Università degli Studi ROMA "Tor Vergata"

Facoltà di Scienze Matematiche, Fisiche e Naturali

Corso di Dottorato in Fisica XX Ciclo–2004/2007

PhD Thesis

Cosmic Rays Propagation in the Galaxy

Candidate:
Emanuele Orazi

Supervisor:
Aldo Morselli

Coordinator:
Prof. Piergiorgio Picozza

Contents

Introduzione

During the last decades physics has not been so exciting since we have not seen any fundamental turning point. The main reason is that, if we exclude astrophysical observation of dark matter and dark energy, we do not have any new key phenomenon that needs an explanation (here we are not considering the experiment supported neutrino oscillation since it has a widely accepted explanation given by endowing neutrinos with masses and mixing). From one side this generated an enormous growth of the number of theories (that is a sign of the crisis that we are living in), with the hope that mathematical consistency could suggest the right way to follow. From another side, it is believed that increasing the energy of particle scattering, could shed light on fundamental interaction, giving eventually rise to new particles.

In this framework a special role is played by cosmic ray physics whose beginning is commonly traced back to the discovery of the increasing of the radiation with altitude observed by the austrian scientist Victor Hess onboard his balloon flight, in 1912. This demonstrated the outer-space origin of the radiation exceeding the prediction based on the know sources of natural background radioactivity. Since then cosmic rays provided a unique tool to understand the most energetic processes in the universe. The main component of cosmic rays comes from outside the solar system but they are mostly (especially for the energy range considered in this work) of galactic origin. We have to think about cosmic rays as probes for astronomical observation since they travel for millions of years, trapped by the galactic magnetic field, passing many times through the galactic disk. While the light rays are weakly influenced by the galactic medium so that they map regions from which they bring information, cosmic rays yield clues on the dynamics and matter content of the galaxy.

The interest in cosmic ray physics is threefold because it embraces particle physics, astrophysics and theoretical physics. In fact upcoming balloon borne and satellite

experiments are equipped with detectors whose energy range acceptance is comparable with the energies reached by new generation accelerators. Moreover earth based experiments on cosmic rays are able to detect energies far beyond future accelerator experiment[1]. Obviously we have a great gain of information on particle physics coming from such experiments. Concerning astrophysics, we are directly connected with new physics coming from dark matter and dark energy that still do not have a compelling explanation. To explain this puzzle the efforts are mainly focused on the existence of new types of particle that are able to explain this "dark-problem". In order to chose which particle has to be taken into account, the scientific community has to draw on theoretical physics. With this general picture in mind, one can argue that the main target is to exploit the high energy component of cosmic ray spectra to identify eventual new physics contribution. Furthermore the recent launch of the satellite borne experiment PAMELA[2], endowed of a variety of specialized detectors that will measure cosmic ray particles over a large range of energy from 50 MeV to hundreds GeV, lead us to commit this work to the study of cosmic rays inside this interval of energy in search of possible new physics. To this end it is necessary to disentangle the standard observations from the non-standard ones that requires a certain degree of knowledge about the standard component of cosmic rays. This thesis is dedicated to this last aspect, namely we try to predict the cosmic ray observations using the standard model of cosmic ray origin and propagation. Even if no new physics will arise from this line of research, we confide in a refinement of our models of galactic cosmic rays. Anyhow this task is rather hard to achieve since it includes several fields of physics and large uncertainties. First of all we need to know where the galactic cosmic ray came into life and which is the medium where they propagate. Thus the key information comes from the branch of astrophysics that gives us the galactic profile, with clear contacts with astronomy. Secondly concerning propagation we have to include in our treatment the main effects that occur during the cosmic ray wandering inside the Milky Way. To study these processes we need to include magnetohydrodynamics and standard nuclear physics. Each area brings with it a certain amount of uncertainty as for instance the cross sections that are not completely known or, the galactic magnetic field which do not show a coherent behavior and so on.

[1] http://www.auger.org/index.html

[2] http://pamela.roma2.infn.it/index.php

There are many ways to treat cosmic ray propagation. The most simple is the so-called Leaky Box (see appendix B), in which the galaxy is described as a finite propagation volume with homogeneous density of sources, interstellar gas and cosmic rays. All the physics is enclosed into only two parameters: the escape length $\lambda_{esc}(E)$ and the gas density. This model find its limits in the failure to predict unstable cosmic rays [1]. To understand why the Leaky Box works so well in reproducing stable nuclei, it is needed to embed it in a more general approach as the Weighted Slab model [2]. The Slab Model is based on the mean density of matter traversed by a particle, the *grammage* x, that is assumed to be the same for all nuclei. Since the secondary over primary ratio are directly related to the grammage by equation involving production and destruction cross sections, one can easily predict these ratios. The simple slab approach leads to contradictions since Li-Be-B/C-N-O data give $x \sim 4.8\, g\, cm^{-2}$ while SubFe/Fe data predict $x \sim 0.8\, g\, cm^{-2}$. The discrepancy is solved in the context of the Weighted Slab model where it is introduced a path length distribution $G(x)$ that weights the probability that a nucleus has crossed the grammage x. The weighted slab technique infers the path length distribution directly from the data and gives the chance to link Leaky Box model to more general diffusion models that is the ultimate and more physical approach to cosmic ray propagation. More precisely it has been shown that the path length distribution associated to diffusion model can be written as a sum of path length distributions of the Leaky Box models with different escape length [3]. Since in the most simple frameworks only the first terms contribute to the propagation, the wide success of the Leaky Box is explained. Nowadays it is clear that the most general approach is based on diffusion processes that is equivalent to say that cosmic rays experience a random walk during their wandering through the galaxy [4]. It is a pity that equations coming from an all-inclusive model are too complex to be solved analytically in general. Only for particular problems one can solve the equations in an analytical or semi-analytical way but to predict the flux of all the nuclei taking into account all the processes in the same frame, one cannot abstract from a numerical approach. For this reason our approach is based on the public GALPROP model[3] (50p version) that has the advantage to include all the current knowledge about cosmic ray physics. Anyway many free parameters are present in the GALPROP model that need to be fixed according to observation. So far no systematic statistical approach has been

[3]GALPROP model is available at http://galprop.stanford.edu/na_home.html

carried out using the code of the GALPROP model to fix these parameters. The reason is that this approach is very time consuming. Luckily the progress in computer science have made a systematic scan of the parameter space affordable, so that we decided to proceed along this way. Thanks to the hardware enhancement reached nowadays we were able to perform our analysis with a common desktop, earning many results and prospects for future refinement.

Among the original contribution we mention that in order to carry out this work we wrote the following programs and routines:

- GRIDGALPROP: that is a program that automatically scan a user defined parameter space, activating a GALPROP run for each set of parameters. The key feature of this program is that it is able to archive the output fitsfiles produced by GALPROP code and to recognize them for following wider scan of the parameter space;

- STATVIEW: designed to analyze the models scanned by GRIDGALPROP, calculating statistical quantities by matching with sets of experimental data chosen by the user;

- BestFitFinder and BestIntervalFinder: that are two routines used to find the best model and models with a χ^2 below a user defined value. In particular the second routine gives the maximum and minimum value of each parameter among the models that do not exceed the imposed χ^2 value.

The main guideline of this thesis is to obtain results that are completely reproducible. That is why we spend many pages describing in detail all the approximation and data that we used. Following this line, the code of the GALPROP model has not been changed.

The thesis is organized as follows: the first chapter is dedicated to the description of the journey of a galactic cosmic ray, from its origin to our instruments, with a survey of each process that occurs during propagation; the second chapter deals with detailed derivation and analysis of the all-in-one propagation equation that include all the physics regarding cosmic rays; the third chapter describes the GALPROP model and finally the fourth chapter collect all the original results that we obtained together with consequences for future developments.

Chapter 1

Propagation Processes

In this chapter we want to give an answer to the main two questions concerning cosmic rays that are:

- what are the production sites
- what are the most relevant acceleration processes.

To this end we follow the complete journey of a cosmic ray, starting from its origin until the detection at earth. Along the way, diffusion, acceleration, spallation and energy losses are among the most important processes that are interesting for the range of energy and typology of cosmic rays that we consider in this work. Less important but still relevant for our purpose are reacceleration, galactic convection, solar modulation etc. Processes involving gamma rays (like inverse compton etc.) are not considered since in the present work we focused completely on massive cosmic rays.

1.1 Origin of Cosmic Rays

If we assume that the energy density is the same as the local one (namely $\rho_E \sim 1\, eV/cm^3$) all over the galactic disk, then the power required to supply all the galactic cosmic rays turns out to be

$$P_{cr} = \frac{\rho_E\, V_D}{\tau_R} \sim 5 \times 10^{40}\, \frac{erg}{sec}\,, \tag{1.1}$$

where V_D is the volume of the galactic disk

$$V_D = \pi\, R^2\, d \sim \pi(15\, kpc)^2(200\, pc) \sim 4 \times 10^{66}\, cm^3 \tag{1.2}$$

and τ_R is the residence time of cosmic rays in the disk

$$\tau_R \sim 6 \times 10^6\, years\,. \tag{1.3}$$

The above value of the residence time can be estimated in the context of the leaky box model (see appendix B) to be

$$\tau_R = \frac{\lambda_{esc}}{\rho v}\,, \tag{1.4}$$

where the value of λ_{esc} which is the mean amount of matter traversed by a particle of velocity v, is approximately $\lambda_{esc} \sim 10\, g/cm^2$ for a nominal disk density of one hydrogen atom per cubic centimeter. Even if the age of cosmic rays is longer than the resident time, a percentage of the lifetime can be spent in the halo, so that what is important for the above estimation of the source power requirement is the equilibrium state in the volume V_D that is determined by the observed energy density, independently from the halo size. It has been observed along the centuries that there are about 3 supernovas per century, that means a mean occurrence of one every 30 years. For 10 $M_\odot$ ejected from a type II supernova with a velocity $v \sim 5 \times 10^8 cm/s$, we figure out the total power

$$P_{SN} \sim 3 \times 10^{42}\, erg/s\,, \tag{1.5}$$

that, even if affected by great uncertainties, make supernovas the most plausible source of galactic cosmic rays. Other possible minor sources that contribute to the observed spectrum can be identified in pulsars, compact objects in close binary systems and stellar wind.

The above observation suggests that the main component of primary cosmic ray is represented by the material ejected during supernova explosion (supernova remnants) so that the composition of cosmic rays should reflects the products of nuclear reactions that occur inside the stars. However this is not completely true because the primaries interact with interstellar medium giving rise to a plenty of other elements. As a consequence, if we compare the elemental abundance of the solar system with the cosmic ray elemental abundance measured at Earth, then we observe a discrepancy regarding the elements that are not final products of stellar nucleosynthesis (see fig. 1.1). This means

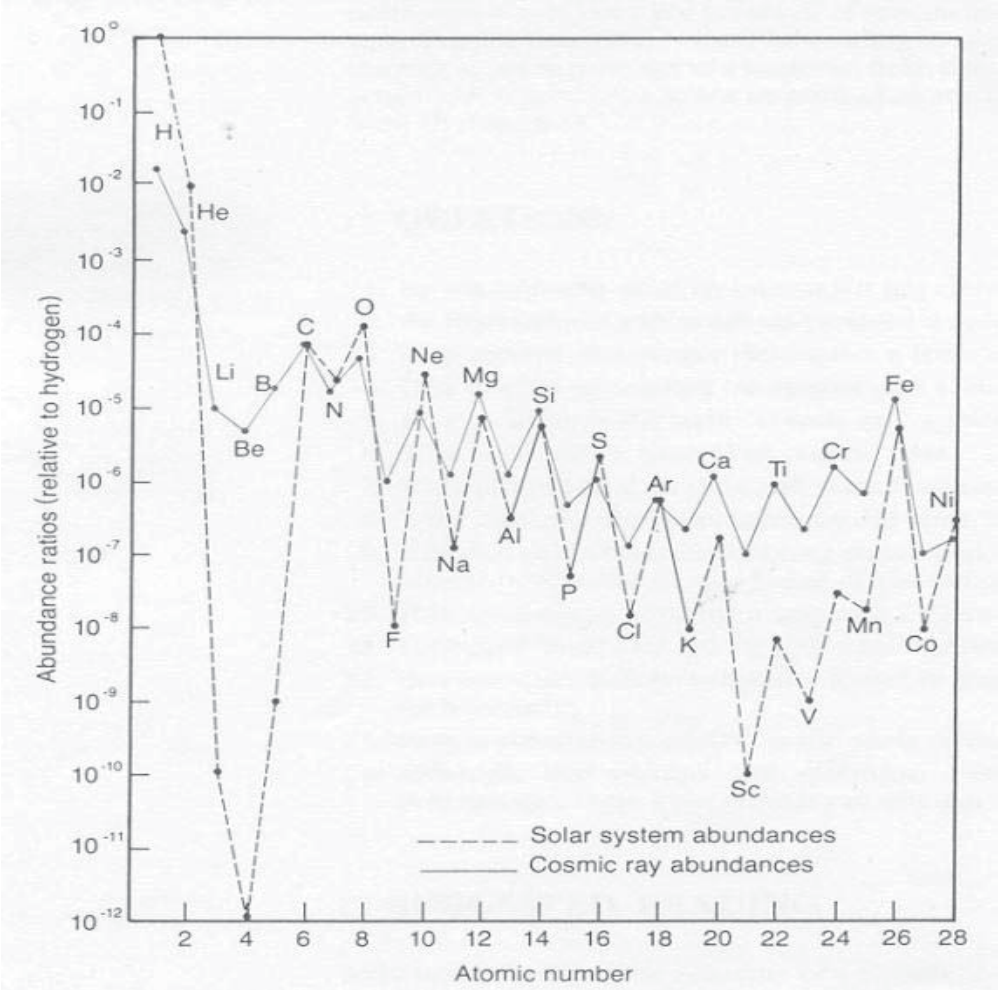

Figure 1.1: Elemental abundance in the solar system (points connected by dashed lines) compared with cosmic rays composition (points connected by solid lines).

that the elements whose abundance exceeds the one measured in the solar system are produced by spallation and deemed as secondary cosmic rays. In this way it is rather easy to single out the purely secondary components of cosmic ray with the following two main groups :

- (^{2}H, ^{3}He) produced by protons and helium;
- (Li, Be, B) produced by carbon and oxygen;
- (Sc, Ti, V, Cr, Mn) produced by iron ,

where the first group has been added even if not reported in figure 1.1. The importance of distinguishing between primary and secondary cosmic rays, resides in the possibility of connecting different type of cosmic ray to different aspects of propagation as we will deepen in the upcoming sections. The protons are by far the most important

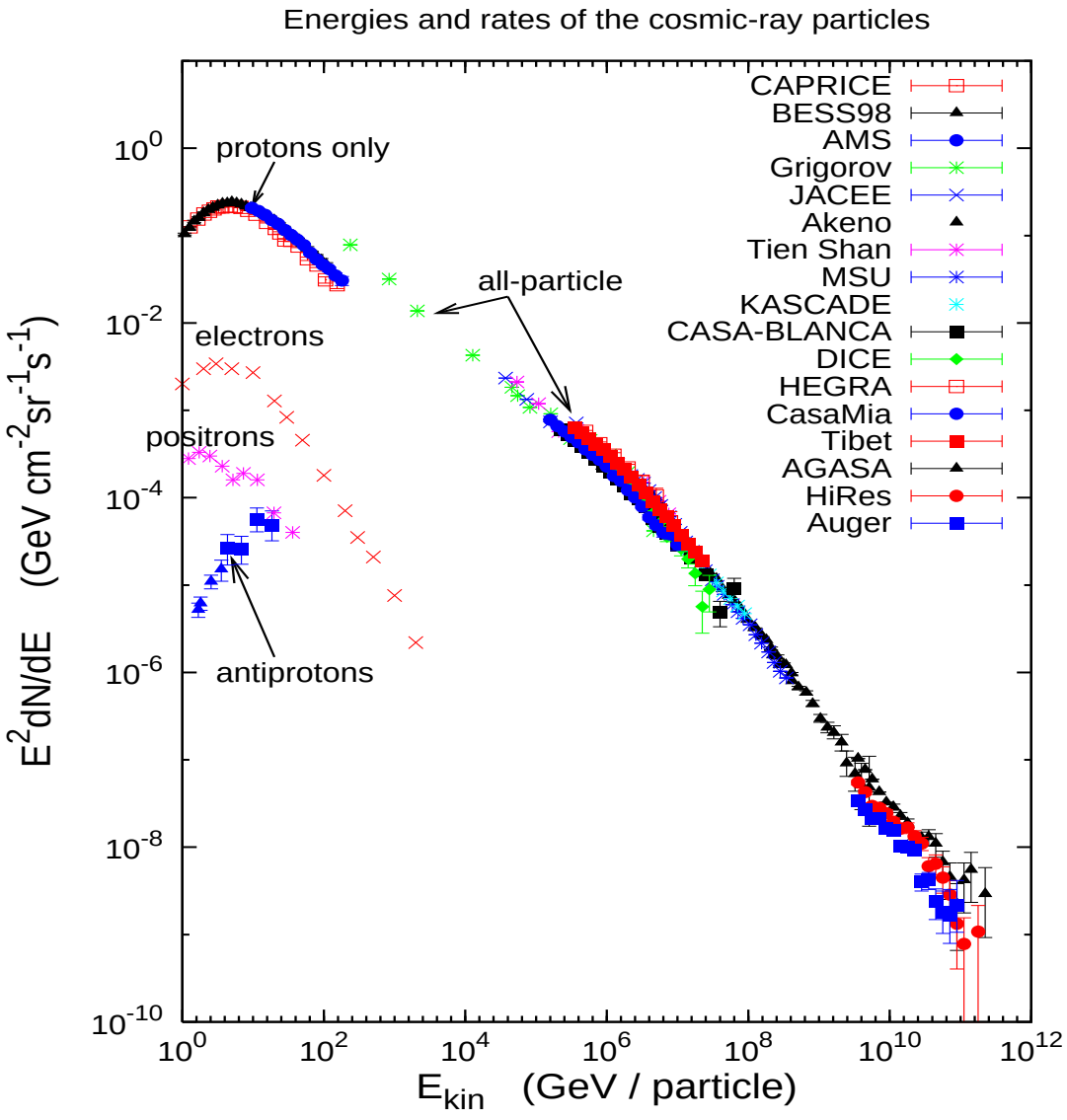

Figure 1.2: Differential energy spectra of galactic cosmic rays in a wide range of kinetic energy [5] .

component of cosmic ray flux. They amount to about the 90% of the total, followed by a 9% of Helium nuclei. Since this main components are primaries, they carry informations about the source spectrum. In figure 1.2 we can see that for energies that are enough high to make the solar modulation not effective, the proton differential flux exhibits a power law behavior that is the same for almost all the cosmic ray

$$\frac{dN}{dE} \propto E^{-(\gamma+1)}\,, \tag{1.6}$$

with $\gamma \sim 1.7$ until $E \sim 10^6\, GeV$ and a steepening to $\gamma \sim 2$ above. Such a dependence of the differential fluxes on the energy is highly constraining for propagation models and will be used in the forthcoming chapters for the interpretation of a plenty of important results.

1.2 Acceleration and Reacceleration

The understanding of cosmic ray acceleration is still a subject of intensive studies. At present the scientific community is mostly focused on ultra high energy cosmic ray with energies around $10^{19}\, eV$, where the theory is not completely established. The range of energies that we encounter in this work will never exceed the TeV (so we are far from considering ultra high energy cosmic ray). In this interval of energy, there is a good agreement on the processes of acceleration that occur during the propagation and it is well known that everything happens inside our galaxy. It is important to have in mind that only charged particles can be accelerated since all the acceleration processes are magnetic in nature. In order to give a easy understanding explanation of the cosmic ray acceleration, we will present in this section both first and second order Fermi acceleration but while the previous is responsible for the initial acceleration of a cosmic ray, the last occurs during the cosmic ray propagation (that is why it is called reacceleration) and is less effective than the other one. However both mechanisms have some features in common so we believe it is better to put them together in order to highlite differences and similarities.

1.2.1 Second Order Fermi Acceleration

One of the milestone of cosmic ray studies is the explanation of an effective mechanism of particle acceleration suggested by Enrico Fermi in 1949 [6]. The original idea was that slowly moving magnetic clouds, about 10-100 times more dense than the interstellar medium and endowed with enhanced "frozen-in" magnetic field, are responsible for the reacceleration of cosmic rays. These many light years wide clouds are now believed to occupy several percent of the interstellar medium. Whenever a fast moving particle enter such clouds, it experiences random irregularities of the magnetic field that change its momentum with a resulting gain or loss of energy according to a collision that sees the particle momentum opposite or in the same direction of the velocity of the cloud, respectively. Since the frontal collision is more probable, the global effect is a gain of energy of the whole galactic particles. There are two types of elastic scattering that end with a reflection of the particle :

- the "magnetic mirror" where the particle get inside a field flux tube whose field lines get closer and closer (increasing of the magnetic field gradient) until the reflection;

- the particle follows a field line that is bent.

Since the magnetic irregularities of the field are random, the multiple scattering inside the cloud can be considered as a random walk.

Let us explain in detail how the second order Fermi acceleration work. Denoting E_1 the energy in the laboratory frame of a relativistic particle that is entering a slowly moving magnetic cloud, Lorentz transformations give

$$E_1' = \gamma E_1(1 - \beta \cos\theta_1)\,, \tag{1.7}$$

where here and in the following, prime stands for the rest frame of the cloud. The angle θ_1 is between the moving directions of the particle and the cloud. β and γ are referred to the velocity of the cloud. If we call E_2' and θ_2' the exiting energy and angle in the cloud rest frame, we can go back to the laboratory frame with

$$E_2 = \gamma E_2'(1 + \beta \cos\theta_2')\,. \tag{1.8}$$

Notice that the β sign has been changed. Since we are assuming that we have elastic scattering, the energy of the particle in the rest frame is conserved

$$E_2' = E_1' \,, \tag{1.9}$$

so that from (1.7) and (1.8) we get

$$E_2 = \gamma^2 E_1 (1 - \beta \cos\theta_1)(1 + \beta \cos\theta_2') \,, \tag{1.10}$$

and

$$\frac{\Delta E}{E} := \frac{E_2 - E_1}{E_1} = \frac{1 - \beta\cos\theta_1 + \beta\cos\theta_2' - \beta^2 \cos\theta_1 \cos\theta_2'}{1 - \beta^2} - 1 \,. \tag{1.11}$$

To exploit the random nature of the process, we average equation (1.11) to end with

$$\frac{\Delta E}{E} = \frac{1 + \beta^2/3}{1 - \beta^2} - 1 \approx \frac{4}{3}\beta^2 \,, \tag{1.12}$$

where we used the all θ_2' equal probability

$$\frac{dn}{d\cos\theta_2'} = const,\ -1 \leq \cos\theta_2' \leq 1 \,, \tag{1.13}$$

that leads to $< \theta_2' >= 0$, and the fact that the angular probability of a particle to enter the cloud with an angle θ_1 is proportional to the relative velocity between particle and cloud

$$\frac{dn}{d\cos\theta_1} = \frac{1}{2}(1 - \beta\cos\theta_1),\ -1 \leq \cos\theta_1 \leq 1 \,, \tag{1.14}$$

so that

$$< \cos\theta_1 >= -\beta/3 \,. \tag{1.15}$$

In conclusion we are left with the net energy gain per collision

$$dE \propto \beta^2 \cdot E \,, \tag{1.16}$$

which labels this effect as the "second order" one because of the β^2 dependence. Equation (1.16) can be integrated to give us the energy reached by the particle after n collision that is

$$E = E_i \cdot e^{\beta^2 n} \,, \tag{1.17}$$

where E_i stands for the injection energy, namely the energy with which the particle enter the cloud. To manifest the time dependence in (1.17) we introduce the average

time between two collision τ_c so that we count the number of collision occurring in the interval of time t that is $n = t/\tau_c$. Substituting this last expression in (1.17), we are left with

$$E(t) = E_i \cdot e^{\beta^2 t/\tau_c} = E_i \cdot e^{t/t_c}\,, \tag{1.18}$$

where $t_c = \tau_c/\beta^2$. To take into account the surviving or leaking of the particles, we define t_l as a mean time of existence of the particle inside the system. Obviously the probability that a particle survive until time t is

$$P(t) = e^{-t/t_l} = E_i^{t_c/t_l}(E_i \cdot e^{-t/t_c})^{-t_c/t_l} = k \cdot E^{-\alpha}\,, \tag{1.19}$$

where we used equation (1.18) and we introduced $\alpha = t_c/t_l$. Therefore the total number of particles with energy greater than E, namely the integral form of the differential energy spectrum, reads

$$J(E) \propto E^{-\alpha}\,, \tag{1.20}$$

that shows the typical power law behavior. Accordingly, the differential energy spectrum is proportional to

$$\frac{dJ}{dE} \propto E^{-(\alpha+1)} =: E^{-\gamma}\,, \tag{1.21}$$

where γ is the already mentioned spectral index. The possibility to explain the observed power law followed by the differential flux of cosmic rays is one of the reason why this kind of acceleration was immediately accepted as a further step toward the understanding of cosmic ray physics.

However, since the particles experience energy loss by ionization during the path inside the dense cloud, there exist a threshold energy beyond which this second order Fermi mechanism do work. More precisely if the energy losses exceed the energy gain due to the cloud, then the net effect on the particle is not an acceleration. The point where the gain overtake the loss is such a threshold energy which depends on the considered particle as the ionization effects do. For instance we have 200 MeV for protons, 20 GeV for oxygen, and 300 GeV for iron. In other words the ionization is more effective for heavier ions because of the increasing charge.

1.2.2 First Order Fermi Acceleration

Another similar acceleration mechanism was proposed by Bell [9] and independently by Blandford and Ostriker [10] in 1978. In this case the propulsion engine is the

supernova remnant shock which generate a non random boost of the particles. Here the framework is the same as the first order Fermi acceleration : the cloud is represented by accelerated gas following a shock front (downstream). This shocked gas moves with a velocity $v = u_2 - u_1$ where $-u_1$ is the velocity if the shock front and u_2 is the relative velocity between the shock and the particles in the downstream region. We can apply again equation (1.11) but this time the angular distribution (1.13) is replaced by the projection of an isotropic distribution on the shock plane, namely

$$\frac{dn}{d\cos\theta_2'} = 2\cos\theta_2', \quad -1 \leq \cos\theta_2' \leq 0\,, \tag{1.22}$$

that gives

$$< \cos\theta_2' >= -\frac{2}{3},. \tag{1.23}$$

Accordingly even the interval of $\cos\theta_1$ in (1.14) is changed by the presence of the plane into $-1 \leq \cos\theta_1 \leq 0$, so that

$$< \cos\theta_1 >= -\frac{2}{3}\,. \tag{1.24}$$

Averaging equation (1.11), we get

$$\frac{\Delta E}{E} = \frac{1 + \frac{4}{3}\beta + \frac{4}{9}\beta^2}{1 - \beta^2} - 1 \approx \frac{4}{3}\beta\,, \tag{1.25}$$

where the approximation is for non relativistic motion of the cloud, namely $\beta << 1$. This time we have a first order dependence on the velocity of the cloud (this gives the name to the effect) so that this last kind of Fermi acceleration is more effective than the second order one simply because β is always less than one. Moreover the second order case can result in loss of energy of the particle for a single encounter (even if after many encounters there is a net gain) while in the first order case, there is always an increase of the particle energy for each encounter.

To end this section let us spend a few word on the source spectral distribution that is generated mostly by the first order mechanism as to say by shock waves. In general the source spectral distribution can be parameterized as follows

$$q^j(E) = q_0^j\, Q^j(E) \tag{1.26}$$

where the j index specifies the nucleus, q_0^j take into account the composition and $Q^j(E)$ encloses the energy dependence. Concerning this last term, different forms, namely

$$\begin{aligned} \frac{Q^j(E)}{dE} &\propto p^{-\gamma_j}\,, \\ \frac{Q^j(E)}{dE} &\propto E_{tot}^{-\gamma_j}\,, \\ \frac{Q^j(p)}{dp} &\propto p^{-\gamma_j}\,, \end{aligned} \tag{1.27}$$

(where γ is the spectral index), has been considered in [7] where the authors realized that the best parametrization for the HEAO data in the leaky box framework with the proper modulation strength, is the first one. This is in agreement with the law directly derived from the shock acceleration theory [8]. Moreover all the heavy elements appear to have very nearly the same spectral index γ with a values ranging in the interval $2.39 - 2.44$ while for protons γ has to be lowered to values around 2.1.

1.3 Diffusion

The most important effect that characterize all the life of a cosmic ray is the diffusion. It takes place whenever a spatial gradient in the density of particles $N(\mathbf{r}, t)$ occurs to be different from zero. In order to flatten the density, a current is generated that brings particles from high density zones to lower density ones

$$\nabla N \neq 0 \;\rightarrow\; \mathbf{J}(\mathbf{r}, t) = -D\nabla N\,, \tag{1.28}$$

where D is the diffusion coefficient. Since in general we can write the continuity equation with a source term $Q(\mathbf{r}, t)$

$$\frac{\partial N}{\partial t} = -\nabla \cdot \mathbf{J} + Q(\mathbf{r}, t)\,, \tag{1.29}$$

we immediately get the diffusion equation

$$\frac{\partial N}{\partial t} = \nabla \cdot (D\nabla N) + Q\,. \tag{1.30}$$

The Green's function associated to (1.30)

$$G(\mathbf{r}, t) = \frac{1}{8(\pi D\, t)^{3/2}} e^{-r^2/(4D\, t)}\,, \tag{1.31}$$

gives us the probability for finding a particle that is injected at the origin, at position **r** after time t. Using (1.31) one can calculate the mean distance from the galactic plane

$$< |z| >= \frac{1}{8(\pi D\, t)^{3/2}} \int z\, e^{-r^2/(4D\, t)}\, dV = 2\sqrt{Dt/\pi}\,, \tag{1.32}$$

and then define the characteristic time to reach an height H as

$$t \equiv \frac{\pi}{4D} H^2 \sim \frac{H^2}{D}\,. \tag{1.33}$$

Finally we are able to define the characteristic averaged velocity to escape from a galaxy whose halo height is H

$$v_D \sim H/t_H \sim D/H\,. \tag{1.34}$$

Let us underline that to obtain the mean distance from the galactic plane, we assumed the diffusion coefficient to be spatially constant all over the halo and the disk that is not strictly true.

1.4 Energy Losses

For nucleon propagation in the ISM neutral matter (90% H and 10% He) the relevant energy losses are due to electromagnetic and nuclear effects according to the type of interaction. The most relevant processes of the first group are ionization and Coulomb scattering while for the second we have spallation, fragmentation and radioactive decay. For electromagnetic processes that involve electrons, even bremsstrahlung in the neutral and ionized medium, as well as Compton and synchrotron losses became important. Although all these processes are well-known and are often explained during academic courses, the formulae for the different cases are rather scattered throughout the literature. A complete derivation of the equations that describe these effects is beyond the purpose of this work but we think that for the sake of completeness it is important to explain what are the equations that are used in the following.

1.4.1 Ionization Losses

The general equation that describes ionization losses for nucleons can be written as ([11], their eq. [4.24])

$$\left(\frac{dE}{dt}\right)_{\rm I}(\beta \geq \beta_0) = -2\pi r_e^2 c\, m_e c^2 Z^2 \frac{1}{\beta} \sum_{s=H,He} n_s \left[B_s + B'(\alpha_f Z/\beta)\right], \tag{1.35}$$

where α_f is the fine structure constant, n_s is the number density of the corresponding species in the ISM, $\beta_0 = 1.4e^2/\hbar c = 0.01$ is the characteristic velocity determined by the orbital velocity of the electrons in hydrogen, and

$$B_s = \left[\ln\left(\frac{2m_e c^2 \beta^2 \gamma^2 Q_{\rm max}}{\tilde{I}_s^2}\right) - 2\beta^2 - \frac{2C_s}{z_s} - \delta_s\right], \tag{1.36}$$

where γ is the Lorentz factor of the ion. The largest possible energy transfer from the incident particle to the atomic electron is defined by kinematics

$$Q_{\rm max} \approx \frac{2m_e c^2 \beta^2 \gamma^2}{1 + [2\gamma m_e/M]}, \tag{1.37}$$

where $M \gg m_e$ is the nucleon mass, and $\tilde{I}_s$ denotes the geometric mean of all ionization and excitation potentials of the atom. The values $\tilde{I}_H = 19$ eV and $\tilde{I}_{He} = 44$ eV are given in [11]. The shell-correction term C_s/z_s, the density correction term δ_s, and the B' correction term (for large Z or small β) in equations (1.35) and (1.36), can be neglected for our purposes.

Concerning electrons, ionization losses has to be treated in a different way. In a medium made of neutral hydrogen and helium the Bethe-Bloch formula ([13], p.360) has to be applied

$$\left(\frac{dE}{dt}\right)_{\rm I} = -2\pi r_e^2 c\, m_e c^2 \frac{1}{\beta} \sum_{s=H,He} Z_s n_s \left[\ln\left\{\frac{(\gamma-1)\beta^2 E^2}{2I_s^2}\right\} + \frac{1}{8}\right], \tag{1.38}$$

where Z_s is the nucleus charge, n_s is the gas number density, I_s is the ionization potential (we use $I_H = 13.6$ eV, $I_{\rm He} = 24.6$ eV, though the exact numbers are not very important), E is the total electron energy, γ and $\beta = v/c$ are the electron Lorentz factor and speed, correspondingly.

1.4.2 Coulomb Scattering

The Coulomb collisions in a completely ionized plasma are dominated by scattering off the thermal electrons. The corresponding energy losses are given by ([11], their eqs. [4.16],[4.22])

$$\left(\frac{dE}{dt}\right)_{\rm Coul} \approx -4\pi r_e^2 c\, m_e c^2 Z^2 n_e \ln\Lambda \frac{\beta^2}{x_m^3+\beta^3}, \tag{1.39}$$

where r_e is the classical electron radius, m_e is the electron rest mass, c is the velocity of light, Z is the *projectile* nucleon charge, $\beta = v/c$ is the nucleon speed, n_e is the electron number density in plasma, $x_m \equiv (3\sqrt{\pi}/4)^{1/3} \times \sqrt{2kT_e/m_e c^2}$, and T_e is the electron temperature. The Coulomb logarithm $\ln\Lambda$ in the cold plasma limit is given by (e.g., [12])

$$\ln\Lambda \approx \frac{1}{2}\ln\left(\frac{m_e^2 c^4}{\pi r_e \hbar^2 c^2 n_e}\cdot\frac{M\gamma^2\beta^4}{M+2\gamma m_e}\right)\ , \tag{1.40}$$

where $\hbar$ is the Planck constant, M is the nucleon mass, and γ is the nucleon Lorentz factor. For the appropriate number density, $n_e \sim 10^{-1}-10^{-3}$ cm^{-3}, and total energy $E \sim 10^3-10^4$ MeV, the typical value of the Coulomb logarithm $\ln\Lambda$ lies within interval $\sim 40-50$, instead of usually adopted value 20.

For the electrons, the Coulomb energy losses in the fully ionized medium, in the cold plasma limit, are described by ([13], p.361)

$$\left(\frac{dE}{dt}\right)_{\rm Coul} = -2\pi r_e^2 c\, m_e c^2 Z n \frac{1}{\beta}\left[\ln\left(\frac{E m_e c^2}{4\pi r_e \hbar^2 c^2 n Z}\right)-\frac{3}{4}\right], \tag{1.41}$$

where $Zn \equiv n_e$ is the electron number density. For an accurate treatment of the electron energy losses in the plasma of an arbitrary temperature see, e.g., [14] and [15].

1.4.3 Bremsstrahlung, Compton Effect and Synchrotron Radiation for Electrons

The energy losses due to the bremsstrahlung became relevant for electrons. Considering electron-proton bremsstrahlung in cold plasma, the effect is ruled by the equation [16]

$$\left(\frac{dE}{dt}\right)_{ep} = -\frac{2}{3}\alpha_f r_e^2 c\, m_e c^2 Z^2 n \cdot \cdot \begin{cases} 8\gamma\beta\left[1-0.25(\gamma-1)+0.44935(\gamma-1)^2-0.16577(\gamma-1)^3\right], & \gamma \le 2; \\ \beta^{-1}\left[6\gamma\ln(2\gamma)-2\gamma-0.2900\right], & \gamma \ge 2. \end{cases} \tag{1.42}$$

For the electron-electron bremsstrahlung one can obtain [17; 15]

$$\left(\frac{dE}{dt}\right)_{ee} = -\frac{1}{2}\alpha_f r_e^2 c\, m_e c^2 Z n \beta\gamma^* Q_{\rm cm}(\gamma^*), \tag{1.43}$$

where

$$\begin{aligned} Q_{\rm cm}(\gamma^*) &= 8\frac{p^{*2}}{\gamma^*}\left[1-\frac{4p^*}{3\gamma^*}+\frac{2}{3}\left(2+\frac{p^{*2}}{\gamma^{*2}}\right)\ln(p^*+\gamma^*)\right], \\ \gamma^* &= \sqrt{(\gamma+1)/2}, \quad p^* = \sqrt{(\gamma-1)/2}, \end{aligned} \tag{1.44}$$

and the asterisk denotes center-of-mass variables. The total bremsstrahlung losses in the ionized gas is the sum $(dE/dt)_{\rm BI} = (dE/dt)_{ep} + (dE/dt)_{ee}$. A good approximation gives the expression ([13], p.408)

$$\left(\frac{dE}{dt}\right)_{\rm BI} = -4\alpha_f r_e^2 c\, m_e c^2 Z(Z+1) n E\left[\ln(2\gamma)-\frac{1}{3}\right]. \tag{1.45}$$

Bremsstrahlung energy losses in neutral gas can be obtained by integration over the bremsstrahlung luminosity ([18]

$$\left(\frac{dE}{dt}\right)_{\rm B0} = -c\beta\sum_{s=H,He} n_s \int dk\, k\frac{d\sigma_s}{dk}. \tag{1.46}$$

A suitable approximation (max 10% error near $E \sim 70$ MeV) for eq. (C.11) gives the combination (cf. equation (1.45))

$$\left(\frac{dE}{dt}\right)_{\rm B0} = \begin{cases} -4\alpha_f r_e^2 c\, m_e c^2 E\left[\ln(2\gamma)-\frac{1}{3}\right]\sum_{s=H,He} n_s Z_s(Z_s+1), & \gamma \le 100; \\ -c\,E\sum_{s=H,He}\frac{n_s M_s}{T_s}, & \gamma \ge 800, \end{cases} \tag{1.47}$$

(see [13], p.386, 409), with a linear connection in between. Here M_s is the atomic mass, and T_s is the radiation length ($T_H \simeq 62.8$ g/cm^2, $T_{He} \simeq 93.1$ g/cm^2).

The Compton energy losses are calculated using the Klein-Nishina cross section ([19; 15])

$$\frac{dE}{dt} = \frac{\pi r_e^2 m_e c^2 c}{2\gamma^2\beta} \int_0^\infty d\omega\, f_\gamma(\omega)[S(\gamma,\omega,k^+) - S(\gamma,\omega,k^-)], \tag{1.48}$$

where the background photon distribution, $f_\gamma(\omega)$, is normalized on the photon number density as $n_\gamma = \int d\omega\, \omega^2 f_\gamma(\omega)$, ω is the energy of the background photon taken in the electron-rest-mass units, $k^\pm = \omega\gamma(1 \pm \beta)$,

$$\begin{aligned} S(\gamma,\omega,k) &= \omega\left\{\left(k + \frac{31}{6} + \frac{5}{k} + \frac{3}{2k^2}\right)\ln(2k+1) - \frac{11}{6}k - \frac{3}{k} + \frac{1}{12(2k+1)} + \right. \\ &\left. + \frac{1}{12(2k+1)^2} + Li_2(-2k)\right\} - \gamma\left\{\left(k + 6 + \frac{3}{k}\right)\ln(2k+1) - \frac{11}{6}k + \right. \\ &\left. + \frac{1}{4(2k+1)} - \frac{1}{12(2k+1)^2} + 2Li_2(-2k)\right\}, \end{aligned} \tag{1.49}$$

and Li_2 is the dilogarithm

$$\begin{aligned} Li_2(-2k) &= -\int_0^{-2k} dx\, \frac{1}{x}\ln(1-x) \qquad (1.50) \\ &= \begin{cases} \sum_{i=1}^\infty (-2k)^i/i^2, & k \le 0.2; \\ -1.6449341 + \frac{1}{2}\ln^2(2k+1) - & \\ -\ln(2k+1)\ln(2k) + \sum_{i=1}^\infty i^{-2}(2k+1)^{-i}, & k \ge 0.2. \end{cases} \end{aligned}$$

The synchrotron energy losses are given by

$$\left(\frac{dE}{dt}\right)_{\rm S} = -\frac{32}{9}\pi r_e^2 c\, U_B \gamma^2 \beta^2, \tag{1.51}$$

where $U_B = \frac{H^2}{8\pi}$ is the energy density of the random magnetic field.

1.4.4 Inelasting Scattering

Whenever a cosmic ray crosses the thin galactic disk it may undergoes a nuclear interaction with an interstellar hydrogen or helium nucleus. This encounter can result in a inelasting scattering that, from one side, destroys the parent nuclei and, from another side, creates new cosmic rays (secondaries). The importance of this effect is ruled by

the corresponding cross sections. In particular the total cross section governs the disappearing of a nucleus while to have informations about the daughter nuclei, we need to know the branching ratio of each channel. In the first case we talk about *fragmentation* while in the second we deal with the so called *spallation*. Concerning fragmentation we can insert this effect in the same way we treat decay (see next section) by associating to cross sections a fragmentation rate λ_f.

The most important aspect of the spallation is that a nucleus can produce a considerable number of lighter nuclei that are not generated by sources. A way to identify such secondary cosmic ray nuclei has been already explained in section 1.1 where we pointed that the most important groups are (^{2}H, ^{3}He) from protons and helium, (Li, Be, B) from carbon and oxygen; (Sc, Ti, V, Cr, Mn) from iron. To have an idea of the importance of the spallation just think that we observe the secondary over primary proportions B/C $\sim$ SubFe/Fe ~ 0.1. Notice that, roughly speaking, if the proton abundance is normalized to one, than in proportion we have 0.1 for helium, 0,01 for CNO and 0.001 for iron. These proportions hold both for the interstellar medium as for the cosmic rays. Since the interstellar medium is mainly composed of H and He, it is clear that the most relevant contribution to secondaries comes from reaction such as

$$n_1 + (p,\, He) \;\rightarrow\; n_2 + X\,, \tag{1.52}$$

where n_1 stands for some kind of primary nucleus while n_2 is referred to secondary one. However even heavier species may contribute significantly to secondary cosmic rays through, for instance, the following reaction

$$n_1 + (C,\, N,\, O) \;\rightarrow\; n_2 + X\,, \tag{1.53}$$

but the cross sections involved are not well known and sometimes these processes are negligible. From (1.52) and (1.53) it follows that the source term for secondary nucleons can be written as

$$q_j(\vec{r},p) = \beta c \sum_i f_i^{prim}(\vec{r},p) \;\cdot\; \Big[\sigma_{ij}^{(H)}(p) n_H(\vec{r}) + \sigma_{ij}^{(He)}(p) n_{He}(\vec{r}) + \\ + \sigma_{ij}^{(CNO)}(p) n_{CNO}(\vec{r}) + \sigma_{ij}^{(Fe)}(p) n_{Fe}(\vec{r})\Big]\,, \tag{1.54}$$

where f_i^{prim} is the primaries density of the parent nucleus i, $\sigma_{ij}^{(H)}$ is the cross section for the production of nucleus j from nucleus i that scatters on a proton ($n_1 + p \rightarrow$

$n_2 + X$), $\sigma_{ij}^{(He)}$ is for the production of nucleus j from nucleus i that scatters on helium ($n_i + He \rightarrow n_j + X$) and so on for the other most abundant elements in the interstellar medium that are grouped in the last terms (here CNO stands for carbon, nitrogen and oxygen). One can disregard the i index by introducing the weighted production cross sections $\sigma_j^{(X)} = \sum_i f_i^{prim} \sigma_{ij}^{(X)}$ for the daughter j-nucleus produced on the X-nucleus target, so that we are left with

$$q_j(\vec{r}, p) = \beta c \quad \cdot \quad \Big[\sigma_j^{(H)}(p) n_H(\vec{r}) + \sigma_j^{(He)}(p) n_{He}(\vec{r}) + \\ + \sigma_j^{(CNO)}(p) n_{CNO}(\vec{r}) + \sigma_j^{(Fe)}(p) n_{Fe}(\vec{r})\Big] \; . \tag{1.55}$$

For each inelastic scattering channel in (1.55) we have to evaluate the importance comparing the mean time of each reaction on the target X $\tau = \beta\, c \sigma_{ij}^{(X)} n_{(X)}$ with the typical propagation time of a cosmic ray ~ 20 Myr. So the knowledge of a cross section immediately gives a estimate of the relevance of a scattering process. To further emphasize the key role of cross sections let us notice that in nuclear reactions in the interstellar medium, the kinetic energy per nucleon is approximately conserved so that all the information are contained in cross sections. The above arguments force to proceed to a deeper analysis of the methods used to construct high energy cross section for energy range of interest for cosmic ray physics. Since for a experimental point of view the determination of total cross sections is a completely different problem with respect to identification of all the nuclei produced (in the previous case it is enough to know that the reaction has occurred), we discuss the two cases separately.

Fragmentation Cross Sections

In principle the ideal approach to the determination of cross sections should be based on fundamental considerations (empirical approach). Anyway none of this models is able to provide quick and precise evaluation of the required cross sections and this makes these methods useless for our purpose. More promising is the semi-empirical approach which is based on simpler considerations but still successful in reproducing all existing data on nuclear reactions.

The most simple evaluation of the cross section uses an effective radius of the nucleus $\sigma \sim \pi R_{eff}^2 \sim A^{2/3}$ that has been slightly modified in [20] to take into account

the overlap of the two nuclei wavefunction

$$\sigma_{inel} = \pi\, r_0 \left(A_{target}^{1/3} + A_{proj}^{1/3} - b_0 \right)^2 , \tag{1.56}$$

where r_0 is the nucleon radius and b_0 is the overlap parameter. To come to a modern characterization that is still widely used we have to reach the eighties, when the asymptotic energy independent form

$$\sigma_{inel}(mb) = 45\, A^{0.7} \left[1 + 0.016\, \sin\left(5.3 - 2.63\, \ln A\right) \right] , \tag{1.57}$$

has been proposed in [67] for high energy reaction with a proton colliding on any kind of target. At low energies the high energy cross section (1.57) needs a refinement by adding a factor as follows

$$\sigma_{inel}(E_k in) = \sigma_{inel}(mb) \cdot \left[1 - 0.62 \exp(-E_k in/200) \sin(10.9\, E_k in^{-0.28}) \right] , \tag{1.58}$$

where the kinetic energy per nucleon E_{kin} is expressed in MeV/nuc. For light nuclei, a energy dependent rescaling $[\sigma_{LN}/\sigma_p](E_{kin})$ has to be introduced. A further enhancement [22] consider the A+A reactions but final formulae that are able to reproduce the whole data with a 2% accuracy from 6.8 MeV/nuc to 9 GeV/nuc, has been presented in [23].

In order to construct a general formalism for all reactions, it has been demonstrated in [24] that the parameterization

$$\sigma_{inel} = \pi\, r_0^2 \left(A_{proj}^{1/3} + A_{targ}^{1/3} + \delta_E \right)^2 \left(1 - R_c \frac{B}{E_{rf}} \right) , \tag{1.59}$$

is the best fit to most measurements. Here we have several effects introduced by the term

$$\delta_E = 1.85\, S + 0.16\, \frac{S}{E_{rf}^{1/3}} + 0.91\, \frac{Z_p(A_t - 2Z_t)}{A_t\, A_p} - C_E \, , \tag{1.60}$$

with:

- $S = A_p^{1/3} A_t^{1/3} / (A_p^{1/3} + A_t^{1/3})$ which is the asymmetrical mass term that is related to the overlapping volume of the colliding system;
- $C_E = D[1 - \exp(-E/T_1)] - 0.292 \exp(-E/792) \cos(0.229\, E^{0.453})$ stands for the energy dependence at intermediate and large energies with E as the colliding kinetic energy and D (related to the system density) as T_1, are parameters fixed once for all reactions;

- $0.91\, Z_p(A_t - 2Z_t)/(A_t\, A_p)$ for the isotopic dependence.

Moreover we have the Coulomb barrier

$$B = 1.44\, \frac{Z_p\, Z_t}{R}\,, \tag{1.61}$$

the radius to evaluate the barrier height

$$R = r_p + r_t + 1.2\, \frac{(A_p^{1/3} + A_t^{1/3})}{E_{rf}^{1/3}}\,, \tag{1.62}$$

E_{rf} is the rest frame kinetic energy per nucleus and $r_0 = 1$. Finally, the parameter R_c is inserted to describe all the reactions with the same formalism. Let us underline that the above parameterization has free parameters that need to be fitted on known data. In some cases we can exploit some data points but in many cases, especially for helium on light nuclei, there are no available data. So predictions are sometimes based on purely theoretical ground that exploit the above parameterization, with uncertainties that run from a 2-5% for protons induced reactions, to 10-20% for reactions involving helium.

Spallation Cross Sections

For a nuclear physicist, the energies that are relevant for cosmic rays are not of great interest. This explain why fast procedures to evaluate cross sections for single channels has been developed by cosmic ray physicists. There are basically two approaches:

- the first one stem from a theoretical motivated work of Silberberg and Tsao [25] and is based on regularities coming from the mass difference between target and parent nuclei and the ratios between the number of neutrons and protons in the daughter nuclei. Even if this approach gives a 35% accuracy with data it is still preferred to propagate heavy nuclei with $Z > 30$ whose cross sections are still unknown;

- the origin of the second approach can be traced back to the work of Webber et al. [26] whose target has been to develop a parameterization fully based on experimental regularities. Without entering into details, we can say that exploiting the

fact that the production of different isotopes has similar dependence on energy, we end with three terms parameterization

$$\sigma^{p+N_i}(Z_i,\, A_i;\, Z_f,\, A_f;\, E) = \sigma_0(Z_f,\, Z_i) f_1(Z_i,\, A_i,\, Z_f,\, A_f) f_2(E,\, Z_f,\, Z_i)\,, \quad (1.63)$$

where $\sigma_0(Z_f,\, Z_i)$ describes the dependence on the fragment charge, $f_1(Z_i,\, A_i,\, Z_f,\, A_f)$ gives the isotopic distribution of fragments for a given species and the last term takes into account the energy dependence with a dependence only on the charges. Notice that this approach holds for nuclei with $Z > 3$ since light systems require specific models [27].

1.4.5 Radioactive Decay

Whenever an unstable nucleus loses energy by emitting particles or electromagnetic waves, we have a radioactive decay that changes the *parent* nucleus into a *daughter* one. For a large population of nuclei we can use a statistical approximation so that by simple considerations one can argue that the variation of the population dN of the parent nuclei is proportional to the population itself and to the interval of time considered

$$dN = -\lambda\, N\, dt\,, \quad (1.64)$$

where the minus sign reflect the population decreasing with time passing and λ is called the decay constant. The solution of (1.64) is easily found to be

$$N(t) = N_0 \exp^{t/\tau_0}\,, \quad (1.65)$$

where N_0 is the initial population while $\tau_0 = 1/\lambda$ is the mean lifetime in the rest frame. The time needed to half the initial population is given by the half-life $t_{1/2} = \ln 2\, \tau$. If we consider a relativistic moving frame, time intervals are contracted by a γ factor so that the lifetime becames $\tau_0 \to \tau = \gamma\tau_0$.

So far the problem seems to be well defined and easy to solve once the half-lifes associated to each nucleus are give as in [28]. Unfortunately different decay modes are affected in a different way by the propagation [29] while the half lifetime is often a combination of all the decay modes. In the context of cosmic ray propagation, the most relevant decay processes are β-decay and electronic capture where the nucleus captures a K-shell electron. The β-decay is independent from the environment while

electronic capture needs an attached electron to occur. At the energy of cosmic rays, the electrons around the nucleus are completely removed and the interstellar medium is very poor in e^- so that the nucleus lifetime may be much longer than the one we measure in ordinary laboratory. The importance of unstable elements resides in the possibility of measuring the propagation time of cosmic rays. Pioneering works on this subject focused on ^{10}Be ([30],[31],[32]) followed by other nuclei as ^{26}Al [33], ^{36}Cl [34], ^{54}Mn [35]. It turns out that the typical propagation time of a cosmic ray is about 10-20 Myr. This value can be used to select the interesting unstable nuclei for cosmic ray physics once the γ factor that enhances the lifetime of the nuclei ($\tau_0 \to \tau = \gamma\tau_0$) is taken into account. In [36] a complete list of such a nuclei is given. Only three purely

Z	Nucleus	Daughter	$t_{1/2}^{unit}$(error)
4	$^{10}_{4}$Be	$^{10}_{5}$B	1.51^{Myr} (0.06)
6	$^{14}_{6}$C	$^{14}_{7}$N	5.73^{kyr} (0.04)
26	$^{60}_{26}$Fe	$(^{60}_{27}\mathrm{Co}\overset{\beta^-}{\to})^{60}_{28}$Ni	1.5^{Myr} (0.3)

Table 1.1: Pure β unstable isotopes ($1\,kyr < t_{1/2} < 100\,Myr$) from [36].

β-decay unstable elements have a half-life $\tau_{1/2}$ which lies within the interval 1 kyr-100 Myr as reported in table 1.1. The third one, which is the transition from Fe to Ni, include the transition from Fe to Co as intermediate step, with a half-life of 1.5 Myr while transition from Co to Ni is immediate from a cosmic ray point of view ($t_{1/2} \sim 5$ yr). Whenever we deal with a situation like this we can refer to the Co as a "ghost nucleus" because it does not need to be propagated having an half life smaller than a kyr. As pointed before, the propagation affect the density $N^j(r,z)$ of β-unstable nuclei as is derived in [39] where a slight modified expression with respect to [40], is presented

$$N^j(r,z) = \exp\left(\frac{V_c z}{2D}\right) \sum_{i=0}^{\infty} \frac{\bar{\mathcal{Q}}^j}{A_i^j} \frac{\sinh\left[\frac{S_i^j(L-z)}{2}\right]}{\sinh\left[\frac{S_i^j L}{2}\right]} J_0(\zeta_i \frac{r}{R}), \tag{1.66}$$

that needs a relatively long explanation since we have

$$\bar{\mathcal{Q}}^j \equiv q_0^j Q(E)\hat{q}_i + \textstyle\sum_k^{m_k > m_j} \tilde{\Gamma}^{kj} N_i^k(0) \tag{1.67}$$

$$S_i^j \equiv (\tfrac{V_c^2}{D^2} + 4\tfrac{\zeta_i^2}{R^2} + 4\tfrac{\Gamma_{rad}^{N^j}}{D})^{1/2} \qquad A_i^j \equiv 2h\tilde{\Gamma}_{N^j}^{tot} + V_c + DS_i^j \coth(\tfrac{S_i^j L}{2}) \tag{1.68}$$

where $\bar{\mathcal{Q}}^j$ is the source function resulting from the sum of the first term for the primary contribution with q_0^j being a normalization factor, $\hat{q}_i$ defined by

$$\hat{q}_i = \frac{1}{\pi R^2 J_1^2(\zeta_i)} \frac{\int_0^1 \rho q(\rho) J_0(\zeta_i \rho) d\rho}{\int_0^1 \rho q(\rho) d\rho}, \qquad \rho \equiv r/R\,, \tag{1.69}$$

($J_k(\zeta_i \rho)$ is a order k Bessel function), and a second term for the parent nuclei contribution; the various Γs are decay rates, V_c is the convection velocity and D the diffusion coefficient. Equation (1.66) can be used to properly select β-decay nuclei reported in table 1.2 where ^{54}Mn and ^{56}Ni have been excluded because electronic capture for these

Table 1.2: Pure β unstable isotopes ($1\,kyr < t_{1/2} < 100\,Myr$) from a propagation point of view as presented in [36].

Z	Nucleus	Daughter	$t_{1/2}^{unit}$(error)
4	$^{10}_{4}$Be	$^{10}_{5}$B	1.51^{Myr} (0.06)
6	$^{14}_{6}$C	$^{14}_{7}$N	5.73^{kyr} (0.04)
13	$^{26}_{13}$Al	$^{26}_{12}$Mg	0.91^{Myr} (0.04)
17	$^{36}_{17}$Cl	$^{36}_{18}$Ar	0.307^{Myr} (0.002)
26	$^{60}_{26}$Fe	$^{60}_{28}$Ni	1.5^{Myr} (0.3)

nuclei cannot be neglected.

The interesting elements that undergoes purely electronic capture are summed in table 1.3. Another set of nuclei that are worth to be considered, show a mixed electronic capture and β decay that means that the half-lives associated to the two channels are comparable. The complete list of this nuclei is presented in table 1.4. Unstable nuclei are interesting not only from a propagation time point of view but even to provide information on whether the cosmic ray acceleration process occurs only over a short initial time or whether significant acceleration occurs throughout the lifetime of a cosmic ray. For instance, this approach has been adopted in [38], where the authors concentrated on the three vanadium isotopes ^{51}V, ^{50}V and ^{49}V that are almost secondaries . From table 1.3 we see that ^{51}V is enhanced by the decay of ^{51}Cr while ^{49}V is depleted as it decays into ^{49}Ti. ^{50}V can be considered as stable. It turned out that about 25% of ^{51}Cr and ^{49}V produced as secondaries, decayed at interstellar energy

Table 1.3: Pure electronic capture unstable isotopes from [36].

Z	unstable (EC)	Daughter	$t_{1/2}^{unit.}$ (error)
4	$^{7}_{4}$Be	$^{7}_{3}$Li	53.29^{d} (0.07)
18	$^{37}_{18}$Ar	$^{37}_{17}$Cl	35.04^{d} (0.04)
20	$^{41}_{20}$Ca	$^{41}_{19}$K	103^{kyr} (4)
22	$^{44}_{22}$Ti	$(^{44}_{21}\mathrm{Sc}\xrightarrow{\beta^+})^{44}_{20}$Ca	49^{yr} (3)
23	$^{49}_{23}$V	$^{49}_{22}$Ti	330^{d} (15)
24	$^{48}_{24}\mathrm{Cr}^{\dagger}$	$(^{48}_{23}\mathrm{V}\xrightarrow{\beta^+})^{48}_{22}$Ti	21.56^{h} (0.03)‡
24	$^{51}_{24}$Cr	$^{51}_{23}$V	27.702^{d} (0.004)
25	$^{53}_{25}$Mn	$^{53}_{24}$Cr	3.74^{Myr} (0.04)
26	$^{55}_{26}$Fe	$^{55}_{25}$Mn	2.73^{yr} (0.03)
27	$^{57}_{27}$Co	$^{57}_{26}$Fe	271.79^{d} (0.09)
28	$^{59}_{28}\mathrm{Ni}^{\S}$	$^{59}_{27}$Co	80^{kyr} (11)

† This nucleus has an allowed β transition, but contrary to ^{54}Mn and ^{56}Ni, it has not been studied recently so that we can set it as a pure electronic capture.

‡ In this two-step reaction, the second transition $^{48}\mathrm{V}\xrightarrow{\beta^+}{}^{48}$Ti has a half-life greater than the first one – $15.9735^{d}(0.0025)$. Nevertheless, this second reaction can be taken as immediate because of its β nature. We thus can consider this second element as a ghost. Finally, only the first reaction ($^{48}\mathrm{Cr}\rightarrow{}^{48}\mathrm{V}$) enters the decay rate.

§ This nucleus has a β decay, but with $t_{1/2} > 100\,Gyr$ thus it is sufficient to take into account the electronic capture channel.

of ∼400 MeV/nuc with a possible energy gain due to reacceleration of ∼100 MeV/nuc. Another obvious application of unstable nuclei in the context of cosmic ray physics, is the evaluation of the halo height. On this line we cite the work [55] of the authors of the GALPROP program that used the ratio $^{10}Be/^{9}Be$ to gain informations about the halo in connection with the *Ulysses* data [93]. Further improvement was presented in [73] where the ACE data were added to obtain the more robust estimate $z_h = 3 - 7$ Kpc. Even if one can find many works that exploit isotopic ratio to have clues about the halo height, in [36] it was noticed that the most probable distance $L = \sqrt{D\gamma\tau_0}$

Table 1.4: Mixed electronic capture-β isotopes from [36] and reference therein.

Z	Nucleus	Daughter (EC)	$t_{1/2}^{unit}$ (error)	Daughter (β)	$t_{1/2}^{unit}$ (error)
13	$^{26}_{13}\mathrm{Al}^{*}$	$^{26}_{12}\mathrm{Mg}$	4.08^{Myr} (0.15)	$^{26}_{12}\mathrm{Mg}$	0.91^{Myr} (0.04)
17	$^{36}_{17}\mathrm{Cl}$	$^{36}_{16}\mathrm{S}$	15.84^{Myr} (0.11)	$^{36}_{18}\mathrm{Ar}$	0.307^{Myr} (0.002)
25	$^{54}_{25}\mathrm{Mn}^{\dagger}$	$^{54}_{24}\mathrm{Cr}$	312.3^{d} (0.4)	$^{54}_{26}\mathrm{Fe}$	0.494^{Myr} (0.006)
28	$^{56}_{28}\mathrm{Ni}^{\ddagger\S}$	$^{\S}(^{56}_{27}\mathrm{Co}\xrightarrow{\beta^+})^{56}_{26}\mathrm{Fe}$	6.075^{d} (0.020)	$^{\S}(^{56}_{27}\mathrm{Co}\xrightarrow{\beta^+})^{56}_{26}\mathrm{Fe}$	0.051^{Myr} (0.022)

§ $^{56}_{27}$Co decays via electronic capture (80%) and β^+ (20%), but as the half-life is of the order of two months, one can consider that the only effective channel is β-decay so that this nucleus vanishes immediately. Notice that these values are taken from [37]. More recent references [28] or nuclear charts on the web are ignored because they give either pure β channel or pure electronic capture channel.

Table 1.5: Propagation distance for unstable nuclei as a function of the energy.

	τ_0 (Myr)	1 GeV/nuc	10 GeV/nuc
^{10}Be	2.17	220 pc	950 pc
^{26}Al	1.31	110 pc	470 pc
^{36}Cl	0.443	56 pc	250 pc

covered by unstable elements is not enough to make them sensitive to the boundaries of the propagation volume. This can be seen clearly in table 1.5 where we find the rest frame lifetimes and corresponding values of L for some β radioactive nuclei at two different energies as presented in [36].

Chapter 2

Propagation Equation

2.1 A Simplified Diffusion Model

Naively, we can think to the propagation of galactic cosmic rays as the result of the sum of different processes. Following this idea we can construct the propagation equation by choosing the physics that we want to include in our model. The relevant processes are

- Diffusion, as derived in section (1.3)

$$\frac{\partial N_i}{\partial t} = \nabla \cdot (D_i \nabla N_i)\,, \tag{2.1}$$

  where $N_i\, d\epsilon = N_i(t, \mathbf{r}, \epsilon)\, d\epsilon$ is the density number of i-particles at time t and position $\mathbf{r}$ with ϵ being the energy per nucleon;

- In presence of systematic large-scale motion of the medium such as galactic convection, we have to consider the term

$$\frac{\partial N_i}{\partial t} = -N_i \nabla \cdot \mathbf{u}\,, \tag{2.2}$$

  but in the following we assume this effect to be absent;

- Continuous energy losses, introduced collectively by defining, for each particle, the energy loss per unit time $b_i = d\epsilon_k/dt$, ϵ_k being the energy per nucleon, so that

by mean of the chain rule and considering that we lose energy by time passing, we have

$$\frac{\partial N_i}{\partial t} = -\frac{\partial}{\partial \epsilon_k}(b_i N_i)\,; \tag{2.3}$$

- inelastic scattering with interstellar medium, given by

$$\frac{\partial N_i}{\partial t} = -nv\sigma_i N_i\,, \tag{2.4}$$

where n is the interstellar medium gas density, v is the velocity of the particle and σ_i is the inelastic scattering cross section of the nucleus of type i with nuclei of the interstellar gas;

- production from inelastic scattering of heavier nuclei is included considering

$$\frac{\partial N_i}{\partial t} = \sum_{j<i} nv\sigma_{ij} N_j\,, \tag{2.5}$$

where σ_{ij} is the production cross section of nucleus i from the heavier nucleus j;

- radioactive decays, which is simply

$$\frac{\partial N_i}{\partial t} = -\frac{N_i}{\tau_i}\,, \tag{2.6}$$

where τ_i is the lifetime of the i-nucleus;

- production from heavier nuclei by radioactive decays, that can be written as

$$\frac{\partial N_i}{\partial t} = \sum_{j<i} \frac{N_j}{\tau_{ij}}\,, \tag{2.7}$$

with τ_{ij} standing for the probability that a nucleus of type j decay into a nucleus of type i.

All the above processes lead to the simplest propagation equation describing a truly diffusion model, namely

$$\frac{\partial N_i}{\partial t} = q_i + \nabla\cdot(D_i\nabla N_i) - \frac{\partial}{\partial \epsilon_k}(b_i N_i) - (nv\sigma_i + \frac{1}{\tau_i})N_i + \sum_{j<i}(nv\sigma_{ij} + \frac{1}{\tau_{ij}})N_j\,, \tag{2.8}$$

where $q_i = q_i(t, \mathbf{r}, \epsilon_k)$ is the source function that describes the power and space-time distribution of point-like sources producing the type i nucleus. In order to decouple

the diffusion of particles from the fragmentation we introduce an integral form for the solution

$$N_i(t,\mathbf{r}) = \int_0^\infty N_i(x) G(t,\mathbf{r},x) dx \,, \tag{2.9}$$

where $G(t,\mathbf{r},x)$ is the path-length distribution function describing the fraction of particles at time t and point $\mathbf{r}$, which have traversed a layer of matter of thickness x. In addition we assume that :

- ionization losses are absent;
- the sources are the same for all kind of nuclei but the production of each nucleus is weighted by the constant coefficient g_i

$$q_i(t,\mathbf{r}) = g_i \chi(t,\mathbf{r}) \,; \tag{2.10}$$

- the diffusion tensor does not depend on the kind of nuclei.

By plugging (2.9) into equation (2.8) we get the system of equations

$$\begin{aligned} &\frac{\partial G}{\partial x} + \frac{\partial G}{\partial t} - \nabla \cdot (D \nabla G) = \chi \delta(x) \,, \\ &\frac{\partial N_i}{\partial x} = -(nv\sigma_i + \frac{1}{\tau_i}) N_i + \sum_{j<i} (nv\sigma_{ij} + \frac{1}{\tau_{ij}}) N_k + g_i \delta(x) \,, \end{aligned} \tag{2.11}$$

provided that the following initial conditions are satisfied

$$[G(t,\mathbf{r},0) + \chi(t,\mathbf{r},0)][N_i(0) + g_i] = 0 \;, G(t,\mathbf{r},\infty) N_i(\infty) = 0 \,. \tag{2.12}$$

The first equation of (2.11) describes the diffusion while the second one encodes the fragmentation and decay and is sometimes considered alone in the so called slab model. Since this last equation is a first order differential equation, we write the solution as a sum of exponential

$$N_i(x) = \sum_{j=1}^{i} a_{ij} e^{-(nv\,\sigma_i + \frac{1}{\tau})x} \,, \tag{2.13}$$

where the coefficient a_{ij} can be determined by solving recurrence relations obtained by substituting (2.13) into the starting equation (2.11). After that, one will get recurrence

relations involving the a_{ij} coefficient. Now we substitute back (2.13) inside (2.9) to get the final solution which is nothing but

$$N_i(t,\mathbf{r}) = \sum_{j=1}^{i} a_{ij} F_j(t,\mathbf{r})\,, \tag{2.14}$$

where we introduced the Laplace transformation in the variable $(nv\,\sigma_i + \frac{1}{\tau})$, namely

$$F_j(t,\mathbf{r}) = \int_0^\infty G(t,\mathbf{r},x) e^{-(nv\,\sigma_i + \frac{1}{\tau})x} dx\,. \tag{2.15}$$

Thus the particle density is determined by $F_i(t,\mathbf{r})$ that is a solution of the equation obtained by integrating (2.11) after multiplying each term by $e^{-(nv\,\sigma_i + 1/\tau_i)}$, namely

$$\frac{\partial F_i}{\partial t} - \nabla\cdot(D\nabla F_i) + (nv\,\sigma_i + \frac{1}{\tau_i})F_i = 0\,, \tag{2.16}$$

where we used

$$\int_0^\infty \frac{\partial G}{\partial x} e^{-(nv\sigma_i + \frac{1}{\tau_i})x} = -G(t,\mathbf{r},0) + nv\,\sigma_i + \frac{1}{\tau_i}F_i\;, \quad G(t,\mathbf{r},0) = -\chi(t,\mathbf{r},0)\,. \tag{2.17}$$

The importance of the function $F(t,\mathbf{r})$ relies in the fact that it plays the role of momentum generating function for the mean path-length traversed by the particles

$$< x >= \frac{\int_0^\infty x\,G\,dx}{\int_0^\infty G\,dx} = -\left(\frac{d}{d(nv\,\sigma_i + 1/\tau_i)} lnF_i\right)\Big|_{\sigma_i=0}\,. \tag{2.18}$$

Moreover, it is important to us to note that without using any explicit expression for the coefficients a_{ij}, we can always say that

$$a_{ij} = \sum_{l=1}^{l=j} a_{ijl} g_l\,, \tag{2.19}$$

to find from (2.13) an expression for the constants g_i defining the nuclear composition of the sources, in terms of the cosmic rays density

$$g_i = \sum_{j=1}^{i} \frac{1}{F_j} \sum_{l=1}^{j} a_{ijl} N_l\,. \tag{2.20}$$

Even in this case the introduction of the Laplace transform F_i is crucial. Equation (2.20) open the way to determine the nuclear composition of cosmic rays at the production sites. In particular, if we focus on secondary nuclei ($g_i = 0$) then we can

determine many propagation parameters once the fluxes of secondary cosmic rays are known by experiments. In fact we can solve the set of linear equations coming from (2.20), namely

$$\sum_{j=1}^{i} \frac{1}{F_j} \sum_{l=1}^{j} a_{ijl} N_l = 0 \,, \tag{2.21}$$

to get information on any propagation parameter that enters in the function F_j.

Even if equation (2.8) offers the possibility to find analytic solutions under a number of assumption, it is nevertheless not completely physical since it does not include reacceleration processes occurring in the interstellar medium such like Fermi-type acceleration. In the following paragraphs we face the problem of finding a propagation equation that include all the known processes occurring in the interstellar medium. To this end we work in the context of the kinetic theory following the derivation of the propagation equation given in [41] to which we remind the reader for further explanations.

2.2 The Boltzmann Kinetic Equation

Let us define $f(t, \mathbf{x}, \mathbf{p})$ as the density distribution of particles at the time t in the phase space. Integrating this quantity we have

$$N(t) \;=\; \int_\Gamma d\mathbf{x}\; d\mathbf{p}\; f(t, \mathbf{x}, \mathbf{p}) \;=\; \int_\Gamma dn \;, \tag{2.22}$$

which is the probable number of particles at the time t contained in the phase space volume Γ. Increasing the time by δt, position and momentum of the particles change according to

$$\begin{aligned} \delta\mathbf{x} \;&=\; \dot{\mathbf{x}}\; \delta t \;=\; \frac{\mathbf{p}}{m}\delta t \;, \\ \delta\mathbf{p} \;&=\; \dot{\mathbf{p}}\; \delta t \;=\; \frac{\mathbf{F}}{m}\delta t \;, \end{aligned} \tag{2.23}$$

where $\mathbf{F}$ is the external force. The total change of the number of particles in the phase space infinitesimal volume turns out to be

$$\delta dn \;=\; d\mathbf{x}\; d\mathbf{p}\; \delta f(t, \mathbf{x}, \mathbf{p}) \;=\; d\mathbf{x}\; d\mathbf{p} \left(\frac{\partial f}{\partial t} + \dot{\mathbf{x}} \nabla f + \dot{\mathbf{p}} \frac{\partial f}{\partial \mathbf{p}} \right) \delta t \;. \tag{2.24}$$

If no collision is supposed to occur, then each particle can be considered as a closed system. Consequently the Liouville theorem holds, asserting that

$$\delta f(t, \mathbf{x}, \mathbf{p}) \;=\; 0 \; . \tag{2.25}$$

If we want to take into account the collisions, we are forced to introduce the variation velocity R of the distribution function due to collisions

$$dn' - dn \;=\; R\delta t \; , \tag{2.26}$$

where the rate R has to be specified case by case, following the properties of each interaction.

The full kinetic equation coming from (2.23) and (2.26) reads

$$\frac{\partial f}{\partial t} + \dot{\mathbf{x}}\nabla f + \dot{\mathbf{p}}\frac{\partial f}{\partial \mathbf{p}} \;=\; R \; . \tag{2.27}$$

Since the collisions between particles are always mediated by an interaction, we need proper arguments to distinguish between forces whose contribution can be included into the collision term, and forces that are inserted through the $\dot{\mathbf{p}}$ term in (2.27). The two relevant quantities to be compared in order to solve this distinction, comes out to be the interaction range and the mean free path of the particles.

For instance, if we consider a gas of neutral atoms or molecules, then we have interactions whose range extends for distances of the order of atomic dimensions which are very short if compared to the mean free path. In this case we have a genuine collision framework and the $\dot{\mathbf{p}}$ term in (2.27) can be neglected if not external field is applied to the system.

Collisions of this kind are necessarily caotic in nature, being responsible of the relaxation mechanism that end up with an equilibrium state through the increasing of entropy.

For the plasma, the situation is completely different. Each particle, being ionized, carries a charge which is responsible of a long range interaction so that, taken together, the plasma particles generate a collective macroscopic field whose effect is to reduce the free mean path to zero. This justify the choice of neglecting collisions whenever we deal with a sufficiently not rarefied plasma. What happens when we work with a rarefied plasma? The answer involve the Debye length (see appendix B) which characterizes the

interaction range of the macroscopic field. Anytime the Debye length is much greater than the mean distance between particles, we can disregard collisions and write down the kinetic equation as

$$\frac{\partial f}{\partial t} + \dot{\mathbf{x}}\nabla f + e\left(\overrightarrow{\mathcal{E}} + \frac{\dot{\mathbf{x}} \times \overrightarrow{\mathcal{H}}}{c}\right)\frac{\partial f}{\partial \mathbf{p}} \;=\; 0 \;, \tag{2.28}$$

where the Lorentz force has been introduced.

2.3 Quasi-Linear Approximation

The standard quasi-linear approximation is based on the assumption that the distribution $f(t, \mathbf{x}, \mathbf{p})$ can be expressed as the sum of two terms

$$f(t, \mathbf{x}, \mathbf{p}) \;=\; f_0(\mathbf{p}) + f_1(t, \mathbf{x}, \mathbf{p}) \;, \tag{2.29}$$

where $f_0(\mathbf{p})$ describes a slowly evolving background (it can be considered spatially uniform if the wavelength of the perturbation is of the order of a few Debye length) while $f_1(t, \mathbf{x}, \mathbf{p})$ stands for the fluctuating part which is required to be small with respect to f_0. We also assume to consider an instability such that a continuous spectrum of waves is excited. Averaging (2.29) over this spectrum the fluctuating part goes to zero

$$< f_1 > = \; 0 \;, \tag{2.30}$$

to leave us with

$$< f > = \; f_0 \;, \tag{2.31}$$

specifying the meaning of f_0. The magnetic field undergoes the same treatment so that

$$\overrightarrow{\mathcal{H}} \;=\; \overrightarrow{\mathcal{H}}_0 + \overrightarrow{\mathcal{H}}_1 \;, \tag{2.32}$$

where $\overrightarrow{\mathcal{H}}_1$ represents the random fluctuating part of $\overrightarrow{\mathcal{H}}$

$$< \overrightarrow{\mathcal{H}} > = \; \overrightarrow{\mathcal{H}}_0 \;, \qquad < \overrightarrow{\mathcal{H}}_1 > = \; 0 \;. \tag{2.33}$$

Moreover, since we are interested in interstellar space which is supposed to be a highly conducting medium, it is reasonable to assume that the mean value of the electric field $\overrightarrow{\mathcal{E}}$ over the ensemble of waves, vanishes

$$< \overrightarrow{\mathcal{E}} > = \; 0 \;. \tag{2.34}$$

The perturbations $\overrightarrow{\mathcal{H}}_1$ and $\overrightarrow{\mathcal{E}}$ can be thought as a superposition of waves with random continuous phases so that we can use the Fourier expansion

$$\begin{aligned}\overrightarrow{\mathcal{H}}_1 &= \sum_\alpha \int d^3k e^{-i[w^\alpha(\mathbf{k})\mathbf{t}-\mathbf{k}\cdot\mathbf{r}]} \overrightarrow{\mathcal{H}}_1^\alpha(\mathbf{k}) \ , \\ \overrightarrow{\mathcal{E}} &= \sum_\alpha \int d^3k e^{-i[w^\alpha(\mathbf{k})\mathbf{t}-\mathbf{k}\cdot\mathbf{r}]} \overrightarrow{\mathcal{E}}^\alpha(\mathbf{k}) \ , \end{aligned} \tag{2.35}$$

where the summation over α is referred to different types of waves propagating into the plasma. As a consequence of the conditions (2.33) and (2.34) applied to the homogeneous maxwell equation

$$\overrightarrow{\nabla} \times \overrightarrow{\mathcal{E}} = -\frac{1}{c}\frac{\partial \overrightarrow{\mathcal{H}}}{\partial t} \ , \tag{2.36}$$

that, once averaged, leave us with

$$\frac{\partial \overrightarrow{\mathcal{H}}_0}{\partial t} = 0 \ , \tag{2.37}$$

we have

$$\overrightarrow{\nabla} \times \overrightarrow{\mathcal{E}} = -\frac{1}{c}\frac{\partial \overrightarrow{\mathcal{H}}_1}{\partial t} \ . \tag{2.38}$$

This equation, in turn, offers the possibility to express magnetic Fourier coefficients in terms of electric Fourier coefficients through

$$\overrightarrow{\mathcal{H}}_1^\alpha(\mathbf{k}) = \frac{c}{w^\alpha(\mathbf{k})}[\mathbf{k} \times \overrightarrow{\mathcal{E}}^\alpha(\mathbf{k})] \ , \tag{2.39}$$

giving us the chance to eliminate one type of coefficient.

2.4 Approximated Solution for the Slowly Varying Distribution

In order to solve equation (2.28) we want to use a slightly relaxed quasi-linear approximation where f_0 dependence on space and time is not disregarded. The needed requirements are restricted to the smallness of the fluctuating parts f_1 , $\overrightarrow{\mathcal{E}}$ and $\overrightarrow{\mathcal{H}}_1$, if compared with equilibrium values. Our aim is to find a closed differential equation for f_0 where the effects on the slowly varying distribution f_0 due to the perturbations $\overrightarrow{\mathcal{E}}$ and $\overrightarrow{\mathcal{H}}_0$ are taken into account. To this end we look for a solution for f_1 which

satisfies a differential equation that is approximated up to linear terms in f_1 , $\overrightarrow{\mathcal{E}}$ and $\overrightarrow{\mathcal{H}}_1$. Then we will use this first order expression for the fluctuating distribution part, to close a second order averaged differential equation for f_0. We begin by inserting equations (2.29)(2.32) into (2.28)

$$\begin{aligned}\tfrac{\partial(f_0+f_1)}{\partial t} + \left(\dot{\mathbf{x}}\cdot\overrightarrow{\nabla}\right)(f_0+f_1) + Ze\left[\overrightarrow{\mathcal{E}} + \tfrac{\dot{\mathbf{x}}}{c}\times\left(\overrightarrow{\mathcal{H}}_0+\overrightarrow{\mathcal{H}}_1\right)\right]\tfrac{\partial f_0}{\partial \mathbf{p}} + \\ + Ze\left[\tfrac{\dot{\mathbf{x}}}{c}\times\left(\overrightarrow{\mathcal{H}}_0+\overrightarrow{\mathcal{H}}_1\right)\right]\tfrac{\partial f_1}{\partial \mathbf{p}} \;=\; 0\;, \end{aligned} \tag{2.40}$$

then we go on averaging equation (2.40)

$$\frac{\partial f_0}{\partial t} + \left(\dot{\mathbf{x}}\cdot\overrightarrow{\nabla}\right) f_0 + Ze\left(\frac{\dot{\mathbf{x}}}{c}\times\overrightarrow{\mathcal{H}}_0\right)\frac{\partial f_0}{\partial \mathbf{p}} \;=\; -\langle Ze\left(\overrightarrow{\mathcal{E}} + \frac{\dot{\mathbf{x}}}{c}\times\overrightarrow{\mathcal{H}}_1\right)\frac{\partial f_1}{\partial \mathbf{p}}\rangle\;, \tag{2.41}$$

where (2.30), (2.33) and (2.34) have been used.

So far we included second order term in the r.h.s. of the last equation. If we neglect all the quadratic terms in f_1 , $\overrightarrow{\mathcal{E}}$ and $\overrightarrow{\mathcal{H}}_1$, equations (2.40) and (2.41) reduce to

$$\begin{aligned}\tfrac{\partial(f_0+f_1)}{\partial t} + \left(\dot{\mathbf{x}}\cdot\overrightarrow{\nabla}\right)(f_0+f_1) + Ze\left[\overrightarrow{\mathcal{E}} + \tfrac{\dot{\mathbf{x}}}{c}\times\left(\overrightarrow{\mathcal{H}}_0+\overrightarrow{\mathcal{H}}_1\right)\right]\tfrac{\partial f_0}{\partial \mathbf{p}} + \\ + Ze\left(\tfrac{\dot{\mathbf{x}}}{c}\times\overrightarrow{\mathcal{H}}_0\right)\tfrac{\partial f_1}{\partial \mathbf{p}} \;=\; 0\;,\end{aligned}$$

$$\tfrac{\partial f_0}{\partial t} + \left(\dot{\mathbf{x}}\cdot\overrightarrow{\nabla}\right) f_0 + Ze\left(\tfrac{\dot{\mathbf{x}}}{c}\times\overrightarrow{\mathcal{H}}_0\right)\tfrac{\partial f_0}{\partial \mathbf{p}} \;=\; 0\;. \tag{2.42}$$

Subtracting the last equation from the previous one, we obtain

$$\frac{\partial f_1}{\partial t} + \left(\dot{\mathbf{x}}\cdot\overrightarrow{\nabla}\right) f_1 + Ze\left(\frac{\dot{\mathbf{x}}}{c}\times\overrightarrow{\mathcal{H}}_0\right)\frac{\partial f_1}{\partial \mathbf{p}} \;=\; -Ze\left(\overrightarrow{\mathcal{E}} + \frac{\dot{\mathbf{x}}}{c}\times\overrightarrow{\mathcal{H}}_1\right)\frac{\partial f_0}{\partial \mathbf{p}}\;, \tag{2.43}$$

that is a closed equation for f_1. Notice that the same result can be achieved directly, without the subtraction procedure, if we assume that $f_0 = f_0(\mathbf{p})$.

We propose as first order solution of (2.43) the following expression

$$f_1 \;=\; -\int_{-\infty}^{t} dt'\; Ze\left(\overrightarrow{\mathcal{E}} + \frac{\dot{\mathbf{x}}}{c}\times\overrightarrow{\mathcal{H}}_1\right)\frac{\partial f_0}{\partial \mathbf{p}}\;, \tag{2.44}$$

that can be inserted into the the second order differential equation (2.41) that becomes

$$\begin{aligned}&\frac{\partial f_0}{\partial t} + \left(\dot{\mathbf{x}}\cdot\overrightarrow{\nabla}\right) f_0 + Ze\left(\frac{\dot{\mathbf{x}}}{c}\times\overrightarrow{\mathcal{H}}_0\right)\frac{\partial f_0}{\partial \mathbf{p}} \;= \\ &= \langle Ze\left(\overrightarrow{\mathcal{E}} + \frac{\dot{\mathbf{x}}}{c}\times\overrightarrow{\mathcal{H}}_1\right)\frac{\partial}{\partial \mathbf{p}}\int_{-\infty}^{t} dt'\; Ze\left(\overrightarrow{\mathcal{E}} + \frac{\dot{\mathbf{x}}}{c}\times\overrightarrow{\mathcal{H}}_1\right)\frac{\partial f_0}{\partial \mathbf{p}}\rangle\;,\end{aligned} \tag{2.45}$$

which is the searched closed differential equation for f_0.

Now let us introduce cylindrical coordinates $(p_\parallel,\ p_\perp,\ \varphi)$ in the momentum space with

$$\mathbf{p}\cdot\overrightarrow{\mathcal{H}}_0 \ = \ p_\parallel \mathcal{H}_0 \ . \tag{2.46}$$

The time scale

$$\Delta t \sim \omega_H^{-1}\,, \tag{2.47}$$

of the particle motion in a magnetic field is given by the gyrofrequency ω_H associated to the circular motion of a particle of charge Ze induced by the surrounding magnetic field, namely

$$\omega_H \ = \ \frac{ZeHc}{E}\ , \tag{2.48}$$

where E stands for the particle energy

$$E^2 \ = \ p^2c^2 + m^2c^4\ . \tag{2.49}$$

The "weak turbulence approximation" corresponds to the assumption that the time scale (2.47) is much smaller than the time scale associated to the frequency of the random fluctuations of $\vec{\mathcal{E}}$ and $\vec{\mathcal{H}}_1$. As a consequence the field fluctuations have no effect on the circular motion of fast moving particles, allowing a reasonable average over the angle φ so that $f_0(t,\vec{r},\vec{p})$ is replaced by

$$\bar{f}_0(t,\vec{r},p_\parallel,p_\perp) = \frac{1}{2}\int_0^{2\pi} d\varphi < f_0(t,\vec{r},p_\parallel,p_\perp) > \ . \tag{2.50}$$

It can be demonstrated (for more details see [42] and [43] that exploiting the above approximation, equation (2.45) can be reduced to

$$\begin{aligned}
&\frac{\partial \bar{f}_0}{\partial t} + v_\parallel \frac{\partial \bar{f}_0}{\partial z} = \\
&= \pi Z^2 e^2 \sum_\alpha \int d^3k \sum_{s=-\infty}^{\infty} \left\langle \left[\mathcal{E}_\parallel^\alpha J_s \hat{\mathcal{P}}_\parallel^\alpha + \mathcal{E}_\perp^\alpha \hat{\mathcal{P}}_\perp^\alpha + \frac{\mathcal{E}_\perp^\alpha}{p_\perp}\left(1 - \frac{k_\parallel v_\parallel}{\omega^\alpha(\mathbf{k})}\right) - \frac{\mathcal{E}_\parallel^\alpha}{p_\perp}\frac{v_\parallel}{v_\perp}\frac{s\,\omega_H}{\omega^\alpha(\mathbf{k})} J_s \right]^\star \cdot \right. \\
&\qquad \left. \cdot \left[\mathcal{E}_\parallel^\alpha J_s \hat{\mathcal{P}}_\parallel^\alpha + \mathcal{E}_\parallel^\alpha \hat{\mathcal{P}}_\perp^\alpha \right] \cdot \delta\left(\omega^\alpha(\mathbf{k}) - k_\parallel v_\parallel - s\,\omega_H\right) \right\rangle \bar{f}_0\,,
\end{aligned} \tag{2.51}$$

where

$$\hat{\mathcal{P}}^{\alpha}_{\parallel} = \frac{\partial}{\partial p_{\parallel}} - \frac{s\,\omega_H}{\omega^{\alpha}(\mathbf{k})}\frac{1}{v_{\perp}}\left(v_{\perp}\frac{\partial}{\partial p_{\parallel}} - v_{\parallel}\frac{\partial}{\partial p_{\perp}}\right), \tag{2.52}$$

$$\hat{\mathcal{P}}^{\alpha}_{\perp} = \frac{\partial}{\partial p_{\perp}} + \frac{k_{\parallel}}{w^{\alpha}(\mathbf{k})}\left(v_{\perp}\frac{\partial}{\partial p_{\parallel}} - v_{\parallel}\frac{\partial}{\partial p_{\perp}}\right), \tag{2.53}$$

$$\mathcal{E}^{\alpha}_{\perp} = \frac{1}{2}\left(\mathcal{E}^{\alpha}_{R}(\mathbf{k})e^{i\psi}J_{s+1} + \mathcal{E}^{\alpha}_{L}(\mathbf{k})e^{-i\psi}J_{s-1}\right), \tag{2.54}$$

$$\mathcal{E}^{\alpha}_{L,R}(\mathbf{k}) = \mathcal{E}^{\alpha}_{x}(\mathbf{k}) \pm \mathcal{E}^{\alpha}_{y}(\mathbf{k}), \tag{2.55}$$

$$\mathcal{E}^{\alpha}_{\parallel}(\mathbf{k}) = \mathcal{E}^{\alpha}_{z}(\mathbf{k}), \tag{2.56}$$

with the last being the component of $\vec{\mathcal{E}}^{\alpha}$ projected along $\mathcal{H}_0$, ψ the azimutal angle of the wave vector and $J_s(k_{\perp}v_{\perp}/\omega_H)$ the Bessel function of order s. The appearance of the δ-function in (2.51) introduce the resonance character of the particle-wave interaction that is realized by the condition

$$\omega^{\alpha}(\mathbf{k}) = k_{\parallel}v_{\parallel} + s\,\omega_H, \quad s \in \mathbb{Z} \tag{2.57}$$

where the $k_{\parallel}v_{\parallel}$ term takes into account the Doppler effect while $s\,\omega_H$ stands for the cyclotron rotation in the magnetic field $\mathcal{H}_0$.

In order to simplify the propagation equation (2.51) we focus our attention on the effective scattering frequency and wave typology that mostly interact with particles in the interstellar medium. To this end let us introduce the Larmor radius $r_H = v/|\omega_H|$ that is the curvature induced by the magnetic field $\mathcal{H}_0$. The comparison between the Larmor radius and the wavelenght tells us if the wave is seen by the particle. If this is the case then the particle is said to be magnetized. More precisely we have two limiting cases

- magnetized particle: $k_{\perp}v_{\perp}/\omega_H \ll 1 \quad \Rightarrow \quad$ the armonics involved are

  1. $s = 0 \quad$ for $\quad \vec{\mathcal{E}}^{\alpha}_{\parallel} \neq 0 \quad \Rightarrow \quad \omega^{\alpha} = k_{\parallel}v_{\parallel}$;
  2. $s = \pm 1 \quad$ for $\quad \mathcal{E}^{\alpha}_{\perp} \neq 0 \quad \Rightarrow \quad \omega^{\alpha}(\vec{k}) = k_{\parallel}v_{\parallel} \pm \omega_H$;

- unmagnetized particle: $k_{\perp}v_{\perp}/\omega_H \gg 1 \quad \Rightarrow \quad$ the armonics involved are

  $s \sim k_{\perp}v_{\perp}/\omega_H \quad \Rightarrow \quad \omega^{\alpha}(\vec{k}) - k_{\parallel}v\| - s\omega_H \sim \omega^{\alpha}(\vec{k}) - \vec{k}\cdot\vec{v} = 0.$

In this last case, where we consider short magnetized waves since $\lambda \ll 2\pi r_H$, the effective scattering rate of ultrarelatistic particles has an energy dependence E^{-2} that is ruled out by the weak energy dependence observed for the escape time

$$T \propto E^{-\mu},\ \mu = 0.3 - 0.7\,. \tag{2.58}$$

In the case when $\lambda \sim 2\pi r_H$, each kind of spectrum determines a different energy dependence of the effective scattering rate so that we are forced to consider separately different kind of waves.

We restrict ourselves to the case when

$$v_s \ll v_A\,, \tag{2.59}$$

where

$$v_s = \sqrt{\frac{K\,T_e}{m}}\,, \tag{2.60}$$

is the velocity of sound in the medium with T_e being the temperature of thermal electrons and

$$v_A = \frac{\mathcal{H}_0}{\sqrt{4\pi\rho}}\,, \tag{2.61}$$

is the Alfvén velocity, with ρ indicating the density of the medium. With this assumption there are only two type of oscillation that are left in the magnetohydrodynamic region ($\omega \ll \omega_H$):

- Alfvén waves identified by the dispersion relation

$$\omega^\alpha(\vec{k}) = \pm|k_\parallel| v_A\,, \tag{2.62}$$

  and by the following properties

$$\begin{aligned} &v \perp (\vec{k}, \vec{\mathcal{H}}_0) \\ &\vec{\mathcal{E}} \in (\vec{k}, \mathcal{H}_0)\,, \end{aligned} \tag{2.63}$$

  where $(\vec{k}, \vec{\mathcal{H}}_0)$ is the plane identified by $\vec{k}$ and $\vec{\mathcal{H}}_0$;

- magnetosonic waves with dispersion relation

$$\omega^\alpha(\vec{k}) = \pm k\, v_A\,, \tag{2.64}$$

and

$$\begin{aligned} & v \in (\vec{k}, \vec{\mathcal{H}}_0) \\ & \vec{\mathcal{E}} \perp (\vec{k}, \mathcal{H}_0)\,, \end{aligned} \tag{2.65}$$

that is transverse to the previous and with opposite circular polarization while propagating along the magnetic field.

Since for $k_b ot \neq 0$ the magnetohydrodynamic waves are strongly damped, we restrict ourselves to the case where the waves propagate along the regular magnetic field $\mathcal{H}_0$, so that $k = k_\parallel$, $\mathcal{E}_\perp \neq 0$ and the resonance condition 2.57 reduces to

$$k_\parallel = \pm \frac{\omega_H}{\omega^\alpha(\mathbf{k})/k_\parallel - v\cos\theta} \approx \pm \frac{Ze\mathcal{H}_0}{p\,c\,(\omega^\alpha(\mathbf{k})/kv - \mu)}\,, \tag{2.66}$$

where in the last step we exploited the relativistic approximation $E \sim p\,c$ and $v \sim c$; here $\mu = \cos\theta$, θ is the angle between $\vec{p}$ and $\vec{\mathcal{H}}_0$ (so that $v_\parallel = v\cos\theta = v\mu$), and we solved with respect to $k_\parallel$ thinking that $\omega^\alpha(\mathbf{k}_\parallel)/k = v_A$ is independent of k. With all the above approximation taken into account, equation (2.51) becomes

$$\begin{aligned} \frac{\partial \bar{f}_0}{\partial t} + \mu\, v \frac{\partial \bar{f}_0}{\partial z} &= \pi^2 Z^2 e^2 \sum_\alpha \left(\frac{\omega^\alpha(\mathbf{k})}{k\,c}\right)^2 \frac{1}{p^2} \left(\frac{\partial}{\partial p} + \frac{\partial}{\partial \mu}\left(\frac{k_{res} v}{\omega^\alpha(k_{res})} - \mu\right)\right) \times \\ &\times \frac{p(1-\mu^2) W^\alpha(k_{res})}{|v\mu - \omega^\alpha(k_{res})/k|} \left(\frac{\partial}{\partial p} + \left(\frac{k_{res} v}{\omega^\alpha(k_{res})} - \mu\right) \frac{1}{p} \frac{\partial}{\partial \mu}\right) \bar{f}_0\,, \end{aligned} \tag{2.67}$$

where the following variable replacement has been performed

$$(p_\parallel,\, p_\perp) \;\rightarrow\; (p = |\vec{p}|,\, \mu) \;\Rightarrow\; \bar{f}_0(t,\, \vec{r},\, p_\parallel,\, p_\perp) \;\rightarrow\; \bar{f}_0(t,\, \vec{r},\, p,\, \mu)\,, \tag{2.68}$$

and we used

$$k_{res} = \left|\frac{Z\,e\,\mathcal{H}_0}{p\,c\,\mu}\right| = \frac{1}{r_H\,|\mu|}\,, \tag{2.69}$$

together with the energy density of waves of type α, namely $W^\alpha(k)$, assumed to be not dependent on phase and polarization. Let us notice that the energy of the waves that we considered is equally parted between the kinetic energy of the particles of the medium and magnetic field energy

$$\int_0^\infty dk_\parallel\, W^\alpha(k_\parallel) = \frac{1}{4\pi} \int_{-\infty}^\infty dk_\parallel \left|\vec{\mathcal{H}}_1^\alpha(k_\parallel)\right|^2\,, \tag{2.70}$$

in virtue of the approximation $v_A \ll v$.

2.5 Diffusion Approximation

As suggested by the term that mostly contribute to (2.67), the effective scattering rate can be defined by

$$\begin{aligned}\nu_\mu^\alpha &:= 2\pi^2|\omega_H|\frac{k_{res}W^\alpha(k_{res})}{\mathcal{H}_0^2}\left(1-\frac{\omega^\alpha(k_{res})}{k_{res}v}\mu\right)^2 \\ &\approx 2\pi^2|\omega_H|\frac{k_{res}W^\alpha(k_{res})}{\mathcal{H}_0^2}\,,\end{aligned} \tag{2.71}$$

from which we can get the relaxation time needed to estabilish isotropy for the α-type wave

$$\tau_{rel} := (\nu_\mu^\alpha)^{-1} \approx \frac{1}{2\pi^2|\omega_H|}\frac{\mathcal{H}_0^2}{k_{res}W^\alpha(k_{res})}\,. \tag{2.72}$$

Accordingly the relaxation length is defined as $\lambda_{rel} := v\,(\nu_\mu^\alpha)^{-1}$. The approximation of weak turbulence $\nu_\mu^\alpha \ll |\omega_H|$ that we assumed, now acquire the explicit form

$$W^\alpha(k_{res}) \ll \frac{\mathcal{H}_0^2}{2\pi^2 k_{res}}\,. \tag{2.73}$$

In order to further simplify the propagation equation (2.67), we divide the contribution of the waves propagating along and opposite to the field $\vec{\mathcal{H}}_0$ by defining the scattering rates

$$\nu_\mu^\pm :\approx 2\pi^2|\omega_H|\frac{k_{res}W^\pm(k_{res})}{\mathcal{H}_0^2}\,, \tag{2.74}$$

where $W^\pm(k)$ are the spectral energies associated to the two propagation directions; by introducing these rates we are left with

$$\begin{aligned}\frac{\partial\bar{f}_0}{\partial t}+\mu\,v\frac{\partial\bar{f}_0}{\partial z} &= \frac{v_A^2}{p^2}\left(\frac{\partial}{\partial p}p+\frac{v}{v_A}\frac{\partial}{\partial\mu}\right)\frac{1-\mu^2}{2}\nu_\mu^+\frac{p^3}{v^2}\left(\frac{\partial}{\partial p}+\frac{v}{v_A}\frac{1}{p}\frac{\partial}{\partial\mu}\right)\bar{f}_0 + \\ &+ \frac{v_A^2}{p^2}\left(\frac{\partial}{\partial p}p-\frac{v}{v_A}\frac{\partial}{\partial\mu}\right)\frac{1-\mu^2}{2}\nu_\mu^-\frac{p^3}{v^2}\left(\frac{\partial}{\partial p}-\frac{v}{v_A}\frac{1}{p}\frac{\partial}{\partial\mu}\right)\bar{f}_0\,,\end{aligned} \tag{2.75}$$

where we exploited again the approximation $|\omega^\alpha(k)/k\,v| = v_A/v \ll 1$. Let us notice that equation (2.67) tells us that the scattering changes rapidly the angle but slowly the energy of the particles. This is a consequence of the large value of the factor

$$\left|\frac{k_{res}v}{\omega^\alpha(k_{res})}-\mu\right| \approx \frac{v}{v_A} \gg 1\,, \tag{2.76}$$

that weights the $\partial/\partial\mu$ term. Therefore, if the anisotropic part of the distribution is large enough to satisfy the condition

$$\bar{f}_0 - \hat{f}_0 \gg \hat{f}_0 \frac{v_A}{v}\,, \tag{2.77}$$

where $\hat{f}_0$ is the mean value of $\bar{f}_0$ over the angles

$$\hat{f}_0 = \frac{1}{2}\int_{-1}^{1} d\mu\, \bar{f}_0\,, \tag{2.78}$$

then it is reasonable to neglect the energy change of the particle in favor of the angular diffusion. In other words if the time intervals considered are large enough, then the distribution can be assumed almost isotropic. Since in the following we want to move to the diffusion approximation framework, namely we consider time intervals and distances such that

$$\Delta t \gg \tau_{rel}\,, \quad \Delta x \gg \lambda_{rel}\,, \tag{2.79}$$

respectively, the expansion

$$\bar{f}_0 = \hat{f}_0 + \delta f(\mu)\,, \quad \delta f(\mu) \ll \hat{f}_0\,, \tag{2.80}$$

is justified. At this point we proceed by substituting (2.80) in (2.75), keeping only the leading terms (remember that $\delta f \ll \hat{f}_0$)

$$\mu\, v \frac{\partial \hat{f}_0}{\partial z} = \frac{1}{p^2}\frac{\partial}{\partial \mu}\frac{v_A}{v}\frac{1-\mu^2}{2}\left(\nu_\mu^+ - \nu_\mu^-\right) p^3 \frac{\partial \hat{f}_0}{\partial p} + \frac{\partial}{\partial \mu}\frac{1-\mu^2}{2}\left(\nu_\mu^+ + \nu_\mu^-\right)\frac{\partial}{\partial \mu}\delta f\,, \tag{2.81}$$

and we go on averaging over μ to get

$$\frac{\partial}{\partial \mu}\delta f = -\frac{v}{\nu_\mu^+ + \nu_\mu^-}\frac{\partial \hat{f}_0}{\partial z} - \frac{v_A}{v}\frac{\nu_\mu^+ - \nu_\mu^-}{\nu_\mu^+ + \nu_\mu^-} p \frac{\partial \hat{f}_0}{\partial p}\,, \tag{2.82}$$

which allows to express δf in terms of $\hat{f}_0$. Turning back to (2.75), we insert (2.80) and perform an average over μ to obtain

$$\begin{aligned}\frac{\partial \bar{f}_0}{\partial t} + \frac{v}{2}\int_{-1}^{1} d\mu\, \mu \frac{\partial \delta f}{\partial z} &= \frac{v_A^2}{p^2}\frac{\partial}{\partial p}\int_{-1}^{1} d\mu \frac{1-\mu^2}{2}\left(\nu_\mu^+ + \nu_\mu^-\right)\frac{p^4}{v^2}\frac{\partial \hat{f}_0}{\partial p} \\ &+ \frac{v_A}{p^2}\frac{\partial}{\partial p} p \int_{-1}^{1} d\mu \frac{1-\mu^2}{4}\left(\nu_\mu^+ - \nu_\mu^-\right)\frac{p^2}{v}\frac{\partial \delta f}{\partial \mu}\,;\end{aligned} \tag{2.83}$$

by recasting the second term of the left-hand side as follows

$$\frac{v}{2}\int_{-1}^{1} d\mu\,\mu\,\frac{\partial \delta f}{\partial z} = \frac{v}{2}\frac{\partial}{\partial z}\int_{-1}^{1} d\mu\,\frac{1-\mu^2}{2}\,\frac{\partial \delta f}{\partial \mu}\,, \tag{2.84}$$

and using the δf expression that can be derived from (2.82), we end with

$$\frac{\partial \hat{f}_0}{\partial t} - \frac{\partial}{\partial z}D_{zz}\frac{\partial \hat{f}_0}{\partial z} + \frac{1}{3p^2}\frac{\partial (p^3 u_w)}{\partial p}\frac{\partial \hat{f}_0}{\partial z} - \frac{\partial u_w}{\partial z}\frac{p}{3}\frac{\partial \hat{f}_0}{\partial p} = \frac{1}{p^2}\frac{\partial}{\partial p}p^2 D_{pp}\frac{\partial \hat{f}_0}{\partial p}\,, \tag{2.85}$$

where we defined the effective velocity of the convective particle transport by the waves

$$u_w := v_A \int_0^1 d\mu \frac{3(1-\mu^2)}{2}\frac{\nu_\mu^+ - \nu_\mu^-}{\nu_\mu^+ + \nu_\mu^-}\,, \tag{2.86}$$

the spatial diffusion coefficient along the regular field $\vec{\mathcal{H}}_0$

$$D_{zz} = \frac{v^2}{2}\int_0^1 d\mu \frac{1-\mu^2}{\nu_\mu^+ + \nu_\mu^-}\,, \tag{2.87}$$

and the momentum diffusion coefficient that enters in the stochastic acceleration term

$$D_{pp} = p^2 (v_A/v)^2 \int_0^1 d\mu 2(1-\mu^2)\frac{\nu_\mu^+ \nu_\mu^-}{\nu_\mu^+ + \nu_\mu^-}\,. \tag{2.88}$$

The particle flux can be written as

$$J_z = \frac{v}{2}\int_{-1}^{1} d\mu\,\mu\,\delta f = -D_{zz}\frac{\partial \hat{f}_0}{\partial z} - \frac{u_w}{3}p\frac{\partial \hat{f}_0}{\partial p}\,, \tag{2.89}$$

with the contribution of a diffusion and a convective term. To finish this paragraph, let us underline two particular but still relevant cases that greatly simplify equation (2.85)

- if the energy density propagating in opposite directions is the same, then $\nu_\mu^+ = \nu_\mu^-$ so that the convection velocity (2.86) vanishes;

- if the energy density propagates only in one direction, then the diffusion in momentum space disappears since the coefficient in (2.88) vanishes.

2.6 Large-Scale Motion of the Medium

So far we restricted ourselves to the case where the medium in which waves propagate is at rest. Now we want to include a medium that is moving with a velocity $\vec{u}(\vec{r}) \ll v$ whose variation scale is much larger than the mean path length of the particles. It turns out that the large-scale motion of the medium can be easily introduced in equation (2.85) provided that the replacements

$$u_w \to u_z + u_w\,, \quad \omega^\alpha(k) \to \omega^\alpha(k) + k\,u_z\,, \tag{2.90}$$

are performed, where the velocity of the medium along the regular field is assumed to be

$$\vec{u} = \frac{\vec{\mathcal{H}}_0}{|\vec{\mathcal{H}}_0|} u_z\,. \tag{2.91}$$

This can be seen by transforming the fields associated with the waves propagating in the medium, from the reference system, moving with velocity u_z, to the system at rest. If this transformation is applied to the starting kinetic equation (2.28), then we realize that, up to terms of order v_A/c and u/c, the magnetic field does not change while the electric field becomes

$$\vec{\mathcal{E}}^\alpha = -\frac{1}{c}\left(\frac{\omega^\alpha(k)}{k} + u_z\right)\left(\frac{\vec{\mathcal{H}}_0}{|\vec{\mathcal{H}}_0|} \times \vec{\mathcal{H}}_1^\alpha\right)\,, \tag{2.92}$$

from which we deduce (2.90). The steps that we followed until equation (2.85), are still working and in conclusion we have

$$\frac{\partial \hat{f}_0}{\partial t} - \frac{\partial}{\partial z} D_{zz} \frac{\partial \hat{f}_0}{\partial z} + \frac{1}{3p^2}\frac{\partial [p^3(u_z+u_w)]}{\partial p}\frac{\partial \hat{f}_0}{\partial z} - \frac{\partial (u_z+u_w)}{\partial z}\frac{p}{3}\frac{\partial \hat{f}_0}{\partial p} = \frac{1}{p^2}\frac{\partial}{\partial p} p^2 D_{pp} \frac{\partial \hat{f}_0}{\partial p}\,. \tag{2.93}$$

Accordingly the particle flux is replaced by

$$J_z = -D_{zz}\frac{\partial \hat{f}_0}{\partial z} - \frac{u_z + u_w}{3} p \frac{\partial \hat{f}_0}{\partial p}\,. \tag{2.94}$$

In addition to the motion of the medium along the field, there could be a component of the velocity which is ortogonal to the field, usually called drift component. This is generated by spatial inhomogeneities of the system, by gravitational forces or by the action of the electric field $\vec{\mathcal{E}}_0 \perp \vec{\mathcal{H}}_0$. We consider the case of drift

$$\vec{u}_\perp = c\frac{\vec{\mathcal{E}}_0 \times \vec{\mathcal{H}}_0}{|\vec{\mathcal{H}}_0|^2}\,, \tag{2.95}$$

that is generated only by the slowly changing electric field ($u_\perp \ll v$)

$$\vec{\mathcal{E}}_0 = \frac{1}{c}\left(\vec{\mathcal{H}}_0 \times \vec{u}_\perp\right) , \tag{2.96}$$

which does not contribute to the particles scattering. The electric field due to drift (2.96) has to be added to (2.92). In order to introduce the renewed $\vec{\mathcal{E}}_0$ field, we recall equation (2.45) that has to be modified as follows

$$\begin{aligned} \frac{\partial \tilde{f}_0}{\partial t} &+ \left(\vec{v}\cdot\vec{\nabla}\right)\tilde{f}_0 + \frac{Ze}{c}\left[(\vec{v}-\vec{u}_\perp)\times\vec{\mathcal{H}}_0\right]\frac{\partial \tilde{f}_0}{\partial \mathbf{p}} - \\ &- \langle Ze\left(\overrightarrow{\mathcal{E}} + \frac{\vec{v}}{c}\times\vec{\mathcal{H}}_1\right)\frac{\partial}{\partial \mathbf{p}}\int_{-\infty}^{t} dt'\; Ze\left(\vec{\mathcal{E}} + \frac{\vec{v}}{c}\times\vec{\mathcal{H}}_1\right)\frac{\partial \tilde{f}_0}{\partial \mathbf{p}}\rangle . \end{aligned} \tag{2.97}$$

The newly added term is proportional to $u_\perp$ that is assumed to be much smaller than v. This suggests the expansion

$$\tilde{f}_0 = f_0 + \triangle f , \tag{2.98}$$

where f_0 is the solution of equation (2.45) while $\triangle f$ has to be understood as a small variation induced by the presence of the drifting. Substituting (2.98) in (2.97) and keeping only leading terms, we get

$$\frac{Ze}{c}\left(\vec{v}\times\vec{\mathcal{H}}_0\right)\frac{\partial \triangle f}{\partial \mathbf{p}} - \frac{Ze}{c}\left(\vec{u}_\perp\times\vec{\mathcal{H}}_0\right)\frac{\partial f_0}{\partial \mathbf{p}} , \tag{2.99}$$

solved by

$$\triangle f = -\frac{\mathbf{u}_\perp\cdot\mathbf{p}}{v}\frac{\partial f_0}{\partial \mathbf{p}} . \tag{2.100}$$

The diffusion approximation can be applied through

$$\tilde{f}_0 = f_0 + \delta f + \triangle f , \tag{2.101}$$

whose net effect on the propagation equation (2.97) is to introduce tensorial quantities

$$\frac{\partial f_0}{\partial t} - \nabla_i D_{ij}\nabla_j f_0 + \frac{1}{3p^2}\frac{\partial[p^3(\vec{u}+\vec{u}_w)]}{\partial p}\cdot(\nabla f_0) - \frac{p}{3}\nabla\cdot(\vec{u}+\vec{u}_w)\frac{\partial f_0}{\partial p} = \frac{1}{p^2}\frac{\partial}{\partial p}p^2 D_{pp}\frac{\partial f_0}{\partial p} , \tag{2.102}$$

where

$$D_{ij} = D_\parallel h_i h_j \quad \vec{u}_w = u_w\vec{h} , \quad \vec{h} = \frac{\vec{\mathcal{H}}_0}{|\vec{\mathcal{H}}_0|} , \tag{2.103}$$

with $D_{\parallel} = D_{zz}$. Finally if the magnetohydrodinamic waves equally propagate in both directions, we have ($\vec{u}_w = 0$ and $\partial\vec{u}/\partial p = 0$)

$$\frac{\partial f_0}{\partial t} - \nabla_i D_{ij} \nabla_j f_0 + (\vec{u} \cdot \nabla) f_0 - \frac{p}{3} \nabla \cdot \vec{u} \frac{\partial f_0}{\partial p} = \frac{1}{p^2} \frac{\partial}{\partial p} p^2 D_{pp} \frac{\partial f_0}{\partial p} \,, \tag{2.104}$$

which is the propagation equation we are searching for.

2.7 Solar Modulation

When a cosmic ray approach the solar system it undergoes the effect of the solar wind which lower the cosmic ray flux below $10 - 20$ GeV. The propagation equation (2.104) can be applied as well to the solar system interplanetary space provided that some specific approximations are taken into account. First of all spherical symmetry can be assumed so that after the introduction of spherical coordinates in (2.104), only the radial component of the diffusion tensor is left. Moreover reacceleration is absent and the solar wind is radially directed to the outer space. At the end we are left with

$$\frac{\partial f}{\partial t} - \frac{1}{r^2} \frac{\partial}{\partial r} \left(r^2 D_{rr} \frac{\partial}{\partial r} f \right) + u_r \frac{\partial f}{\partial r} - \frac{1}{r^2} \frac{\partial}{\partial r} \left(r^2 u_r \right) \frac{p}{3} \frac{\partial f}{\partial p} = 0 \,. \tag{2.105}$$

Gleeson and Axford ([44]) showed that it is possible to solve analytically the differential equation (2.105) under a number of reasonable assumption. We start by saying that the diffusion coefficient and convective velocity can be assumed to be spatially constants. Next we consider the steady-state case where $\partial f/\partial t = 0$. Now equation (2.105) can be written as

$$D_{rr} \frac{\partial^2 f}{\partial r^2} + \frac{2 D_{rr}}{r} \frac{\partial f}{\partial r} - u_r \frac{\partial f}{\partial r} + \frac{2\, u_r\, p}{3r} \frac{\partial f}{\partial p} = 0 \,. \tag{2.106}$$

To further simplify the propagation equation (2.106), we estimate the importance of the first three terms by considering a simple diffusion case where the inward diffusion flux is balanced by the outward convection flux

$$D_{rr} \frac{\partial f}{\partial r} = u_r f \,, \tag{2.107}$$

so that in this zero approximation case the cosmic rays density is given by

$$f = F_0 \cdot \exp^{\frac{u_r}{D_{rr}} r} \,. \tag{2.108}$$

Substituting (2.108) in (2.106) we realize that the first three terms are of order $\frac{u_r^2}{D_{rr}}f$, $\frac{2\,u_r}{r}f$ and $\frac{u_r^2}{D_{rr}}f$, respectively. We conclude that we have to compare u_r/D_{rr} with $2/r$ associated respectively to first-third terms and second term. Roughly speaking, for diffusion we have $D_{rr} = \frac{1}{3}\lambda\, v$, with v velocity of the particle; therefore the comparison is between u_r/v and λ/r but remember that we assumed $u_r/v \ll 1$ during the derivation of the propagation equation. From a quantitative point of view we can say that for 1 GeV protons we have $\lambda \approx 1\,AU$ and $v \approx c$, so

$$\frac{u_r}{c} \approx 1.3 \cdot 10^{-3} \ll \frac{\lambda}{r} \approx 0.1 - 10\,. \tag{2.109}$$

The considerations above lead to the force-field approximation that neglect the first and third term in (2.106) to end with

$$\frac{\partial f}{\partial r} + \frac{u_r\, p}{3\, D_{rr}}\frac{\partial f}{\partial p} = 0\,. \tag{2.110}$$

Notice that this approximation holds for energies above few hundreds MeV but the effect became negligible at 10-20 GeV, as will be cleared in the following. At this point we focus on a particular aspect which is the variation of energy of the flux of cosmic rays travelling from the heliosphere boundary to the earth. Since we excluded all the effect that modify the particle density, we can consider curves identified by constant f, namely curves defined by $df/dr = 0$. In other words we have to solve the system

$$\begin{cases} \frac{df}{dr} = \frac{\partial f}{\partial r} + \frac{dp}{dr}\frac{\partial f}{\partial p} = 0 \\ \frac{\partial f}{\partial r} + \frac{u_r\, p}{3\, D_{rr}}\frac{\partial f}{\partial p} = 0 \end{cases}\,, \tag{2.111}$$

which gives us

$$\frac{dp}{dr} = \frac{u_r\, p}{3\, D_{rr}}\,. \tag{2.112}$$

In order to make manifest the dependence of the diffusion coefficient we can decide to work in the quasi-linear theory, so that D_{rr} becames coordinate independent

$$D_{zz} = D_0 \cdot \beta p\,, \tag{2.113}$$

that can be inserted in (2.112) to give

$$\beta\, dp = \frac{u_r}{3\, D_0} dr\,. \tag{2.114}$$

The last step is the introduction of the relativistic energy $dE = \beta \cdot dp$ in (2.114)

$$dE = \frac{u_r}{3D_0} dr \,, \tag{2.115}$$

that brings us to the final very simple solution

$$E_{ISM} - E(r) = T_{ISM} - T(r) = \Phi \frac{R_{ISM} - r}{R_{ISM} - 1} \,, \tag{2.116}$$

where $T(r)$ is the kinetic energy, the subscript ISM stands for the distance between the earth and the interstellar medium and the factor $(R - 1)$ has been introduced to give to the modulation strength

$$\Phi = \frac{u_r (R_{ISM} - 1)}{3D_0} \,, \tag{2.117}$$

the meaning of the loss of energy from the outer limit to 1 AU as can be seen by setting $r = 1$ AU

$$\Phi = T_{ISM} - T(1\,AU) \,. \tag{2.118}$$

Let us point that the units that we are using are MeV for the energy, AU for the distance and consequently MV for the modulation strength. The equation (2.117) is widely used because of its simplicity in calculating the spectrum of particles at the earth orbit. On the other hand, one can argue that it is rather simplistic to enclose the solar modulation problem in one single parameter Φ.

Chapter 3

The GALPROP Model

Concerning the software used to produce cosmic rays fluxes, our choice fell on the GALPROP [1] model. Among the reason for this choice we have

- the code that comes with the GALPROP model (hereafter GALPROP) is public so that without asking or paying anything, everyone is able to check or reproduce our results
- it is the most physical approach since a real propagation environment and all the known effects (up to human knowledge) are included
- it has been demonstrated that this code is able to reproduce simultaneously almost all the data from space missions.

3.1 The Galaxy

The fundamentals of any cosmic ray model reside in the assumptions that we make on the properties of our galaxy. To have a complete description we take advantage of different fields of astronomy and astrophysics. In this section we will try to give an exhaustive description of the galactic frame in GALPROP model focusing on the parameters that in our work are fixed but in the literature are sometimes different from ours.

[1] GALPROP model is available at http://galprop.stanford.edu/na_home.html

3.1.1 Geometry of the Galaxy

GALPROP is designed to treat both two and three spatial dimensional models. We chose the first option where a cylindrical symmetry is assumed as, for instance, in [40]). In this framework the galaxy is considered as a denser central disk of thickness $2h$ where h is assumed to be $100\,pc$, surrounded by a cylindrical halo where cosmic rays are still trapped by the galactic magnetic field. In the central disk are located the sources and it is the only place where interactions with matter take place. The half height of the halo is one of the most important parameter defined by the user, usually running in an interval from few Kpc to $\sim 20 Kpc$ as suggested by previous studies on radioactive nuclei [45] and distribution of synchrotron radiation [46]. The radial extension of the halo is fixed to $30 Kpc$ (other models use $20\,Kpc$). Beyond the halo cylindrical box, free escape of cosmic rays is assumed while inside diffusion and reacceleration are supposed to work. The solar system is located at $8.5\,Kpc$ from the center of the galaxy even if a distance of $8\,Kpc$ comes from [47] and [48].

3.1.2 Supernovae Distribution in the Galaxy

In section 1.1 we argued that supernovae may be a reasonable source of cosmic rays. Therefore in GALPROP particular attention is dedicated to the supernovae distribution inside the thin disk that is tuned to agree with EGRET gamma-ray data [49]. The best distribution parameterization turns out to be

$$q(r,z) = q_0 \left(\frac{r}{R_\odot}\right)^\eta e^{-\xi \frac{r-R_\odot}{R_\odot} - \frac{|z|}{0.2\ \mathrm{kpc}}} \delta(r - R_{max}) \ , \tag{3.1}$$

where q_0 is a normalization constant and η, ξ and R_{max} are parameters. We see that there is a exponential decrease along the galaxy height modulated by 0.2 kpc factor to take into account the confinement of sources to the disk. A cutoff at R_{max} is inserted via a delta function. Such an r dependence has been already considered for supernovae remnants in [50] but we fix different parameter values, namely $\eta = 0.5$, $\xi = 1$ and $R_{max} = 20$ kpc. The galactocentric position of the sun $R_\odot$ is fixed at 8.5 kpc as stated above. In GALPROP is offered the possibility of introducing point-like supernovae but we did not consider this option. In addition to the position, the supernovae occurrence has to be specified. Following what we said in section 1.1, we assumed to have a supernova event every 10^4 yr inside a volume of a cubic kpc. Moreover the supernovae

remnants cosmic ray acceleration is assumed to work for 10^4 yr. This means that we have at least one cosmic ray acceleration site every cubic kpc at any time. Let us mention that in [51] has been suggested that considerable amount of C and O is accelerated in C- and O- enriched pre-supernovae Wolf-Rayet wind material but this do not affect our source model since the origine sites still coincide with supernovae remnants.

3.1.3 Gas Distribution in the Galaxy

The most important component of the interstellar medium gas is hydrogen followed by helium. The hydrogen is present in the medium in three possible forms: atomic hydrogen HI, molecular hydrogen H_2 and ionized hydrogen HII. A good fit to the

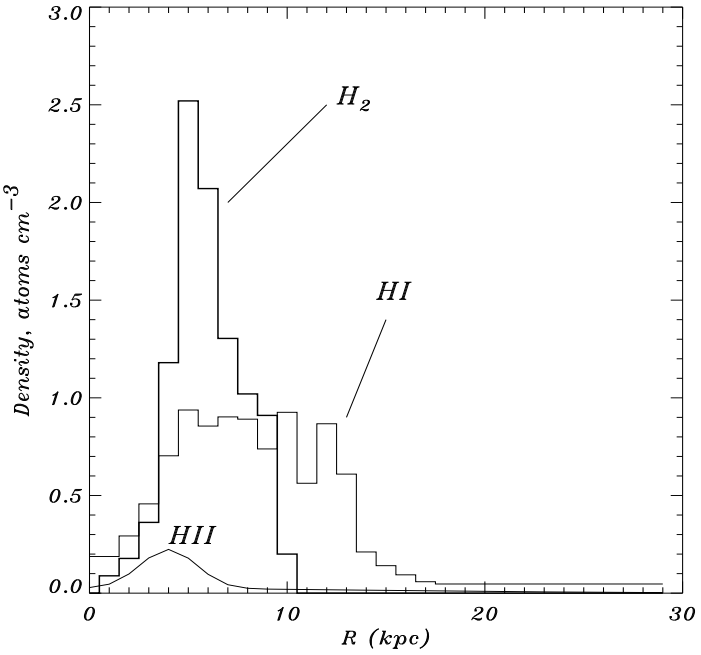

Figure 3.1: A schematic profile of the radial dependence of the three components of hydrogen as a function of the radius at $z = 0$ from [55].

atomic hydrogen distribution is parameterized as an exponentially decreasing function of the halo height and can be represented by

$$n_{HI}(r, z) = n_{HI}(r) e^{-(\ln 2)(z/z_0(r))}\,, \tag{3.2}$$

where $n_{HI}(r)$ is taken from [52] and represented in figure 3.1 while $z_0(r)$ has the form proposed in [53], namely

$$z_0(r) = \begin{cases} 0.25 \text{ kpc}, & r \leq 10 \text{ kpc} \\ 0.083\, e^{0.11\, r} \text{ kpc}, & r > 10 \text{ kpc}. \end{cases} \tag{3.3}$$

with a breaking at the galactocentric radius approximately equal to the one of the solar system. Concerning the molecular hydrogen, the distribution can be found using CO surveys as in [54]

$$n_{H_2}(r, z) = n_{H_2}(r)\, e^{-\ln 2 \cdot (z/70 \text{ pc})^2}\,, \tag{3.4}$$

where the radial dependence $n_{H_2}(r)$ is again reported in figure 3.1. For the last component we consider a first term which represents extensive warm ionized gas (similar to the distribution given by [56]) added to a second component that take into account the concentration around $r = 4$ kpc. Thus we have the following parameterization taken from [57]

$$n_{HII}(r, z) = 0.025\, e^{-\frac{|z|}{1 \text{ kpc}} - \left(\frac{r}{20 \text{ kpc}}\right)^2} + 0.2\, e^{-\frac{|z|}{0.15 \text{ kpc}} - \left(\frac{r}{2 \text{ kpc}} - 2\right)^2} \text{ cm}^{-3}\,. \tag{3.5}$$

Going back to equation (1.39) that describes Coulomb energy losses we have to say that in order to compute such losses we fixed the temperature of the electrons (that enters in (1.39) through x_m) at $T_e = 10^4$. Finally the helium distribution in interstellar medium has been determined exploiting photospheric methods in [58]. It turns out that the helium follows the hydrogen distribution with a factor $He/H = 0.10 \pm 0.08$. Our choice fell on the value $He/H = 0.11$, compatible with the previous estimation. Another approach [59] predict the local value $He/H = 0.08$ using helioseismological methods but there are uncertainties due to the models details and to the extension to interstellar medium. However, even if the true value is 0.08, the influence of the discrepancy on the secondary production will not exceed 10%.

3.1.4 Galactic Magnetic Field

The direction and strength of the uniform magnetic field is a key information for cosmic ray physics because not only it influences the cosmic ray propagation (in particular synchrotron radiation) but even the trapping of particles around the galaxy

(consequently the halo height) is directly connected to the magnetic profile. Investigations on the uniform component of the galactic magnetic field are complicated by the random component of the field, whose strength exceeds that of the uniform component (for instance in [60] the non random component is estimated to be $\sim 5\,\mu$G with a scale length for fluctuations ~ 100 pc). Various techniques has been applied to the determination of the magnetic field. We cite the detailed analysis based on the pulsar rotation and dispersion measures carried out in [61], where a local field strength of $1.4\pm0.2\ \mu$G and direction $\theta_0 = 88^o \pm 5^o$ are found. Some problems arise if one consider a magnetic model of concentric circular field lines as in [61]. In fact in other galaxies has been observed that the galactic magnetic field closely follows the spiral configuration. The work presented in [62] develops this spiral-frame line of research which is based on the large-scale data set on starlight polarization [63] with nearly 7000 stars. The advantage of this kind of data is that they are free of systematic errors and the polarization is accompanied by the source location and estimate of extinction. In the GALPROP model the uniform magnetic field is consistent with the conclusions in [62] and is parameterized as

$$B_\perp = 6\, e^{-|z|/5\,kpc - r/20\,kpc}\,\mu G\,. \tag{3.6}$$

Random fluctuation are not included in the model.

3.2 Propagation Equation

The propagation of cosmic rays in the GALPROP model is completely based on the kinetic theory that we explained in chapter 2. However to have contact with the code, it is important to notice that a change of variable that concerns the cosmic ray phase space density $f(\vec{r}, p, t)$ in propagation equation (2.104) has to be performed. More precisely we introduce the density per unit of total particle momentum $\psi(\vec{r}, p, t)$ defined by

$$\psi(\vec{r}, p, t)dp = \int_{-1}^{1} d\cos\theta \int_0^{2\pi} d\varphi f(\vec{r}, p, t)dp\,, \tag{3.7}$$

and we notice that the fourth term in (2.104) can be rewritten as follows

$$-\frac{1}{3}p\,(\nabla\vec{u})\,\frac{\partial}{\partial p}\left(\frac{\psi}{p^2}\right) = -\frac{1}{3}p\,(\nabla\vec{u})\,\frac{\partial}{\partial p}\left(\frac{1}{p^3}\cdot p\psi\right) = -\frac{1}{p}\,(\nabla\vec{u})\,\psi - \frac{1}{3p^2}\,(\nabla\vec{u})\,\frac{\partial}{\partial p}\,(p\psi)\ , \tag{3.8}$$

so that using (3.8), (3.7) and multiplying the whole equation by p^2 we end with

$$\frac{\partial \psi}{\partial t} = \vec{\nabla} \cdot (D_{zz} \vec{\nabla} \psi - \vec{u} \psi) + \frac{\partial}{\partial p} p^2 D_{pp} \frac{\partial}{\partial p} \frac{1}{p^2} \psi + \frac{1}{3} \frac{\partial}{\partial p} \left[(\vec{\nabla} \cdot \vec{u}) p \psi \right] , \tag{3.9}$$

where it is assumed that the drift velocity (2.95) is absent so that the diffusion coefficient only has the diagonal component which is parallel to the regular magnetic field directed toward the z direction. The z-component of the convection velocity is assumed to follow a linear increasing with distance from the galactic plane, as suggested by self-consistent models of cosmic ray-driven magnetohydrodynamic winds as derived in [64] and [65]. The wind velocity at z=0 is a model parameter but we fixed $u(z = 0) = 0$. In general we have $u > 0$ for $z > 0$, $u < 0$ for $z < 0$, and $dV/dz > 0$ for all z that imply a constant adiabatic energy loss. To take into account decay and fragmentation we use (1.64) that add the two terms $-1/\tau_d$ and $-1/\tau_f$ to the right hand side of (3.9). Energy losses enter the propagation through a momentum loss rate $\dot{p}$. Finally we need to add a source term $s(\vec{r}, p)$ that includes both primary and secondary contribution as explained in the next section. The complete propagation equation used in GALPROP is given by

$$\frac{\partial \psi}{\partial t} = s(\vec{r}, p) + \vec{\nabla} \cdot (D_{xx} \vec{\nabla} \psi - \vec{u} \psi) + \frac{\partial}{\partial p} p^2 D_{pp} \frac{\partial}{\partial p} \frac{1}{p^2} \psi - \frac{\partial}{\partial p} \left[\dot{p} \psi - \frac{p}{3} (\vec{\nabla} \cdot \vec{u}) \psi \right] - \frac{1}{\tau_f} \psi - \frac{1}{\tau_d} \psi \, . \tag{3.10}$$

3.3 Injection Spectrum

The source function distribution for primary cosmic rays has been discussed at the end of section 1.2.2, where it was explained that the best choice fall on a power law in momentum

$$q(E) = q_0 \, Q(E_{kin}) \, , \quad \frac{dQ(E_{kin})}{dE_{kin}} \propto p^{-\gamma} \, . \tag{3.11}$$

Here the flux $Q(E)$ is introduced because it is useful for comparisons with observations that are usually quoted as a flux. For our purposes we need to find a connection between (3.11) and the cosmic ray density per unit of total particle momentum $\psi(\vec{r}, p, t)$. To this end we notice that $dE_{kin}/dp = \beta/A$ where A is the mass number and E_{kin} is the kinetic energy per nucleon, so that we can write (3.11) in terms of the momentum

$$\frac{dQ(p)}{dp} \propto \frac{\beta}{A} p^{-\gamma} \, . \tag{3.12}$$

Now we go on using the relation between the cosmic ray density and the flux $dQ(p) \propto (c/4\pi)\beta\, s(\vec{r},p)dp$ with $s(\vec{r},p)$ indicating the proper source term that appears in the kinetic equation (2.27) to take into account the variation velocity of the distribution function $\psi(\vec{r},p,t)$ (see the definition in eq. (2.26)). In conclusion we can say that the injection spectrum enters the propagation equation in the following way

$$\frac{\partial\psi}{\partial t} = s(\vec{r},p)\,, \quad \frac{\partial s}{\partial p} \propto p^{-\gamma}\,. \tag{3.13}$$

Since the rigidity $\rho = p/Z$ is the most likely parameter governing the propagation and escape of particles moving in the galactic magnetic field, it is preferable to replace equation (3.13) with

$$\frac{\partial\psi}{\partial t} = s(\vec{r},\rho)\,, \quad \frac{\partial s}{\partial \rho} \propto \rho^{-\gamma}\,, \tag{3.14}$$

that, in turn, is implemented in GALPROP as $\frac{\partial s}{\partial \rho} \propto \left(\frac{\rho}{\rho_0}\right)^{-\gamma}$ to take into account possible breaking in the injection spectrum at a reference rigidity ρ_0.

The secondaries are generated by a source term that enters the propagation equation as

$$s_{sec}(\vec{r},p) = \beta\, c\psi_{prim}(\vec{r},p)\left[\sigma^{(H)}(p)n_H(\vec{r}) + \sigma^{(He)}(p)n_{He}(\vec{r})\right]\,, \tag{3.15}$$

where the production cross sections that are relevant for spallation (see section 1.4.4) are introduced. Here we consider only the production on hydrogen and helium targets, with the ψ_{prim} being the progenitors density and n_H, n_{He} the distribution of hydrogen and helium in the interstellar medium as given in section 3.1.3.

3.4 Diffusion Coefficients

The spatial diffusion coefficient (2.87) and momentum diffusion coefficient (2.88) have been deduced for cosmic ray particles that are scattered by random weak hydromagnetic waves propagating along the regular magnetic field $\mathcal{H}_0$. Now we restrict our attention to a power law energy spectrum in wavenumber k so that wave energy density is

$$W(k) = \frac{w\mathcal{H}_0^2 L}{4\pi(1-a)}(kL)^{(-2+a)}\,, \quad kL \geq 1\,, \quad a = const.\,, \tag{3.16}$$

where

$$w = \frac{4\pi}{\mathcal{H}_0^2}\int_{1/L} W(k)dk\,, \tag{3.17}$$

characterizes the turbulence level being equal to the ratio of magnetohydrodynamic wave energy density to magnetic field energy density; L is the principal scale of the turbulence. Moreover we assume that the energy density is the same for both the waves propagating in opposite directions along the regular magnetic field. This imply, as we said at the end of section 2.5, that the effective velocity of the convective particle transport by the wave (2.86) vanishes so that the only contribution to convection comes from the large movements of the medium that in our case is only along z. Substituting (3.16) in (2.87) and (2.88) we have

$$D_{zz} = \frac{2}{3\pi} \frac{(1-a)}{a(2+a)} \frac{vL}{w} \left(\frac{r_g}{L}\right)^a \tag{3.18}$$

and

$$D_{pp} = p^2 \frac{v_A^2}{vL} \frac{2\pi}{(1-a)(2-a)(4-a)} \left(\frac{r_g}{L}\right)^{-a}, \tag{3.19}$$

where we introduced the particle gyroradius $r_g = v/|\omega_H|$. Notice that the spatial diffusion coefficient (3.18) has been reduced of a factor 3 with respect to the local diffusion coefficient as a consequence of the large-scale wandering of magnetic field lines. From equations (3.18) and (**??**) we deduce that there exists the following correlation between the two coefficient

$$D_{pp} D_{zz} = \frac{4p^2 v_A^2}{3a(4-a^2)(4-a)w}, \tag{3.20}$$

so that once the expression of the spatial diffusion coefficient is given and the Alfvén velocity v_A is fixed, the momentum diffusion coefficient is determined according to (3.20). After analyzing all the quantities in (3.18) one can argue that a convenient form for the spatial diffusion coefficient is

$$D_{zz} = \beta D_0 (\rho/\rho_0)^\delta, \tag{3.21}$$

where ρ is the rigidity, ρ_0 is a reference rigidity introduced for an eventual break, D_0 is a normalization factor and δ is a free parameter of the model. In conclusion we reduced the problem of diffusion to two fundamental parameter D_0 and δ (plus ρ_0 in case of a breaking) while the reacceleration is connected to diffusion by specifying the Alfvén velocity v_A that is a third fundamental parameter.

3.5 Specific Models in the GALPROP Frame

Among the working effects in the GALPROP model we can chose to turn off convection or reacceleration. We consider the cases of diffusion+reacceleration (DR model) and diffusion+convection (DC model), since these are the minimum combinations which can reproduce the key observations. Attempts to consider both effects has been strongly excluded in [66].

Reacceleration provides a natural mechanism for reproducing the energy dependence of the B/C ratio [67; 68; 69]. In particular in [70] it is shown that the Kolmogorov spectrum that fixes $\delta = 1/3$ for all rigidities, is the best choice to fit the B/C data. Thus the value $\delta = 1/3$ is often assumed as a reference for fitting secondaries over primaries. In the DC model a reacceleration has to be simulated through a breaking in the spatial diffusion coefficient at reference rigidity. We assume that the breaking takes place at $\rho_0 = 4\,GV$ as suggested in [69]. Other models use a breaking at $\rho_0 = 1\,GV$ but this is not important because this parameter can be absorbed into the other diffusion coefficient parameters D_0 and δ in (3.21).

The idea of the breaking stems from the results obtained in the past for the leaky-box model. The connection between the leaky box model and diffusion model is explicitly shown in [68], for instance. If we consider a diffusion model where sources, gas and reacceleration are confined in a galactic disk that is much thinner than the halo and we restrict to stable particles, then the diffusion propagation equation can be reduced to the leaky-box propagation equation and there is a direct connection between the spatial diffusion coefficient and the escape length that characterizes the leaky-box model, namely

$$\lambda_{esc} = \frac{\rho_0\, v\, h_g\, H}{D(p)}\,, \tag{3.22}$$

where H is the halo height, h_g and ρ_0 enter the gas distribution confined to the thin disk as $\rho(z) = 2\rho_0 h_g \delta(z)$. The available data require a path length for the leaky-box model that presents a break at the reference rigidity

$$\lambda_{esc} = \begin{cases} \lambda_0\beta \text{ g cm}^{-2} & at\, \rho < \rho_0 \text{ GV} \\ \lambda_0\beta(\rho/\rho_0)^{-\delta} \text{ g cm}^{-2} & at\, \rho \geq \rho_0 \text{ GV}. \end{cases} \tag{3.23}$$

Such a breaking has no physical meaning but it makes sense if one notice that one of the condition to link the leaky-box model to a diffusion model is the confinement of

the reacceleration to the thin disk. Since this is not strictly true since reacceleration occurs wherever we have diffusion, the breaking simulates the reacceleration in the halo. Following this last observation one can argue that the path length (3.23) suggests a way to reproduce B/C for the DC model where the reacceleration is completely absent. A possible physical explanation is given in [2] by saying that below a particular rigidity kinetic diffusion becomes slower than the convective transport in removing particle from the galaxy and the particle residence time becomes independent of rigidity or energy. Another attempt to explain such a breaking could be that at low energy the particles propagate following the magnetic field lines rather than scatter on magnetic turbulence. Since the magnetic field lines are essentially tangled, such a process can still behave like diffusion [41]. In conclusion we set a constant value of the diffusion coefficient $D_{xx} = D_0$ for the DC model below reference rigidity $\rho_0 = 4$ GV (that means)and a rigidity dependence as in (3.21), which depends on the parameter δ, above the reference rigidity. For the DR model we do not include any breaking in the diffusion coefficient.

Another breaking is often introduced in the injection spectrum to obtain compatibility with data on primary spectra of protons and helium. This is our choice for the DC model but not for the DR one. The existence of an upturn below few GeV/nucleon is predicted from supernova remnants shock acceleration theory [71]. The explanation is based on a transition between thermal and non-thermal particle population in the shock. We set the injection breaking for protons at 9 GV.

The normalization is such that at kinetic energy $E_{kin} = 100\,GeV$ the proton flux is always equal to $\Phi = 4.90 \times 10^{-9}\,cm^{-2}sr^{-1}s^{-1}MeV^{-1}$. For electron normalization the flux is set to $\Phi = 4 \times 10^{-10}\,cm^{-2}sr^{-1}s^{-1}MeV^{-1}$ at $E_{kin} = 34.5\,GeV$.

Chapter 4

A Comprehensive Model of Cosmic Ray Propagation

This chapter is completely devoted to original results. The main task that we achieved in the following paragraphs, is to find the set of parameters that better describe the cosmic rays observation coming from balloon and satellite experiments. As already pointed out in the introduction, we describe in detail the method that we used, underlying all the adopted approximation in order to present a work that can be reproduced at any time. The range of energy from hundreds of MeV to hundreds GeV, that we chosen is the more interesting from a propagation point of view. Moreover these energies contain the interval covered by PAMELA, making this work particularly relevant in view of a future comparison between theory prediction and observation coming from this satellite born experiment.

4.1 Strategy of Analysis

The most simple statistical approach to the selection of the best model parameters is a scan of a parameter grid. At first sight, one can argue that this procedure is very time consuming since a single GALPROP run takes about twenty five minutes, using our hardware resources (to produce the right amount of secondaries we set the iteration number to two, so that each set of parameters takes two GALPROP run). Thus we were forced to find a way to reduce the time needed to complete the scan. Obviously

the number of parameters N dramatically influences the time of the scan which follows a power law in N

$$\Delta t = \mathcal{O}\left(e^N\right) , \tag{4.1}$$

so that it is our priority to reduce the number of parameters. To this end, we first notice that one of the most important constraint on model propagation is represented by unstable nuclei because their fluxes are directly connected to the halo height [55]. In fact unstable nuclei with life comparable to τ_{esc}, such as isotopes ^{10}Be and ^{26}Al, can be used as "cosmic ray clocks". For instance, let us consider the mostly studied ^{10}Be case which is unstable to β-decay with $\tau \sim 2.2 \times 10^6\, yrs$. In the framework of the leaky box model, one can argue that if the ^{10}Be will escape before decaying (i.e. decay will not affect the expected flux), that means $\tau_{esc} \leq \tau_{^{10}Be}$, then the observed ratio of unstable to stable beryllium is comparable with the ratio expected at production from the ratio of the fragmentation cross sections of the parent nuclei, according to

$$\frac{N_{sec}}{N_{prim}} = \frac{\sigma_{P\to S}}{\sigma_P} \frac{\lambda_{esc}}{\lambda_P[1 + \lambda_{esc}/\lambda_S + \tau_{esc}/(\gamma\tau_S)]} . \tag{4.2}$$

On the contrary, if $\tau_{esc} > \tau_{^{10}Be}$ then the measured ratio is much less than its value at production. These considerations has been applied to show that the containment volume in the leaky box model extents over the galactic disk embracing the halo. In particular the ratio $^{10}Be/^{9}Be$ has been already used in the GALPROP framework [55] to gain informations about the halo in connection with the *Ulysses* data [93]. The resulting halo height interval compatible with measurements was $z_h = 4 - 12$ kpc. Further developments of this kind of approach were presented in [73] where the ACE data where exploited to obtain the more robust estimate $z_h = 3 - 7$ kpc. In [74] is introduced a new evaluation of the production cross sections by the improved Cascade-Extinction Model code CEM2k together with Los Alamos compilation of all available data. This last investigation lead to the range $z_h = 4 - 6$ kpc. Other important estimations come from [75] that predicts $z_h = 2 - 4$ kpc from HEAO-3 and from [76] that gives $z_h = 4.9^{+}_{-2}4$ kpc.

Using the above argument we can split the halo height parameter from the other, performing a first stage analysis involving primaries and secondary over primaries ratios to fix propagation parameters, followed by a second stage where unstable nuclei are used to understand the halo height for which there is an agreement in the literature

around a value of 4 kpc. Thus for the first stage we considered this value. Concerning the parameter range, we were mainly influenced by the theoretical uncertainties claimed in [66] where precise limits for a reduced chi-squared less than two were obtained (see table 4.1). All the above consideration finally lead us to chose the values given in table

Model	z (Kpc)	D_0 (cm^2/s)	δ	γ_1	γ_2	dV_C/dz $(Km\,s^{-1}$ $Kpc^{-1})$	dV_A (Km/s)
DC	3-5	$(2.3-2.7)$ $\times 10^{28}$	0.48-0.62	2.42-2.50	2.14-2.22	5-7	//
DR	3-5	$(5.2-6.7)$ $\times 10^{28}$	0.25-0.36	2.35-2.52	//	//	22-35
DRB	3.5-4.5	$(5.9-6.3)$ $\times 10^{28}$	0.28-0.36	1.88-2.02	2.36-2.50	//	25-33

Table 4.1: Range of parameters that correspond to DC, DR and DRB models with a chi-squared less than two for a fit with about 50 B/C data [66].

4.2 for the DC model and in table 4.3 for the DR model. The steps were chosen in order to match the time required for the simulation with the time at our disposal. It is worth noting that the analysis can be refined at any time in the future thanks to the structure of the ad hoc programs (GRIDGALPROP and STATVIEW) without any loss of the models already analyzed. The amount of sets of parameters scanned for the DC model turns out to be 7200 for an approximate simulation time of 10 months. On the other side, for the DR model, we have 2352 sets for a total time of approximately 3.3 months.

Parameters	D_0 (cm^2/s)	δ	γ_1	γ_2	dV_C/dz $(Km\,s^{-1}\,Kpc^{-1})$
Range	$(2.2-2.7)$ $\times 10^{28}$	0.48-0.62	2.42-2.50	2.14-2.22	5-10
Step	0.1×10^{28}	0.02	0.02	0.02	1

Table 4.2: Range of parameters of the DC model analysis.

Parameters	D_0 (cm^2/s)	δ	γ_1	dV_A $(Km\,s^{-1})$
Range	$(5.2-6.7)$ $\times 10^{28}$	0.25-0.37	2.35-2.53	22-36
Step	0.3×10^{28}	0.02	0.03	2

Table 4.3: Range of parameters the DR model analysis.

4.2 Chi-Squared Approximations

By definition, the chi-squared with ν degrees of freedom is nothing but a random variable resulting from the sum of ν Z-variable

$$\chi^2_\nu = \sum_{i=1}^{\nu} Z_i^2\,, \tag{4.3}$$

where a Z-variable is a gaussian random variable such that

$$< Z >= 0\,, \qquad \sigma_Z^2 = \frac{1}{N-1}\sum_{k=1}^{N}(Z_k - < Z >)^2 = 1\,. \tag{4.4}$$

It is well know that the distribution associated to the χ^2_ν turns out to be

$$D(\chi^2,\nu)\,d\chi^2 = \frac{1}{2^{\frac{\nu}{2}}\Gamma(\nu/2)} exp\left\{-\frac{\chi^2}{2}\right\}(\chi^2)^{\frac{\nu}{2}-1}d\chi^2\,, \tag{4.5}$$

and it can be easily proven that the following properties hold

$$< \chi^2_\nu >= \nu\,; \qquad \sigma^2_{\chi^2_\nu} = 2\nu\,; \qquad \chi^2_{\nu_1+\nu_2} = \chi^2_{\nu_1} + \chi^2_{\nu_2}\,. \tag{4.6}$$

It is important to us to define the reduced chi-squared

$$\tilde{\chi}^2_\nu = \frac{\chi^2_\nu}{\nu} \tag{4.7}$$

so that the first two of (4.6) reduce to

$$< \tilde{\chi}^2_\nu >= 1\,; \qquad \sigma^2_{\tilde{\chi}^2_\nu} = 2\,. \tag{4.8}$$

It can be proven that to count the number of degree of freedom associated to the chi-squared one should pay attention to the dependence between normal variables: if mathematical relations such as

$$\begin{aligned} f_1(Z_1, Z_2, \ldots, Z_\nu) &= 0 \\ f_2(Z_1, Z_2, \ldots, Z_\nu) &= 0 \\ &\vdots \\ f_k(Z_1, Z_2, \ldots, Z_\nu) &= 0 \end{aligned} \tag{4.9}$$

hold, then

$$\chi^2 = \sum_{i=1}^{\nu} Z_i^2 \tag{4.10}$$

will be a chi-squared variable with $\nu - K$ degrees of freedom.

The chi-squared variable is used to test hypothesis and to determine confidence intervals. To describe the observed data coming from an experiment, we usually assume

the hypothesis that a mathematical model is the right one to explain what we see. Since the measurements are always affected by random and eventually systematic errors, observation and prediction will never coincide. Thus we are forced to construct a proper random variable based on the model and observed data. Let us suppose that such a variable, assuming the hypothesis to be true, is distributed according to a chi-squared variable with ν degrees of freedom. If we obtain from an experiment the particular value χ^2_{obs} then we need a test to verify if this value is in agreement with the distribution $D(\chi^2, \nu)$ in (4.5). If it is so, then it is reasonable that the hypothesis is true. To quantify the agreement, a confidential level α is chosen (typically 0.5 percent). If the a priori probability to have a value of the χ^2 greater than the observed one χ^2_{obs}, which is given by

$$P\left(\chi^2 > \chi^2_{obs}\right) = \frac{1}{2^{\frac{\nu}{2}}\Gamma(\nu/2)} \int_{\chi^2_{obs}}^{\infty} exp\left\{-\frac{\chi^2}{2}\right\} (\chi^2)^{\frac{\nu}{2}-1} d\chi^2 \,, \tag{4.11}$$

do not exceed the confidence level, than the chosen theory is not expected to describe what is observed to the α confidence level. In fact $P\left(\chi^2 > \chi^2_{obs}\right) < \alpha$ means that we observed something which has a little probability to be seen under the theoretical model considered. Otherwise if $P\left(\chi^2 > \chi^2_{obs}\right) > \alpha$, then the data are well described by the theory. The same test can be performed by matching values of χ^2. In fact we can define χ^2_α through the equation

$$P\left(\chi^2 > \chi^2_\alpha\right) = \frac{1}{2^{\frac{\nu}{2}}\Gamma(\nu/2)} \int_{\chi^2_\alpha}^{\infty} exp\left\{-\frac{\chi^2}{2}\right\} (\chi^2)^{\frac{\nu}{2}-1} d\chi^2 \;=\; \alpha \,. \tag{4.12}$$

Since $P\left(\chi^2 > \chi^2_\alpha\right)$ decrease by increasing χ^2_α, we can say that

$$\begin{aligned} &\chi^2_{obs} > \chi^2_\alpha \Rightarrow P\left(\chi^2 > \chi^2_{obs}\right) < \alpha \Rightarrow \text{theory rejected} \\ &\chi^2_{obs} < \chi^2_\alpha \Rightarrow P\left(\chi^2 > \chi^2_{obs}\right) > \alpha \Rightarrow \text{theory accepted} \quad . \end{aligned} \tag{4.13}$$

It is worth nothing that sometimes the confidence level is given in terms of number of σ's. To avoid misunderstanding let us clarify this misleading approach. When we perform a single measure of a quantity that experience random fluctuation, we can ask ourselves if it is compatible with an expected one. The easiest way to answer to this question is to consider how many σ's is the distance between the true value x_t and the measured one $x_m \pm \sigma$. The approach is the same as for the χ^2 test but this time the

distribution to consider is the gaussian one. The probability that x falls inside a range of n-σ's is given by

$$P(|x - x_t| < n\sigma) = \int_{-n\sigma}^{n\sigma} g(x)dx = \frac{1}{\sqrt{2\pi\sigma^2}} \int_{-n\sigma}^{n\sigma} exp\left\{-\frac{(x - x_t)}{2\sigma^2}\right\} dx\,. \tag{4.14}$$

To make contact with what we said before about the χ^2 test, we have to consider the probability that x falls outside the above interval which is

$$P(|x - x_t| > n\sigma) = \frac{2}{\sqrt{2\pi\sigma^2}} \int_{n\sigma}^{\infty} exp\left\{-\frac{(x - x_t)}{2\sigma^2}\right\} dx = 1 - P(|x - x_t| < n\sigma)\,. \tag{4.15}$$

Again we can fix a confidence level α and associate to it a corresponding n_α, solution of the equation

$$P(|x - x_t| > n_\alpha\sigma) = \alpha\,. \tag{4.16}$$

If we observe x_{obs} such that $|x_{obs} - x_t| > n_\alpha\sigma$ it means that

$$P(|x - x_t| > |x_{obs} - x_t|) < P(|x - x_t| > n_\alpha\sigma) = \alpha\,, \tag{4.17}$$

so that what we observe does not match what we expect. For instance if $\alpha = 0.05$ then the corresponding value in terms of σ's is $n_{0.05} = 1.96$. Encoding the confidential level into n_α makes sense only in the case of a single variable but, we can say that for a given n_α we can derive a value of α which, in turn, can be used for the χ^2-test. To this end it is useful to have in mind the table 4.4.

Turning back to the χ^2-test, it is left to figure out the explicit expression of the Z-variables. Following the gaussian single variable case just described, we can define

$$Z_i = \frac{y_i - f_t(x_i)}{\sigma_{y_i}} \tag{4.18}$$

where y_i is the i-th observed value with associated variance σ_{y_i} and $f_t(x_i)$ is the theoretic curve. It is clear that if y_i is a random variable then (4.18) is a genuine Z-variable that satisfies the properties (4.4). Finally we are left with the following χ^2 expression

$$\chi^2 = \sum_{i=1}^{\nu} \frac{(y_i - f_t(x_i))^2}{\sigma_{y_i}^2}\,. \tag{4.19}$$

Concerning the analysis of cosmic ray spectra, our problem is to compare cosmic ray flux data coming from balloon and satellite borne experiments (y_i in (4.19)) with the

n_α	1	2	3	4	5
α	0.317311	0.045500	0.002700	0.000063	$< 10^{-6}$
$1-\alpha$	0.682689	0.954500	0.997300	0.999937	0.999999

Table 4.4: Confidence levels α in terms of number of σ's.

GALPROP output fluxes associated to each set of parameters ($f(x_i)$ in (4.19)). The fluxes are obviously function of the energy (x_i in (4.19)). The first problem we faced approaching the χ^2 calculation has been that the GALPROP code produces a discrete flux with a kinetic energy step that can be fixed by the user through the GALDEF file. Actually, since the fluxes are always given in logaritmic scale, the next step is calculated by multiplying the previous one by a chosen factor. For our analysis this Kinetic energy factor is equal to 1.3. In order to figure out the χ^2 value, for each given experimental value of the flux at a certain energy, we interpolated the expected flux between the two points given by the GALPROP fitsfile. This linear interpolation is an approximation that could be refined by searching a fitting curve that include all the data points but this is much harder to implement in the STATVIEW code so we decided to postpone to future upgrading.

Let us suppose that an experimental point in the (kinetic-energy,flux) plane is (x_{exp}, y_{exp}) and that this point falls in the kinetic energy range between the fitsfile points (x_1, y_1) and (x_2, y_2). The line passing through the last two points is

$$y = f(x) = \frac{x_1 y_2 - x_2 y_1}{x_1 - x_2} x + \frac{y_1 - y_1}{x_1 - x_2}\,, \tag{4.20}$$

so that we are left with the Z variable expression that reads

$$Z = \frac{(y_{exp} - f(x_{exp}))}{\sigma_{exp}} = \frac{1}{\sigma_{exp}} \left(y_{exp} - \frac{x_1 y_2 - x_2 y_1}{x_1 - x_2} x_{exp} + \frac{y_1 - y_1}{x_1 - x_2} \right)\,. \tag{4.21}$$

We want to stress that the error bars of the flux data points are always asymmetric. This is mainly due to systematic errors of the instruments that are used onboard the spacecrafts, satellites or balloons. This means that we are not dealing with a proper gaussian distribution but we assume the fluxes to be a measure affected only by random fluctuation. To this end we consider as the variance the greatest value between the upper and lower errors, in order to have symmetric error bars even if overestimated. Concerning the energy bin error, all the graphs that are found in the literature report the energy bin (as we will), not the proper error bars. In principle inside the energy bin can be assumed that we have a uniform distribution so that the best value is simply the mean one, while the error is equal to the measure of the bin divided by the square root of twelve

$$\delta_{E_{Kin}} = \Delta E_{bin}/\sqrt{12}\,. \tag{4.22}$$

To include the energy error in the analysis one should know the mathematical relation between the kinetic energy and the flux that is so complex to make this approach not viable. Another way is to use the curve obtained by the above mentioned fitting procedure, as the functional relation that links kinetic energy and flux but this introduce some biasing that should be taken into account. For the sake of simplicity we simply omit the energy errors from the analysis. The net effect of considering the energy errors is to weight in a different way the data with the increasing of the energy; more precisely the low energy measurements (sometimes affected by solar modulation uncertainties) will weight much more than the high energy ones. Disregarding the energy uncertainties amounts to exclude this effect.

Another approximation that is worth to be mentioned concerns with a possible biasing between different sets of data. In principle, a supernova remnant produces cosmic rays of all kind so that a common imprinting could be responsible for a biasing between different type of cosmic rays. In our opinion this effect is canceled enough during propagation to consider the measures as independent. This imply that the χ^2 can be calculated as a sum of squared Z variable as in (4.18) without including biasing terms.

4.3 Experimental Data Selection

One of our main task is to reconcile all the available knowledge about cosmic rays into a model that is able to reproduce what we observe by the experiments. Following this

Name/Type	Φ (MV)	Period
ACE/Satellite [77]	325	Aug. '97 - Apr. '98
Balloon [78]	350	?
Balloon[79]	600	3 flights in'76,'77 and '78
Balloon [80]	600	?
Balloon [82]	640	Sept. '73 and May '74
IMP 8/Satellite [83]	490	'74-'78
HEAO-3-C2/Satellite [84]	750 from [77]	Oct. 17th '79 - July 12th '80
HEN/Balloon [85]	800	'71 and '72
UNH74 and UNH76/Balloon [86]	625	summer and fall '74; fall '76
Balloon [87]	580	Aug. '73
Balloon [88]	580	Sept. 30th '72
Balloon [89]	540	Oct. '76
VOYAGER/Satellite [90]	450	'76-'94

Table 4.5: Solar modulation strength for B/C data-sets.

line we included all the public data that we found on B/C, Sub-Fe/Fe, protons, helium, $^{10}Be/^{9}Be$, $^{26}Al/^{27}Al$, $^{36}Cl/Cl$ and $^{54}Mn/Mn$. However behind our data selection there are precise motivation. For instance the main reason that lead to an extension of the fitting procedure over the B/C data that is often encountered in the literature, is that the secondary over primary ratio does not fix the injection of primaries. This is clear if one consider the flux of primaries that is, roughly speaking, proportional to the injection spectrum $\Phi_i(E) \sim E^{-\gamma}$ modulated by the diffusion that is $\Phi_{prim}(E) \propto D_0^{-1} E^{-(\gamma+\delta)}$. Therefore the flux of secondaries is proportional to the primary flux which undergoes diffusion so that $\Phi_{sec}(E) \propto D_0^{-2} E^{-(\gamma+2\delta)}$. We conclude that secondary over primary

ratios have the following dependence on the model parameters

$$\Phi_{sec}(E)/\Phi_{prim}(E) \propto D_0^{-1} E^{-\delta}\,, \tag{4.23}$$

so that the injection index γ is not influenced by a fitting based on such ratios.

Once the data are chosen, the main problem that is left to solve is the determination of the solar modulation. Mostly the modulation strength parameter Φ is reported inside the paper were the data-points coming from an experiment are presented. Since the

Name/Type	Φ (MV)	Period
ACE/Satellite [77]	325	Aug. '97 - Apr. '98
SANRIKU/Balloon [91]	660	May 25th '89 and '91
HEAO-3/Satellite [84]	600	Oct. 17th '79 - July 12th '80

Table 4.6: Solar modulation strength for SubFe/Fe data-sets.

determination of the proper solar modulation goes beyond the purpose of this work, we trust the value of Φ whenever it is given in the literature. Sometimes, especially

Name/Type	Φ (MV)	Period
ACE/Satellite [94]	325	Aug. '97 - Apr. '99
VOYAGER/Satellite [95]	500	'77-'91
ULYSSES/Satellite ($^{26}Al/^{27}Al$) [81][92]	800	Oct. '90-'95
ULYSSES/Satellite [93] ($^{36}Cl/Cl$)	780	Oct. '90-fall '97
ULYSSES/Satellite [81] ($^{54}Mn/Mn$)	840	Oct. '90- '95

Table 4.7: Solar modulation strength for isotopic data-sets.

for old publications, the modulation is completely unknown. In these cases we made

a rough estimation of the modulation using the neutron monitor. More precisely we used the correlation between the neutron flux and the known values of Φ for precise period of time to extrapolate a mean value of the modulation relative to the period of each considered mission. To this end we exploited the "CLIMAX Neutron Monitor". The values of the solar modulation strength that we used together with the references, are listed in tables 4.5, 4.6, 4.8 and 4.7.

Now let us focus our attention on a subtle aspect of the fitting procedure that we performed. The point is that in the following we will try to treat primaries and secondary over primary ratios on the same footing even if they affect different aspects of propagation and accordingly different parameters.

Payload	Φ (MV)	Period
BESS/Balloon [96]	660 from [98]	'93
BESS/Balloon [97]	600 from [98]	July 29th-30th 1998
CAPRICE/Balloon [99]	600	Aug. 8-9 1994
CAPRICE/Balloon [100]	600	May 28-29 1998

Table 4.8: Solar modulation strength for protons and helium data-sets.

To account for this aspect we include more or less the same amount of information for each set of data. In particular we decided to exclude protons and helium coming from the AMS experiment because their inclusion tends to favor primaries. Anyway, since protons and helium fluxes are determined with great precision with respect to secondary over primaries ratios, our results are mostly influenced by primaries. The total amount of data-points for the B/C, SubFe/Fe, Protons, helium and isotopic ratios are respectively 103, 45, 83, 83 and 9. The last comment that is worth to be addressed here, is that so far we are not sure about the compatibility between data-sets coming from different experiments. In the literature the authors are used to show a qualitative check by plotting results coming from different references but it should be pointed out that it is correct only for kinetic energies above 10 GeV where the solar modulation does not shift the interstellar flux. To understand the degree of matching below 10

GeV one should know the right solar modulation associated to each experiment in order to relate the observation to the interstellar medium where it is possible to carry out a proper comparison. Obviously this kind of analysis is full of uncertainties and require a certain degree of bravery to state that an experiment is not aligned with the other. Anyway no one handled this problem even above 10 GeV, where a comparison is relatively easy to do since no modulation is working. As a consequence, considering different experiments without a proper selection leads to somewhat high values of the χ^2 when we try to fit theoretical predictions. This gives rise to an ambiguity because the incompatibility may be due to a problem pertaining the theoretical assumptions as well as to experiment results that are not in line with the other ones.

4.4 Cosmic Ray Fluxes Based on the B/C Data

Fitting the measured B/C ratio is a standard procedure to derive the propagation parameters. Its importance reside in the entirely secondary origin of boron and in the measurements that are better than for other ratios (available up to 100 GeV). Moreover the production cross sections from the main progenitors C-N-O, are better known for boron than for the Be and Li (the other almost completely secondaries that share the same parent nuclei).

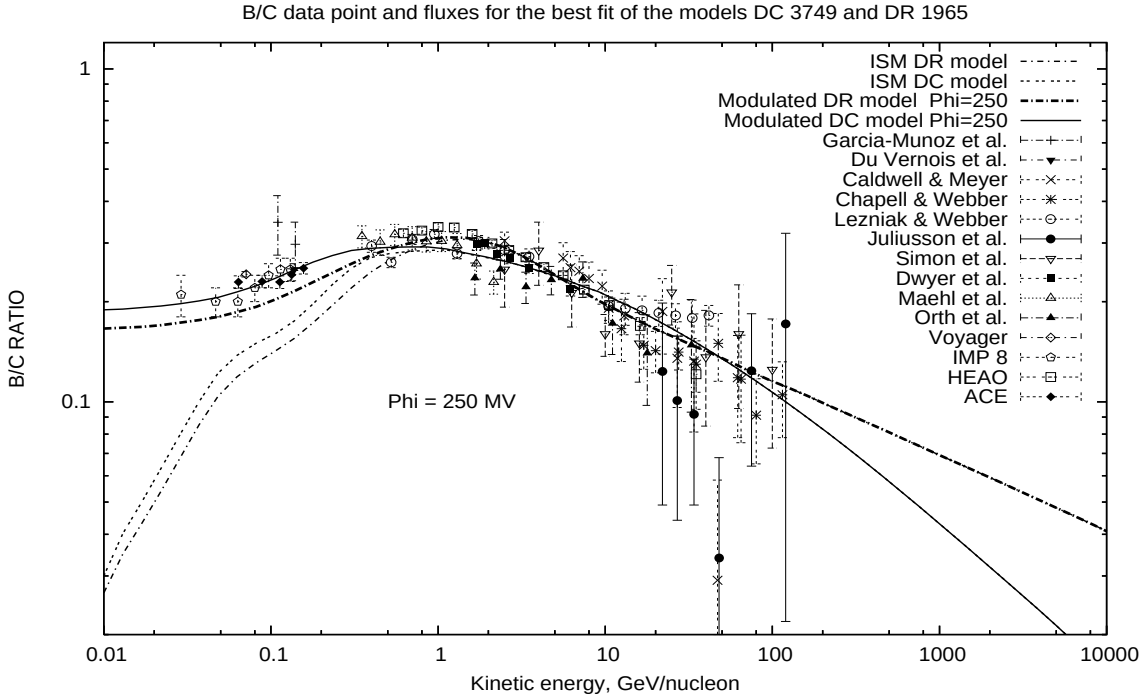

Figure 4.1: Best fits of the DC and DR model and data for the secondary over primary ratio B/C. The fitting has been done considering only B/C ratio.

To have preliminary indications about our parameter space we show the results that we obtain by a fitting procedure applied to the B/C data. Recent remarkable B/C based analysis can be found in [66; 101]. Let us remember once again that the secondary over primary nuclei ratio are sensitive to the value of the diffusion coefficient and its energy density. A larger diffusion coefficient leads to a lower ratio since the primary nuclei escape faster from the galaxy producing less secondary and viceversa.

The best fits are summarized in table 4.9.

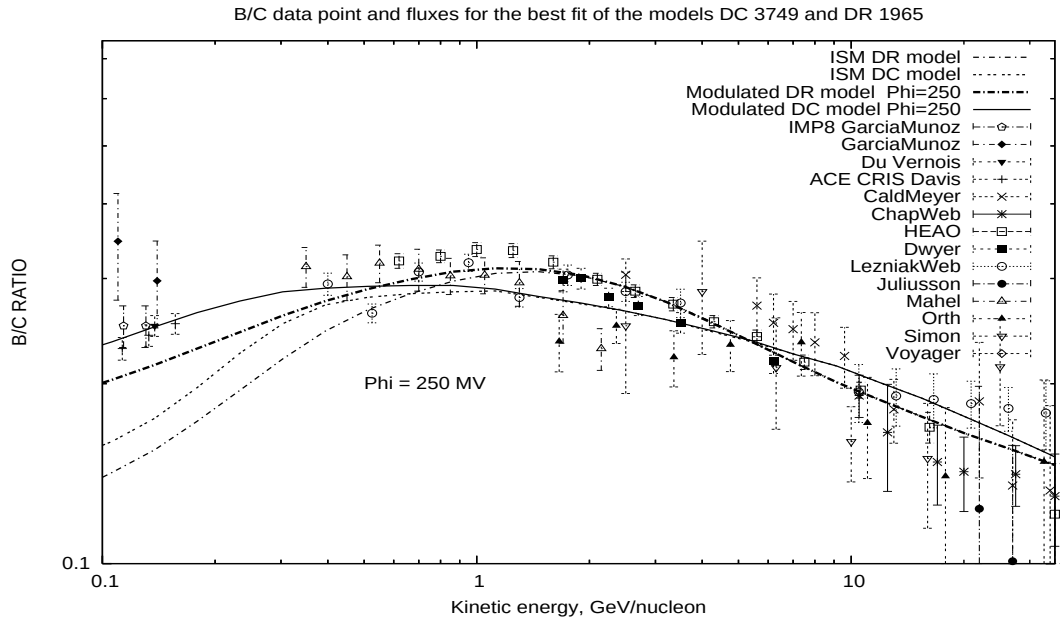

Figure 4.2: Best fits of the DC and DR model and data for the secondary over primary ratio B/C as in figure 4.1, magnified in the energy range 0.1-35 GeV.

$Model - Number$	D_0 (cm^2/s)	δ_1	δ_2	γ_1	γ_2	dV_C/dz $(Km\,s^{-1}$ $Kpc^{-1})$	$V_A(km/s)$	$\tilde{\chi}^2$
$DC - 3749$	2.5×10^{28}	0	0.48	2.5	2.22	10	0	3.79
$DR - 1965$	6.7×10^{28}	0.25	0.25	2.35	2.35	0	32	1.93

Table 4.9: Best models reproducing the B/C data.

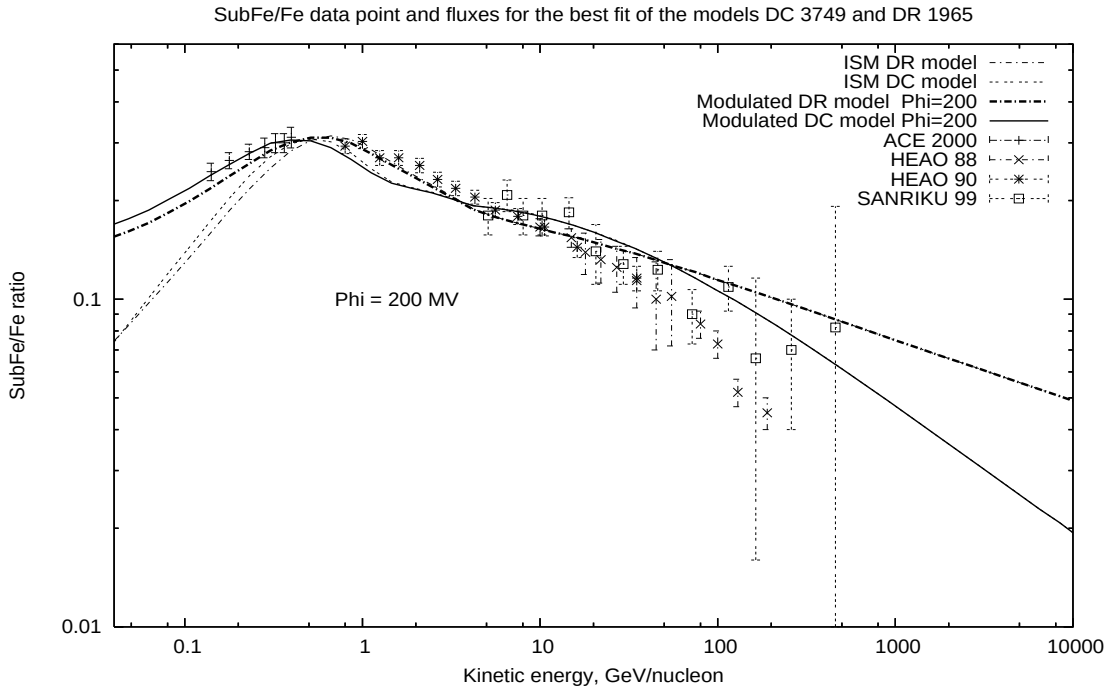

Figure 4.3: Best fit of the DC and DR model and data for the secondary over primary ratio SubFe/Fe. The fitting has been done considering only B/C ratio.

The comparison with previous results from [66] shed light on the unsuitable determination of the theoretical uncertainties on which we based our parameter grid. In fact almost all the parameter touch the limits of the assigned intervals. The reason for this can be attribute to the enlarged set of data or to the different version of the GALPROP code but it is more likely that in [66] no grid scan has been performed (in fact it is not declared the parameter space that they have analyzed and it is reasonable that they searched for the best fit by a reasonable exploration of the parameters). The fitting quality is manifest in figure 4.1 and 4.2. For the DR we get a nice fit but we can not say that we see the same satisfactory agreement for the DC model. This reflects the quantitative results since the $\tilde{\chi}^2$ of the DC model is a factor two more than the DR one. The attitude of the stochastic reacceleration to fit the B/C data is not new as it has been widely emphasized that this is a natural mechanism for reproducing secondary over primary energy dependence without and ad hoc form for the diffusion coefficient [67; 68; 69; 70] as it happens in the DC model. Even the difficulties of the

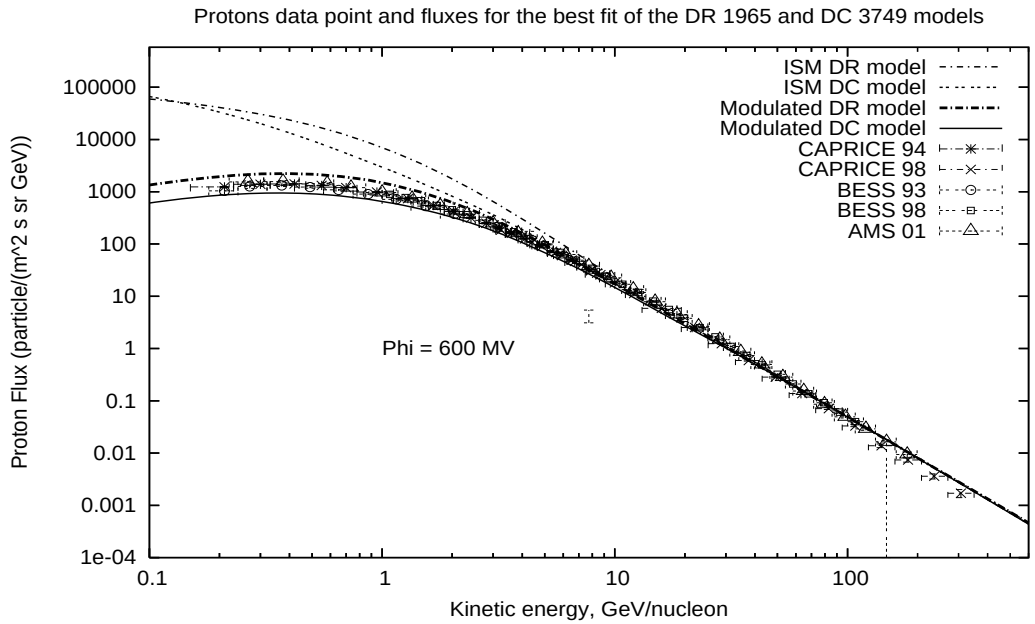

Figure 4.4: Best fits of the DC and DR models together with data for the proton flux. The fitting has been done considering B/C ratio.

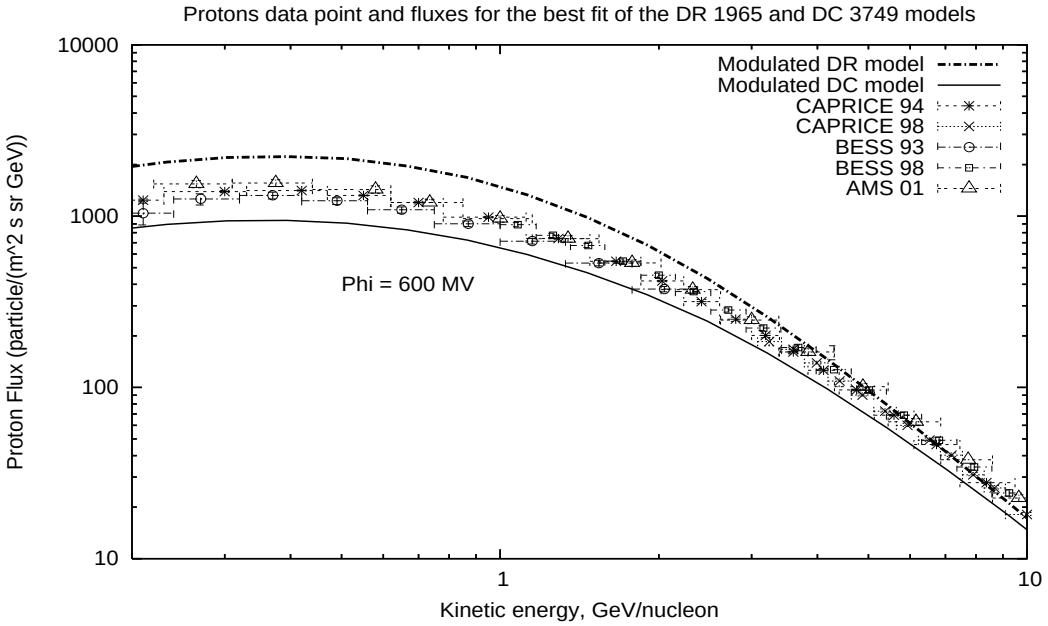

Figure 4.5: Best fits of the DC and DR models from the figure 4.4, magnified in the kinetic energy range 0.1-10 GeV.

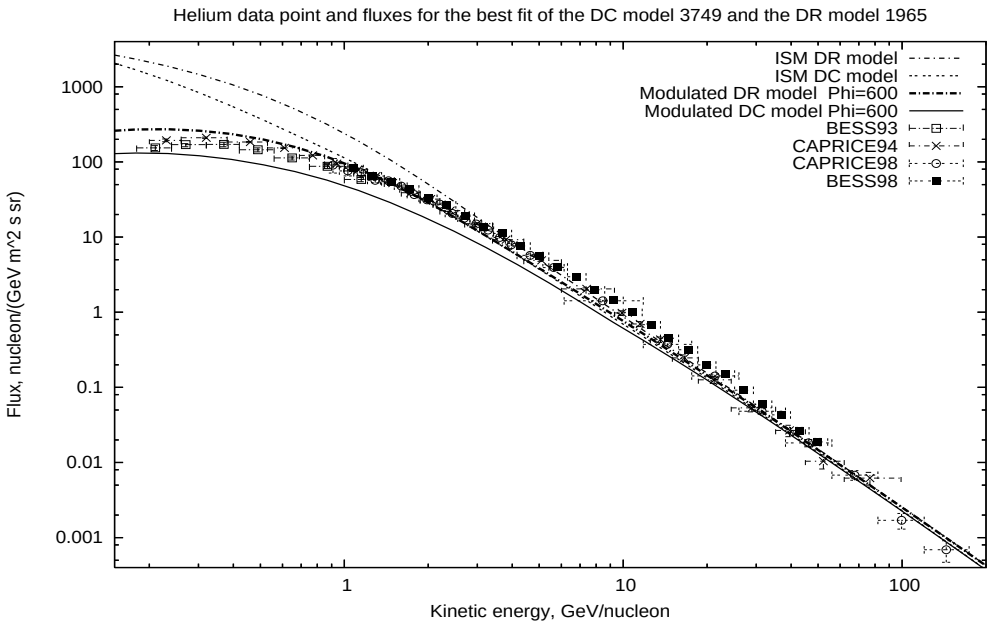

Figure 4.6: Best fit of the DC and DR models with data for helium flux, fitting the B/C ratio.

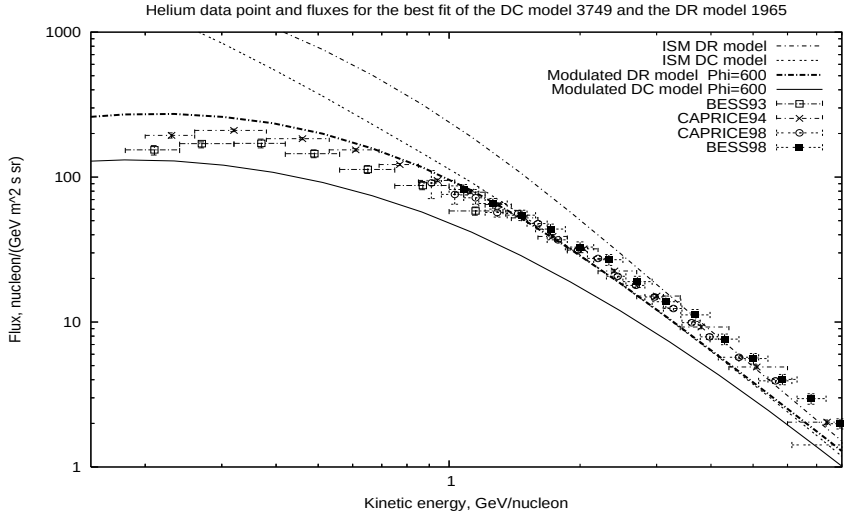

Figure 4.7: Best fits of the DC and DR models from the figure 4.6, magnified in the kinetic energy range 0.1-8 GeV.

DC model to fit the B/C data have been noticed by other authors [55; 105]. The comparison with other results obtained by the authors of the GALPROP model is made

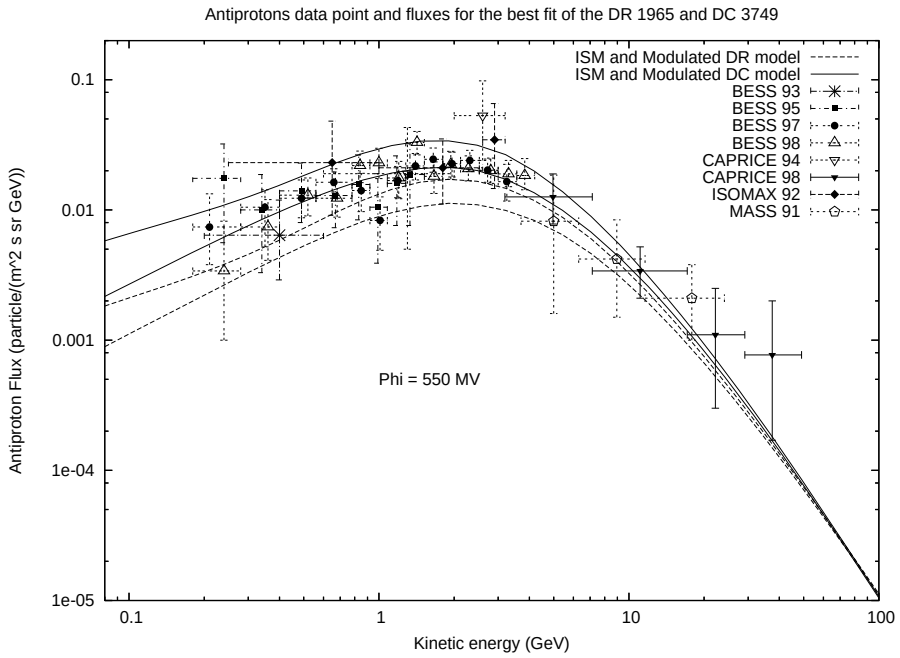

Figure 4.8: Best fits of the DC model and DR model together with data for the antiproton flux. The fitting has been done considering B/C ratio.

difficult by the variation of the parameters involved in the analysis. For instance a change in the reference rigidity at which we set the breaking in the injection spectrum influences the normalization of the primary flux. In addition a fitting that consider the B/C ratio alone has never been explored with the GALPROP model except in [66] to which we are directly linked. The work which is closer to what is presented in this section is [101] where the authors claimed a diffusion coefficient spectral index that is $\delta \gtrsim 0.6 - 0.7$ and a source spectral index $\gamma \sim 2.0$. However we get distance from such esteems from the beginning because our parameter space touch them marginally. Moreover in [101] reacceleration and convection are both turned on in the same model while we consider them separately. Turning back to our best models, we can notice that they present strictly different behavior at energies above one hundred GeV. This reflect the fact that we chosen to let the models unconstrained at high energies even if, in principle, we can say that for sufficiently energetic particles the effects other than diffusion and acceleration, are irrelevant [102; 103]. As a consequence the spectrum is proportional to $\rho^{-\alpha}$ where $\alpha \sim \delta + \gamma \sim 2.8$. Some less relevant discrepancy can

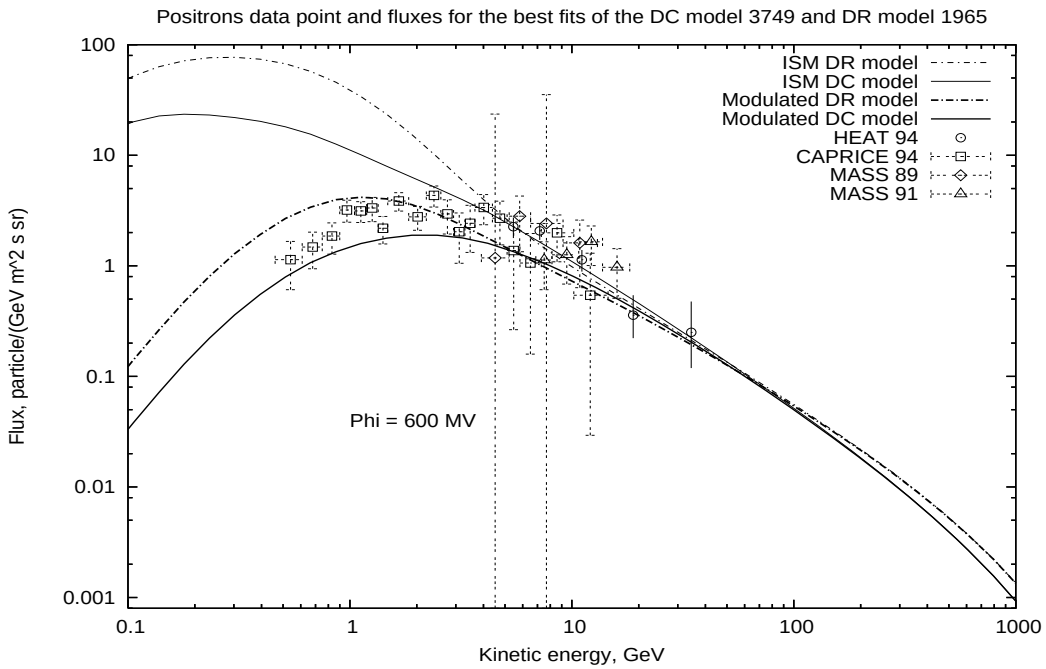

Figure 4.9: Best fits of the DC model and DR model together with data for the positrons flux. The fitting has been done considering B/C ratio.

be found even at lower energies but what is important to stress here is that higher energies data are welcome in order to discriminate between the two models. Another strong result comes from [70] where it has been shown that the Kolmogorov spectrum of weak magnetohydrodynamic turbulence, which corresponds to a diffusion coefficient spectral index $\delta = 1/3$, is the best choice to fit the B/C data. Since then the 1/3-value has been considered as a reference whenever reacceleration is turned on but from the DR model we get a value that is far less than the Kolmogorov one. Since all the secondary over primary ratios are influenced by the same parameters, we expect to obtain a good agreement between the SubFe/Fe data and predictions coming from the best fits obtained by B/C. In fact this is the case as it can be seen from figure 4.3. Moreover we underline that the same high energy behavior that we have seen for the B/C case, is reproduced here.

As we pointed out in the previous paragraph, the injection spectrum of primaries is not controlled by a fitting on B/C [103]. Anyway we want to show the fluxes for protons and helium that comes out from the best fits, in order to compare with the

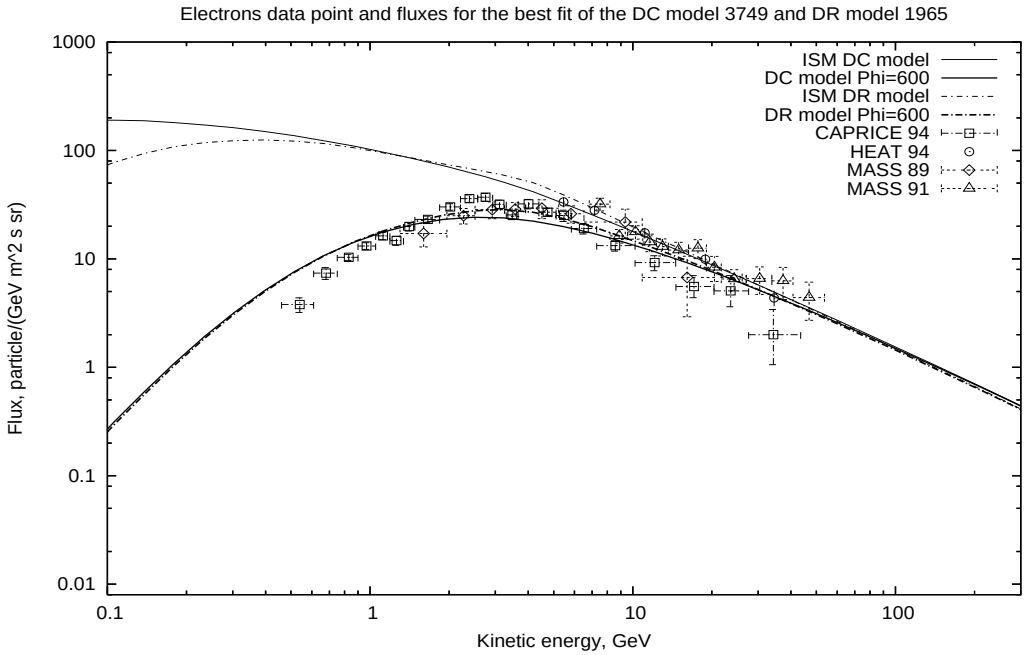

Figure 4.10: Best fits of the DC model and DR model together with data for the electron flux. The fitting has been done considering B/C ratio.

results of the next section, where the fit will be extended to primaries. In the graph 4.4 are reported the energy dependence of the proton flux for DC and DR models.

The low energy data come from experiments that were performed during a period of about 600 MV solar modulation so we chosen this value for the plot. We observe that a fine tuning of the proton flux in the solar modulated region is needed. In fact it turns out that the DC model underestimate the data while the DR model overestimate them. This is a problem that has been already stressed in other works [105]. Notice that even if the flux seem to be graphically close to data, the narrow error bars enhance dramatically the χ^2 value, moving away from compatibility. Quantitatively for protons we have obtained the values $\tilde{\chi}^2_{DC} = 38.40$ and $\tilde{\chi}^2_{DR} = 114$ that are hopelessly large. This means that a fitting based only on B/C ratio is not able to reproduce properly the flux of primaries, as we expected [103]. Concerning the helium flux (figure 4.6), the problems that arise are very similar to the ones faced for the protons. However we do not observe a clear overestimation of the DR model like in the proton case. In fact the reduced chi-squared give $\tilde{\chi}^2_{DC} = 28.97$ and $\tilde{\chi}^2_{DR} = 4.23$. We conclude that the primaries

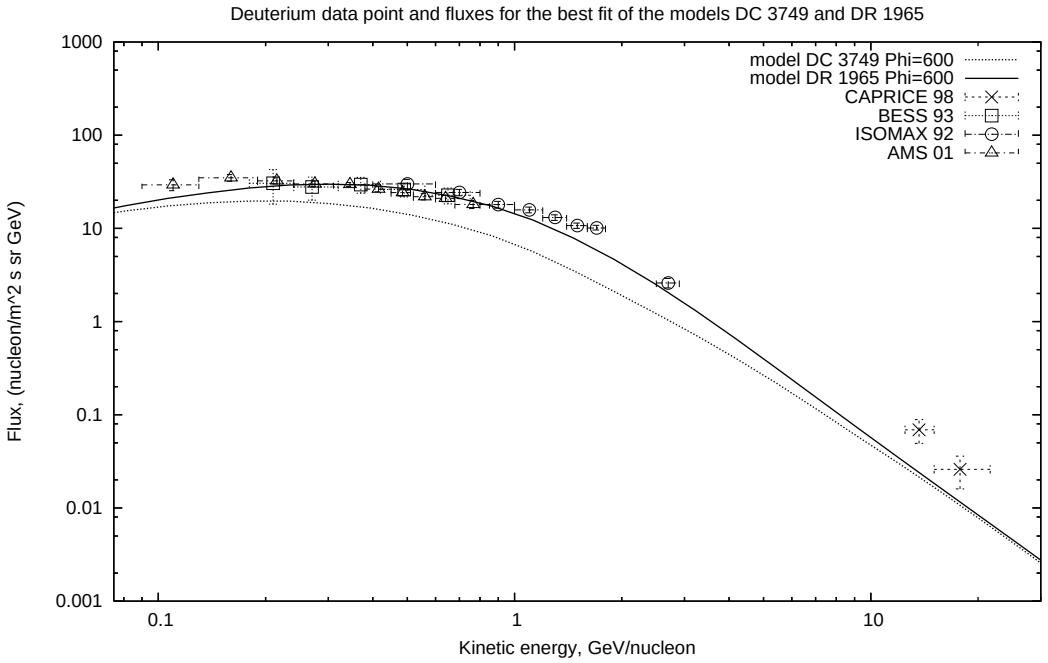

Figure 4.11: Best fits of the DC model and DR model together with data for the Deuterium flux. The fitting has been done considering B/C ratio.

are completely unconstrained by the secondary over primary ratio in contrast to what is claimed in [66]. A more careful approach have to include primaries in the fitting procedure as is done in the next section. For the sake of completeness we show in the following the fluxes of antiprotons (fig. 4.8), positrons (fig. 4.9), electrons (fig.4.10) and deuterium (fig. 4.11).

The antiproton flux is in good agreement with data for the DC model while the DR case exhibits a recurrent well known underestimated flux [104; 105]. We remind the reader that to reach the right amount of antiprotons we added to the primary flux even the secondary and tertiary contribution. Anyway the antiprotons flux that we obtain here have not physical meaning because antiprotons are completely secondaries (a primary source can only be justified with a dark matter contribution) so that their production is strongly correlated to the protons and helium flux that are not properly fixed by B/C (the same argument holds for positrons). Positrons are difficult to be interpreted qualitatively because they are strongly modified by solar modulation, but we notice that the DR flux is clearly higher than the DC flux in the solar modulated

region (see fig. 4.9). Surprisingly the electron flux, that are the most problematic to reproduce because highly modified by the local bubble environment [72], are well described by our models.

4.5 Cosmic Ray Fluxes Based on the Proton, helium, B/C and SubFe/Fe

As demonstrated in the previous section, a fit based only on B/C data is not enough to fix properly all the parameters of a diffusion model. Thus we are forced to introduce some primaries. The most precise measurement are found to be the one relative to protons and helium. Moreover, since in the literature accurate data about the ratio SubFe/Fe can be found easily, we decided to include them too.

$Model - Number$	D_0 (cm^2/s)	δ_1	δ_2	γ_1	γ_2	dV_C/dz $(Km\,s^{-1}$ $Kpc^{-1})$	$V_A(km/s)$	$\tilde{\chi}^2$
$DC - 6897$	2.7×10^{28}	0	0.58	2.5	2.22	8	0	5.12
$DR - 1576$	6.4×10^{28}	0.25	0.25	2.38	2.38	0	22	9.78

Table 4.10: Best models reproducing the protons, helium, B/C and SubFe/Fe data.

As pointed out in the previous section, considering B/C ratio is enough to fix parameters describing diffusion (the injection parameter are not sensible to sec/prim ratio) so that the net effect of introducing the SubFe/Fe ratio is to enlarge the statistic. In principle we could include even other primaries and ratios but the high energy cross sections are well known only for the cases that we considered. The best parameter set for the DC and DR models can be found in table 4.10. One can notice that with respect to the B/C fit, the parameters of the DC model undergoes a changing of the diffusion coefficient normalization and spectral index from the value of 2.5×10^{28} and 0.48 to 2.7×10^{28} and 0.58, respectively. In addiction, the convection velocity turns from 10 to 8. On the other side the injection indices γ_1 and γ_2 are left fixed to the

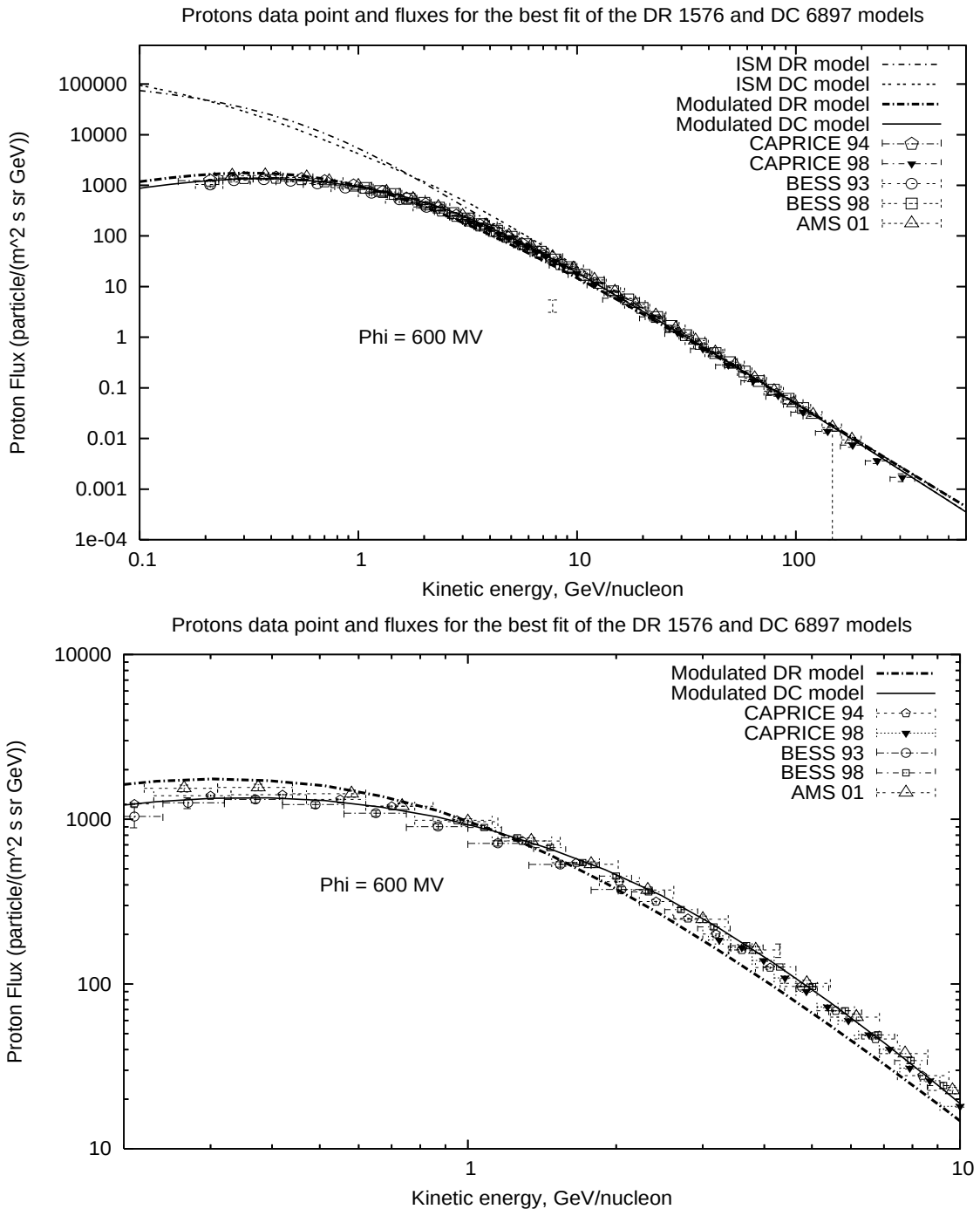

Figure 4.12: Best fits of the DC and DR models with data for the proton flux. The fitting has been done considering protons and helium as primaries together with B/C and SubFe/Fe ratios. In the lower panel the kinetic energy region GeV is magnified.

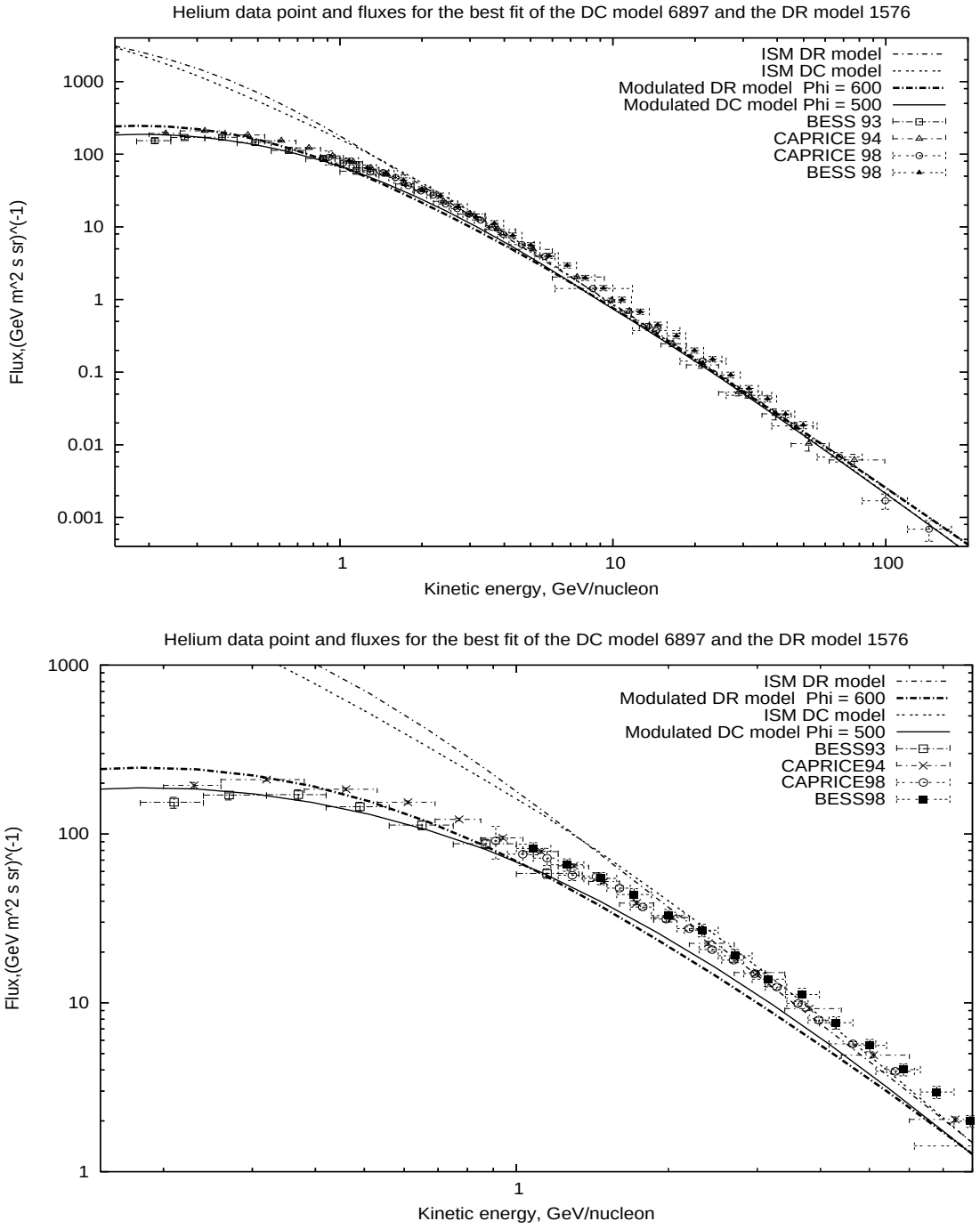

Figure 4.13: Best fit of the DC and DR model with data for the helium flux, fitting protons and helium as primaries together with B/C and SubFe/Fe ratios. In the lower panel the kinetic energy interval 0.1-8 GeV is magnified.

Model-Number	D_0 (cm^2/s)	δ_1	δ_2	γ_1	γ_2	dV_C/dz $(Km\,s^{-1}$ $Kpc^{-1})$	$V_A(km/s)$	$\tilde{\chi}^2$
$DR-2024$	6.7×10^{28}	0.27	0.27	2.38	2.38	0	22	13.27

Table 4.11: Best model for the fit based on protons and helium.

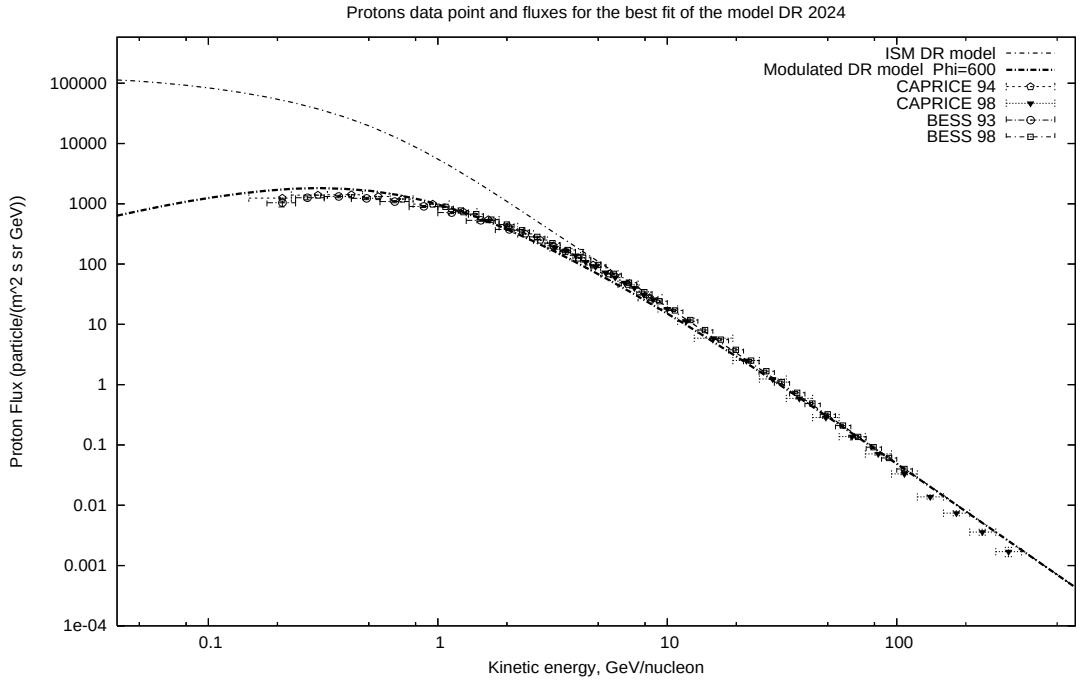

Figure 4.14: Best fits of the DR model together with data for the proton flux. The fitting has been done considering protons and helium.

maximum and minimum value respectively. This suggests that the interval of these two parameters should be enlarged accordingly. Concerning the DR model the situation is completely different since all the parameters are changed and the χ^2 raises dramatically to the value of 9.78. This a consequence of the fact that the DR model is not able to

Dataset	χ^2	$\tilde{\chi}^2$	number of data
BESS 98 - protons [97]	149.91	5.00	31
BESS 93 - protons [96]	10.25	1.28	9
CAPRICE 94 - protons [99]	1079.67	63.51	18
CAPRICE 98 - protons [100]	189.30	7.89	25
BESS 98 - helium [97]	67.04	2.68	26
BESS 93 - helium [96]	21.43	3.57	7
CAPRICE 94 - helium [99]	321.07	13.38	25
CAPRICE 98 - helium [100]	225.85	9.41	25

Table 4.12: χ^2 for the fit between model DR 2024, protons and helium for the considered datasets.

Dataset	χ^2	$\tilde{\chi}^2$	number of data
BESS 98 - protons [97]	166.22	5.54	31
BESS 93 - protons [96]	55.68	0.92	9
CAPRICE 94 - protons [99]	946.60	55.68	18
CAPRICE 98 - protons [100]	220.37	9.18	25
BESS 98 - helium [97]	77.35	3.09	26
BESS 93 - helium [96]	14.24	2.37	7
CAPRICE 94 - helium [99]	368.71	15.36	25
CAPRICE 98 - helium [100]	271.52	11.31	25

Table 4.13: χ^2 for the fit between model DR 1576 and protons for the considered datasets.

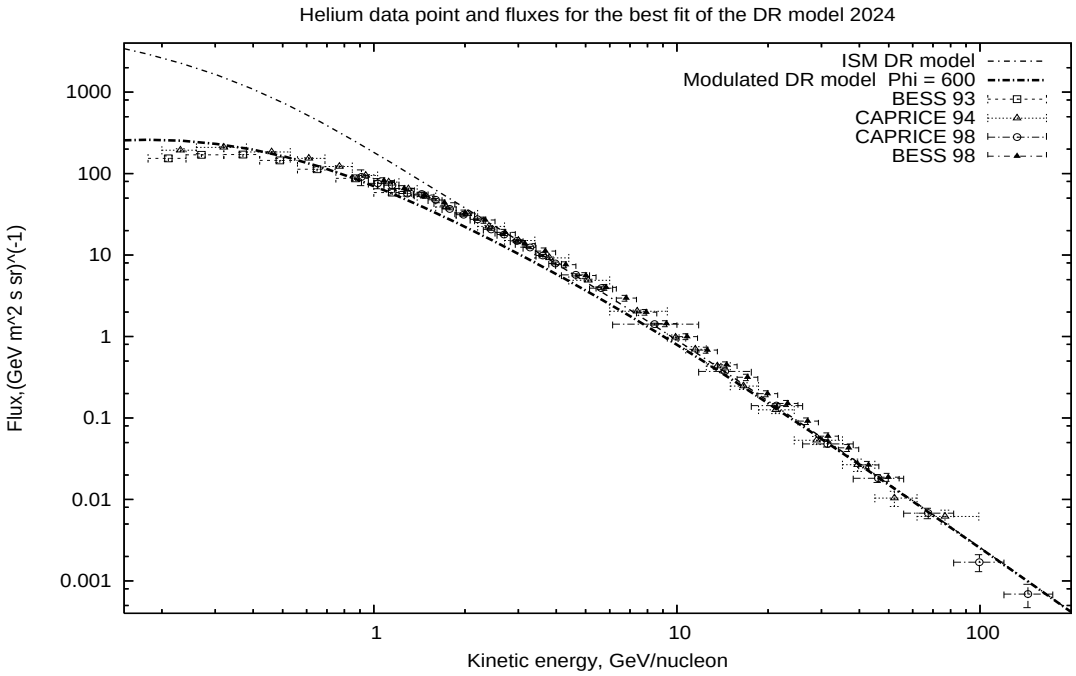

Figure 4.15: Best fit of the DR model and data for helium flux, fitting protons and helium.

agree with primaries data, at least for the parameter space that we are considering. To underline this aspect we try to fit on protons and helium. The best model turns out to be the DR 2024 reported in table 4.11 with a $\tilde{\chi}^2$ equals to 13.17 not so far from the model DR 1576 where $\tilde{\chi}^2 = 13.24$. This demonstrate that the narrow error bars of the primaries data are highly constraining, more than the secondary over primary ratios thus the fitting is almost completely determined by protons and helium. Even the high values of the χ^2 can be addressed to the great accuracy that characterize the experimantal determination of primaries. Just a glance at tables 4.12 and 4.13 is enough to understand that the experiments CAPRICE 94 and CAPRICE 98, where the fluxes are determined with great precision, are responsible for the high value of the $\tilde{\chi}^2$. Anyway the displacement between the DR and DC best fits is reduced with respect to the B/C based fits, in behalf of a better matching with low energy data as manifest by having a look to the protons and helium fluxes reported in figures 4.12 and 4.13. Any improvement of the fit on protons and helium in the DR 2024 model is not appreciated by only looking at 4.14 and 4.15 but a quantitative analysis of the χ^2

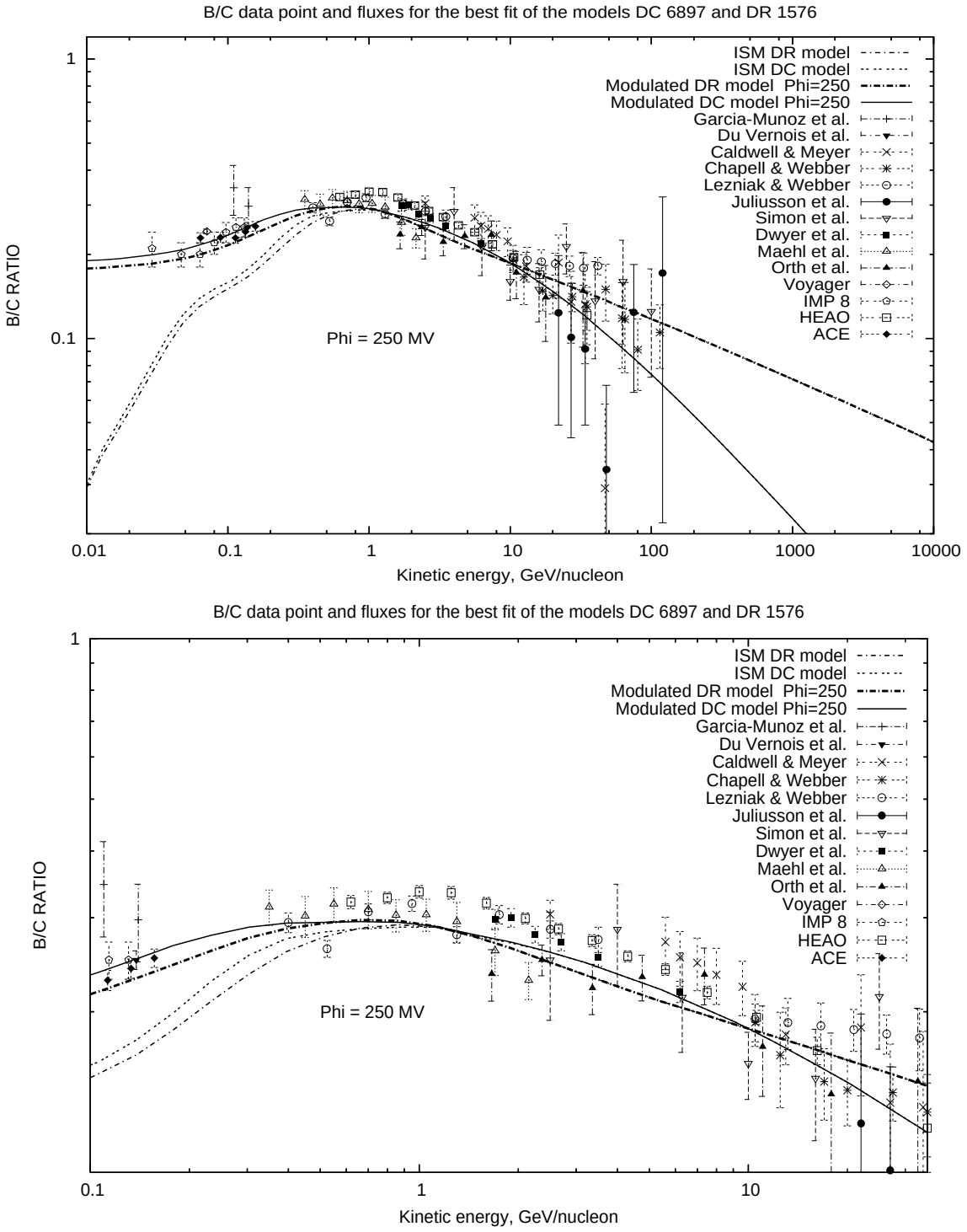

Figure 4.16: Best fits of the DC model and DR model together with data for the B/C ratio. The fitting has been done considering protons and helium as primaries together with B/C and SubFe/Fe ratios. In the lower panel the kinetic energy interval 0.1-35 GeV is magnified.

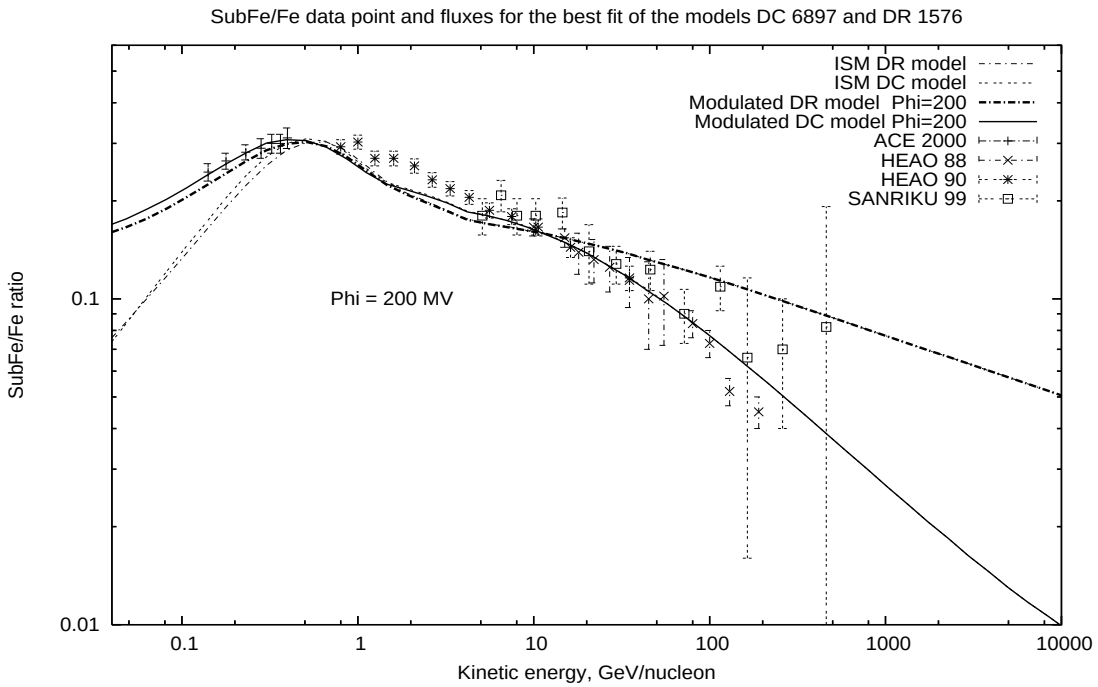

Figure 4.17: Best fit of the DC model, DR model and data for SubFe/Fe ratio, fitting protons and helium as primaries together with B/C and SubFe/Fe ratios.

values reveals the refinement (just compare tables 4.13 and 4.12).

The above considerations lead us to the conclusion that DR models are not able to produce fluxes that fit properly primaries as the DC models do. Honestly, if we take into account the χ^2 values associated to the best models (table 4.10), we are far from a truly compatibility between predictions and observations as for instance is obtained in a weighted slab framework [2] where $\tilde{\chi}^2 \sim 1 - 2$. Anyway we can always search for the set of parameters that better approach the collected data without asking a full matching. In this sense the χ^2 becomes only a index of reference that lead to qualitative conclusions. With this in mind let us pass to the B/C and SubFe/Fe ratios where we observe (see figures 4.16 and 4.17) the same feature of the previous section : strictly different behavior at energies above 20 GeV/nucleon. Again we stress that new high energy measurements are decisive to disentangle the models. This time we want to understand what happens if we introduce the high energy constraint discussed in the previous section. To this end we found the best fits (table 4.14) among the models whose parameters satisfy $\alpha = \delta + \gamma \in [2.68, 2.72]$. The constraint reduce the

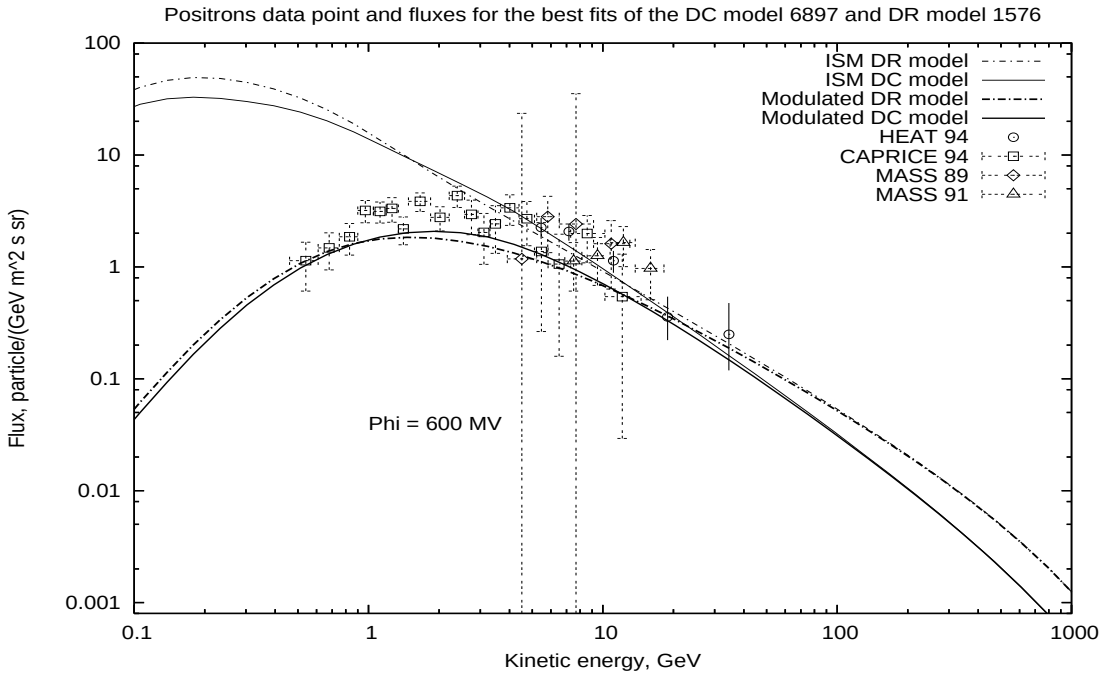

Figure 4.18: Best fits of the DC model and DR model together with data for the electron flux. The fitting has been done considering protons and helium as primaries together with B/C and SubFe/Fe ratios.

number of allowed models to 576 and 240 for the DC and DR cases, respectively. For the DC model the diffusion parameters are not changed but the high energy injection spectral index and the convection velocity are reduced. The final spectrum coefficient turns out to be $\alpha = 2.72$. The DR model allow a nice surprise since the constraint force to select a Kolmogorov spectrum. By reversing this argumentation we can say that the Kolmogorov spectrum selects a high energy behavior described by $\alpha = 2.68$. By matching with the unconstrained result of the DR case we see that the diffusion is enhanced, the injection spectrum weakened and connection between diffusion and reacceleration is left unchanged (this means that the reacceleration is damped since the spatial diffusion coefficient is augmented).

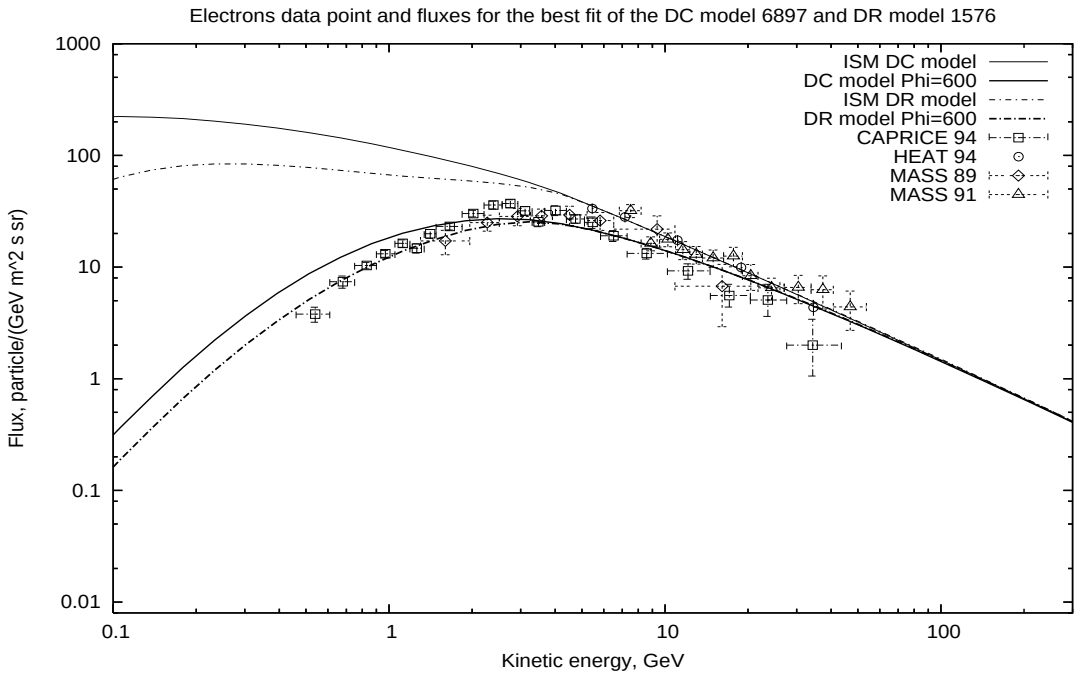

Figure 4.19: Best fits of the DC model and DR model together with data for the electron flux. The fitting has been done considering protons and helium as primaries together with B/C and SubFe/Fe ratios.

$Model$	D_0 (cm^2/s)	δ_1	δ_2	γ_1	γ_2	dV_C/dz $(Km\,s^{-1}$ $Kpc^{-1})$	$V_A(km/s)$	$\tilde{\chi}^2$	$N.\ of$ $Models$
DC	2.7×10^{28}	0	0.58	2.5	2.14	5	0	7.11	576
DR	6.7×10^{28}	0.33	0.33	2.35	2.35	0	22	13.02	240

Table 4.14: Best models reproducing the protons, helium, B/C and SubFe/Fe data with the constraint on the high energy spectral index $\alpha = \delta + \gamma \in [2.68, 2.72]$.

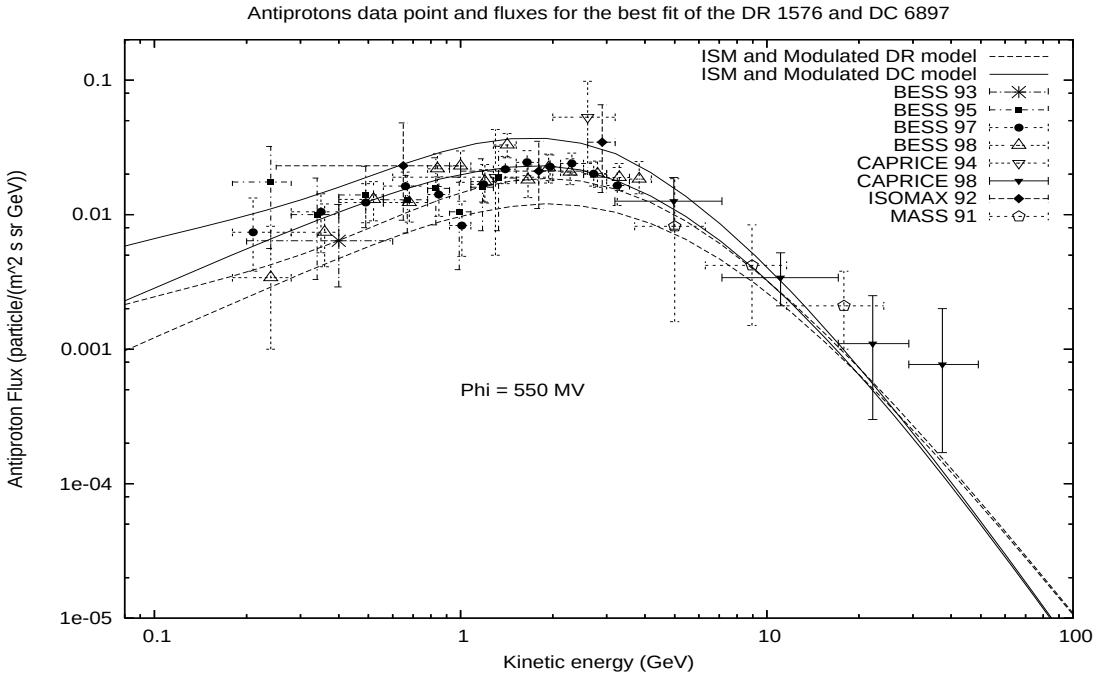

Figure 4.20: Best fit of the DC model, DR model and data for antiprotons, fitting protons and helium as primaries together with B/C and SubFe/Fe ratios.

As expected the $\tilde{\chi}^2$ values restricted to the B/C data are increased with respect to the previous section. Respectively we have $\tilde{\chi}^2_{DC} = 4.97$ and $\tilde{\chi}^2_{DR} = 4.38$ for the DC 6897 and DR 1576 models. This is the price that we have to pay in order to enlarge our analysis.

The positron flux (fig 4.18) is very similar for both models at energies below 20 GeV. In this low energy region the positrons experience a decisive solar modulation so that the gap between our best fits and data can be filled by a proper study of solar modulation. At high energies, where the solar modulation has no more effect, the DR model flux becomes higher and higher than the DC model one but no data are available to select the right model. Concerning electrons (fig. 4.19) we see that the high energy behavior beyond 4 GeV is the same for both models while at low energy the DR model better matches data. The DC model in this case overestimate the expected flux. The electrons are strongly correlated to positrons since in the past a reliable positron spectrum in connection with measurements of positron fraction, has been used to have clues on electron spectra [72]. This happened because the

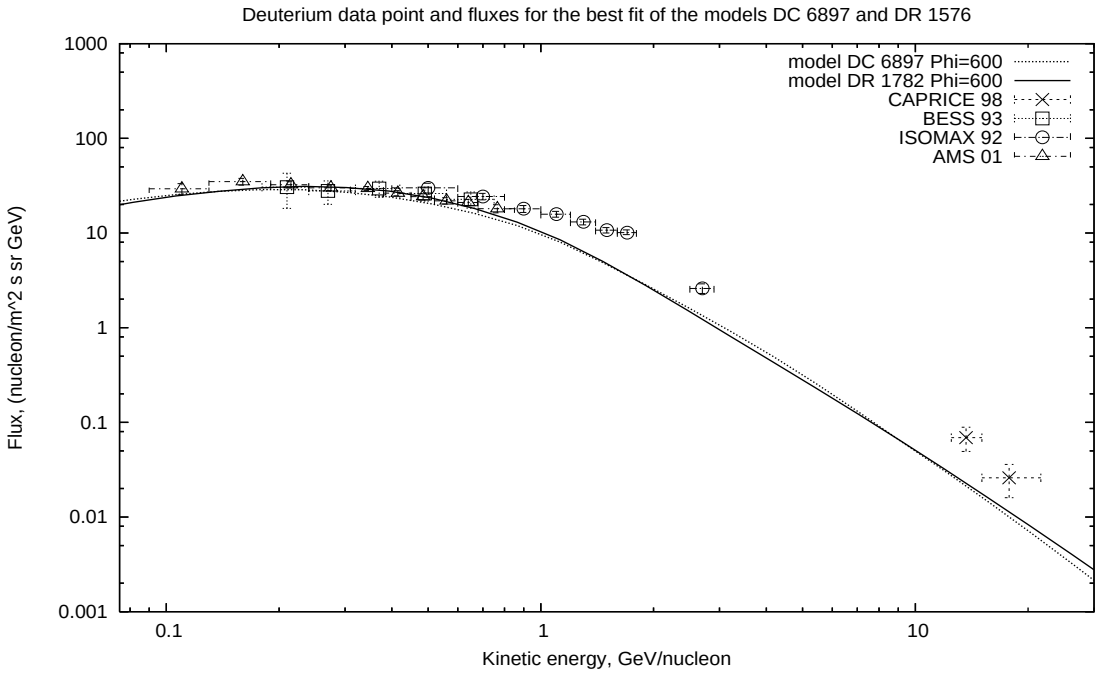

Figure 4.21: Best fit of the DC model, DR model and data for Deuterium, fitting protons and helium as primaries together with B/C and SubFe/Fe ratios.

positron fraction is more easily measured by experiments. Nowadays we have data that are good enough to disentangle positrons and electrons. It is important to notice that our analysis provides a fairly good electron flux without invoking a nucleon flux stronger than the measured one as claimed in [72]. A deeper investigation on electrons and positrons may be carried out by including a fit on positron fraction, synchrotron radiation and gamma rays but this is out of the task of this work where we only give an idea of the fluxes that came out from a nucleon based fitting. The antiprotons (fig. 4.20) are clearly underestimated by the DR model while the DC one seems to be in agreement with experiments. Clearly antiprotons favour the DC model as discussed in the previous section. As is seen in figure 4.21, even the flux of the Deuterium is well estimated by our models, at least below 1 GeV. This is a good result since the disagreement above 1 GeV is due to the absence of proper high energy cross sections for the main channels $p, He + C, N, O \rightarrow He^2$ [106]. Similar results can be found in [107].

Another aspect that we want to examine is the determination of a proper range of

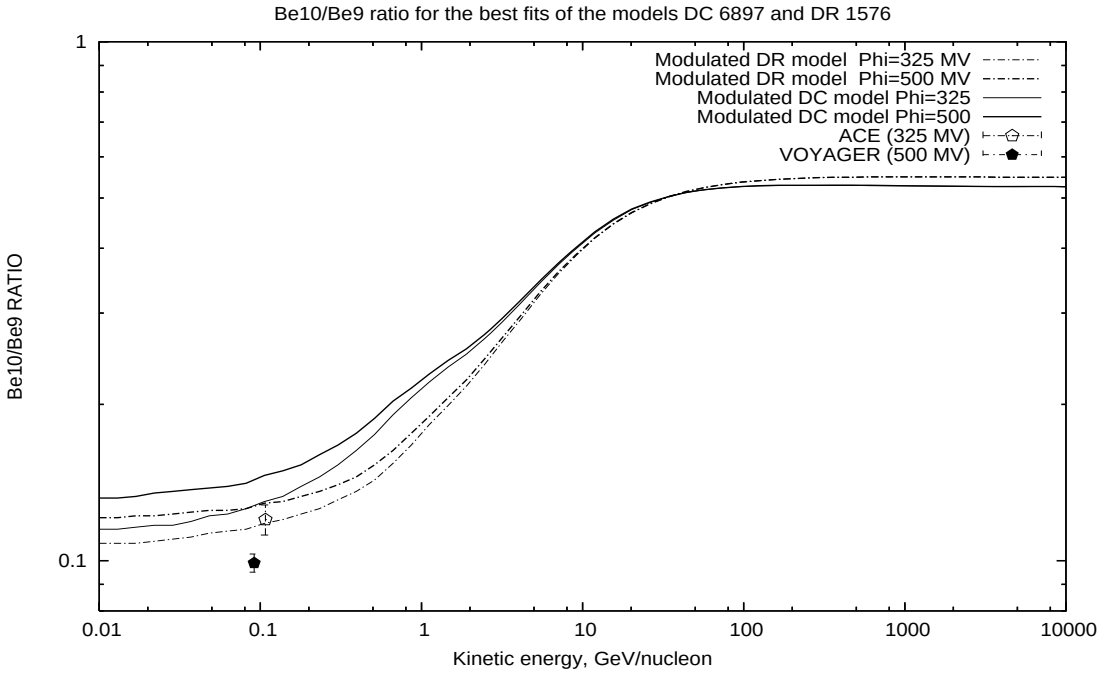

Figure 4.22: Best fits of the DC 6897 model and DR 1576 model together with data for the isotopic $^{10}Be/^{9}Be$ ratio. The fitting has been done considering protons and helium as primaries together with B/C and SubFe/Fe ratios.

parameters as it is suggested by our scanned models. To this end we choose a value of the $\tilde{\chi}^2$ and we look for the models that do not exceed this value. Then we derive interval for each parameter which include all the models satisfying this requirement obtaining what is summed in tables 4.15 and 4.16.

First of all we notice that there are not disconnected island in the parameter space. This tells us that the steps are sufficiently small but it is manifest that the DR models are less thick than the DC case. In fact the steps chosen for the $\tilde{\chi}^2$ of the DR models are ten times more wider than the one adopted for the DC models while for each step we enlarge the sample of more or less the same amount of parameter sets. Concerning the intervals we notice that for almost all parameters there is a edge value that is always touched. This means that to refine the analysis we should enlarge the interval in that direction. We conclude that the suggested guidelines for future developments turn out to be as follows :

- for DC models, D_0, γ_1, γ_2 and dV_C/dz should be pushed beyond the values

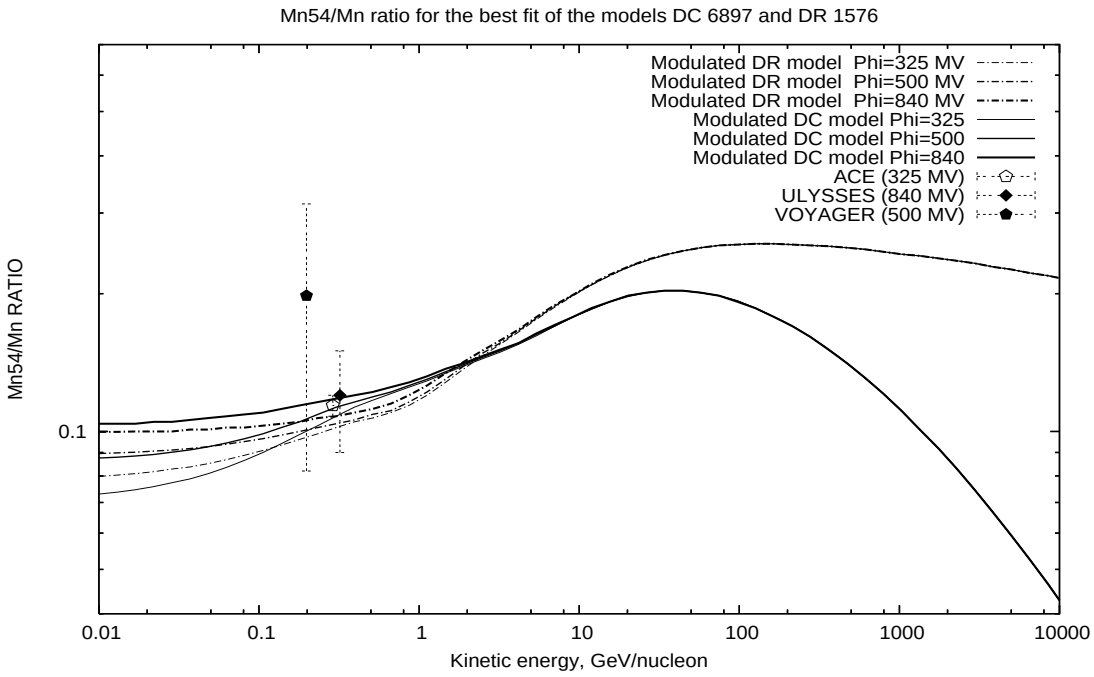

Figure 4.23: Best fits of the DC 6897 model and DR 1576 model together with data for the isotopic $^{54}Mn/Mn$ ratio. The fitting has been done considering protons and helium as primaries together with B/C and SubFe/Fe ratios.

$\tilde{\chi}_0^2$	D_0 (cm^2/s)	δ_2	γ_1	γ_2	dV_C/dz $(Km\,s^{-1}$ $Kpc^{-1})$	$Number$ $of\ Models$
5.2	$(2.5-2.7)\times 10^{28}$	0.58-0.60	2.5	2.22	8-10	4
5.3	$(2.4-2.7)\times 10^{28}$	0.58-0.6	2.48-2.5	2.22	7-10	9
5.4	$(2.3-2.7)\times 10^{28}$	0.58-0.62	2.48-2.5	2.2-2.22	7-10	21
5.5	$(2.2-2.7)\times 10^{28}$	0.56-0.62	2.48-2.5	2.2-2.22	6-10	35

Table 4.15: Intervals spanned by DC models whose $\tilde{\chi}^2$ does not exceed the $\tilde{\chi}_0^2$ limit.

2.7×10^{28}, 2.5, 2.22 and 10 respectively while δ_2 seems to be well centered even if an increasing beyond the 0.62 value is recommended;

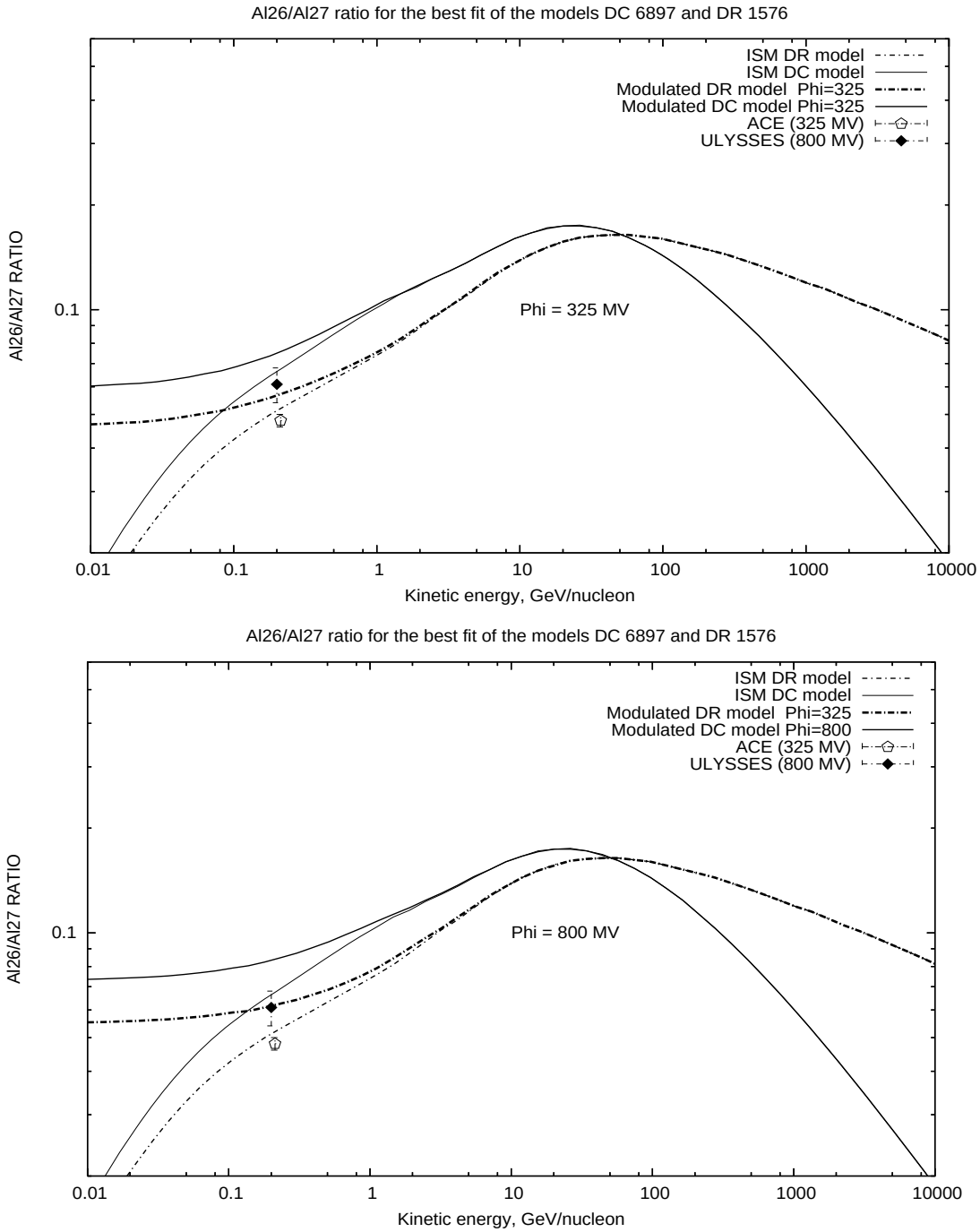

Figure 4.24: Best fits of the DC 6897 model and DR 1576 model together with data for the isotopic $^{26}Al/^{27}Al$ ratio. The fitting has been done considering protons and helium as primaries together with B/C and SubFe/Fe ratios. A solar modulation of $\Phi = 325$ MV which is associated to the ACE experiment, is considered in the upper panel while $\Phi = 800$ MV for the ULYSSES experiment is considered in the lower one.

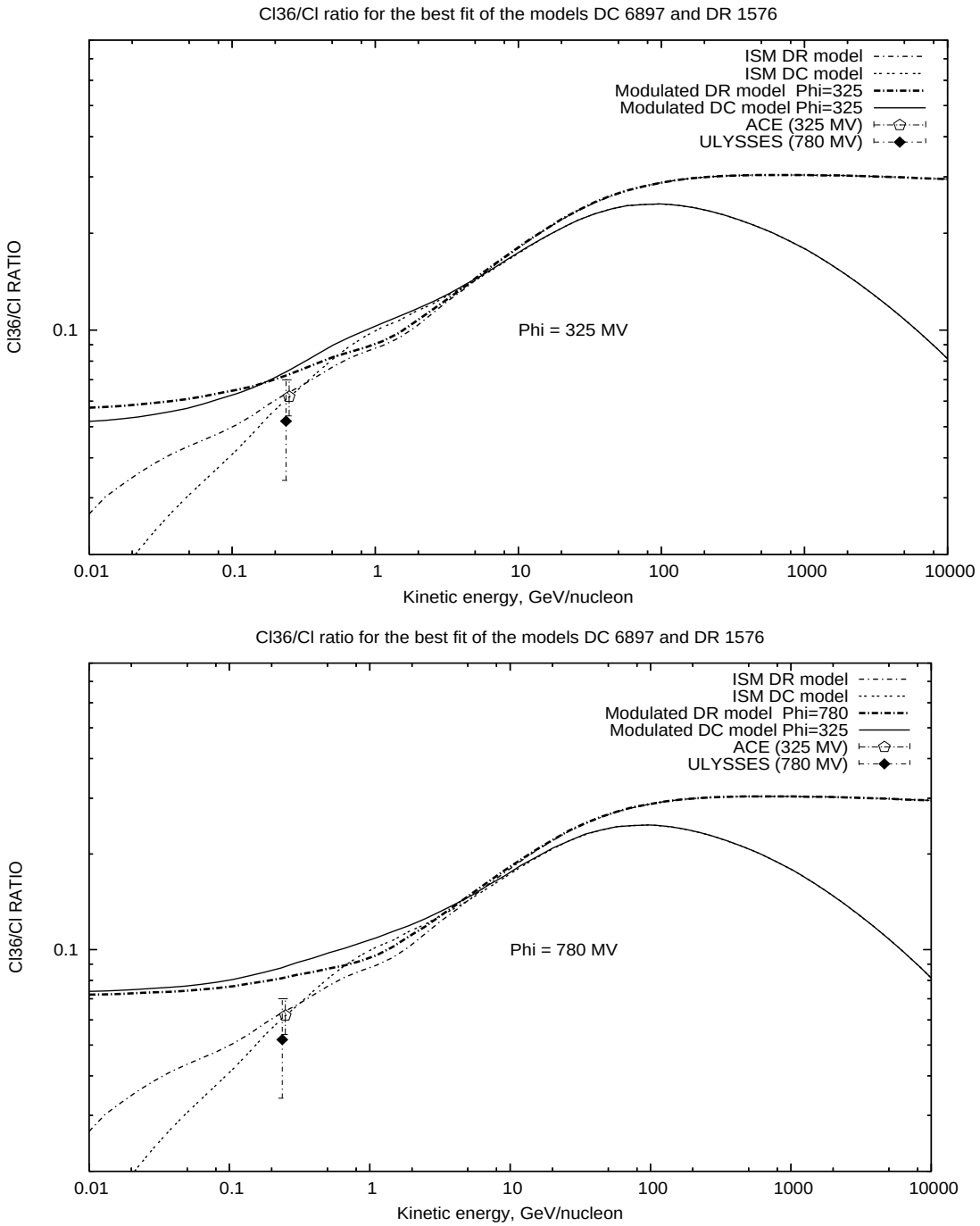

Figure 4.25: Best fits of the DC 6897 model and DR 1576 model together with data for the isotopic $^{36}Cl/Cl$ ratio. The fitting has been done considering protons and helium as primaries together with B/C and SubFe/Fe ratios. A solar modulation of $\Phi = 325$ MV which is associated to the ACE experiment, is considered in the upper panel while $\Phi = 780$ MV for the ULYSSES experiment is considered in the lower one.

$\tilde{\chi}^2_0$	D_0 (cm^2/s)	δ	γ	V_A (Km/s)	$Number\ of\ Models$
10.0	6.7×10^{28}	0.25	2.35-2.38	22	2
10.5	$(5.8 - 6.7) \times 10^{28}$	0.25-0.29	2.35-2.38	22-26	11
11.0	$(5.8 - 6.7) \times 10^{28}$	0.25-0.29	2.35-2.41	22-26	20
11.5	$(5.5 - 6.7) \times 10^{28}$	0.25-0.31	2.35-2.41	22-26	26

Table 4.16: Intervals spanned by DR models whose $\tilde{\chi}^2$ does not exceed the $\tilde{\chi}^2_0$ limit.

- for DR models, a decreasing of the parameters δ, γ and V_{alf} over 0.25, 2.35 and 22 respectively together with an increasing of D_0 beyond 2.7×10^{28}, seems to be the right way.

The fact that the intervals that we considered for our analysis are not exactly the proper ones is not surprising since they are suggested by past works based on B/C data alone. Here we are proving that the primaries necessarily shift the parameters values and consequently the intervals to be considered for the scan.

In order to carry out our analysis plan, we need to include unstable elements to select the right halo height. Before proceeding it is wise to check if it is possible to go further by having a look to what our best fits say about unstable elements. The comparison between models DC 6897, DR 1576 and data is shown in figures 4.22, 4.24, 4.25 and 4.23 respectively for the isotopic ratios $^{10}Be/^{9}Be$, $^{26}Al/^{27}Al$ at $\Phi = 325$ MV, $^{26}Al/^{27}Al$ at $\Phi = 500$ MV, $^{36}Cl/Cl$ at $\Phi = 325$ MV, $^{36}Cl/Cl$ at $\Phi = 500$ MV and $^{54}Mn/Mn$. The point here is that we are analyzing a sector which is highly influenced by solar modulation. All we can do is to trust the modulation values associated to each experiment as are given in the literature (see section 4.3), wondering if we have any chance of agreement. For all the isotopic ratios we observe that the ratio grows with the increasing of the modulation strength. For the Beryllium case the value observed by ACE at $\Phi = 325$ MV is touched by both models but the VOYAGER prediction at

$\Phi = 500$ MV is completely out of scale.

In fact in this last case we have a lower value of the ratio but a higher modulation that lead to an incompatibility with the ACE result. This can be justified by the too large time period considered for the VOYAGER missions which leads to averaged solar modulation strength that is probably not the proper one. Anyway we will include both missions in this work. Concerning the $^{26}Al/^{27}Al$ we have the data points that do not show contradictions as in the $^{10}Be/^{9}Be$ case. In fact the increasing of the ratio data join a growing of the solar modulation strength. However the DC 6897 model clearly overestimate experiments results while the DR 1576 model seems to be promising especially for the ULYSSES case. Turning to the $^{36}Cl/Cl$, we encounter the same problem discussed for the $^{10}Be/^{9}Be$ case which is the value of the ratio estimated by ULYSSES with solar modulation stronger than the ACE one, is smaller than the ratio value deduced by the ACE mission. However the two data are compatible thanks to the relatively wide errors associated to the ULYSSES point. Anyway both models overestimate the $^{36}Cl/Cl$ ratio.

Finally we spend a few words on the $^{54}Mn/Mn$ ratio where the fluxes from our simulation rest inside the error bars even if the data follow the same trend that we observed for the $^{36}Cl/Cl$ and $^{10}Be/^{9}Be$ cases. In conclusion it seems reasonable to proceed further with our analysis including the isotopic ratios commented above.

4.6 The halo height and Local Parameters from isotopic ratios

So far we centered our search for the best fits at a fixed value (4 Kpc) of the halo height. Now we want to perform a variation of this parameter in order to find the value that better fit the isotopic ratio available data. We enlarged the results summed in table 4.1 in favor of a range of the halo height that runs from 2 Kpc to 6 Kpc with a step of 200 pc. For this choice we were influenced by the work [55] of the authors of the GALPROP program that used the ratio $^{10}Be/^{9}Be$ to gain informations about the halo in connection with the *Ulysses* data [93]. The resulting halo height interval compatible with measurements was $z_h = 4 - 12$ Kpc. Further improvement was presented in [73] where the ACE data were added to obtain the more robust estimate $z_h = 3 - 7$ Kpc.

Halo Height (Kpc)	$\tilde{\chi}^2_{u/s}$	$\tilde{\chi}^2_{p,He,B/C,SubFe/Fe}$	$\tilde{\chi}^2_{p,He,B/C,SubFe/Fe,u/s}$
2	65.87	48.16	48.46
2.2	50.31	41.23	41.33
2.4	39.23	34.99	34.99
2.6	31.18	29.41	29.36
2.8	25.23	24.48	24.42
3.0	20.77	20.22	20.17
3.2	17.38	16.66	16.63
3.4	14.77	13.82	13.80
3.6	12.74	11.73	11.71
3.8	11.15	10.38	10.36
4.0	9.89	9.78	9.75
4.2	8.90	9.91	9.85
4.4	8.10	10.75	10.65
4.6	7.45	12.28	12.11
4.8	6.93	14.45	14.21
5.0	6.51	17.22	16.89
5.2	6.17	20.56	20.13
5.4	5.88	24.42	23.87
5.6	5.65	28.76	28.08
5.8	5.46	33.53	32.71
6.0	5.30	38.69	37.71

Table 4.17: χ^2 obtained by different kind of fitting : unstable over stable ratios (second column); protons, helium, B/C and SubFe/Fe (third column); protons, helium, isotopic, B/C and SubFe/Fe ratios. The halo height is varied and the other parameters are taken from the DR 1576 model.

Other important estimations come from [75] that predicts $z_h = 2-4$ Kpc from HEAO-3 and from [76] that gives $z_h = 4.9^{+4}_{-2}$ Kpc. The other parameters are left fixed to the values that we found for the best fits based on protons, helium, boron over carbon and sub-iron over iron. The total number of set of parameters analyzed amount to 40, 20

Halo Height (Kpc)	$\tilde{\chi}^2_{u/s}$	$\tilde{\chi}^2_{p,He,B/C,SubFe/Fe}$	$\tilde{\chi}^2_{p,He,B/C,SubFe/Fe,u/s}$
2	80.58	23.54	24.92
2.2	70.80	18.92	20.19
2.4	63.55	15.24	16.42
2.6	58.05	12.32	13.45
2.8	53.79	10.03	11.12
3.0	50.46	8.29	9.34
3.2	47.80	7.00	8.02
3.4	45.68	6.09	7.08
3.6	43.95	5.51	6.47
3.8	42.55	5.20	6.14
4.0	41.39	5.12	6.03
4.2	40.44	5.23	6.11
4.4	39.65	5.50	6.35
4.6	39.00	5.89	6.72
4.8	38.45	6.40	7.20
5.0	38.00	6.98	7.75
5.2	37.62	7.64	8.38
5.4	37.30	8.34	9.06
5.6	37.04	9.08	9.77
5.8	36.81	9.85	10.51
6.0	36.63	10.63	11.26

Table 4.18: χ^2 obtained by different kind of fitting : unstable over stable ratios (second column); protons, helium, B/C and SubFe/Fe (third column); protons, helium, B/C, SubFe/Fe and isotopic. The halo height is varied and the other parameters are taken from the DC 6897 model.

for the DC model and 20 for the DR one. The values of the χ^2 are summed in tables 4.17 and 4.18 where we see in the second columns a sharp decreasing of the $\tilde{\chi}^2$ with the increasing of the halo height. Thus it is clear that unstable over stable ratios suggest a value of the halo height that exceeds our maximum value. Since we assumed from the

beginning that the fit based on primaries and secondary over primary ratios is weakly influenced by the halo dimensions, it is reasonable to check if it is true. To this end we reported the $\tilde{\chi}^2$ obtained from primaries and secondary over primary ratios, in the third columns of tables 4.17 and 4.18. It is obvious that we have a correlation that suggest 4 Kpc as the best halo height. This justifies the predictions already presented in the literature [73; 75; 76]. In fact the value of 4 Kpc is often used as a reference to study other parameters [105]. Moreover we have to admit that our choice of fixing the halo height is not completely correct but a simultaneous scan of all the parameters should be carried out. In the last columns of tables 4.17 and 4.18 we show that isotopic data do not influence the fits based on stable nuclei because of the small statistic coming from just 9 data-points. It turns out that the best DC and DR models are always the same and only the $\tilde{\chi}^2$ values are increased to 6.03 and decreased to 9.75 respectively. This lead to the conclusion that it is too early to include unstable over stable data in this kind of global analysis even if we can always say that we determined the best fits based on the wider knowledge that we can draw from the literature. More interesting is to single out the unstable nuclei to gain some specific information as we have done for the halo height estimation. Let us ask ourselves how the isotopic data affect the propagation parameters. The answer to this question is found in [36]. As explained in section 1.4.5, a deep understanding of the travel-distance of an unstable nucleus reveals that the kinetic energies of our experimental data are not sufficient to reach the halo boundary (see table 1.5). Anyway it is almost sure that there is some kind of linking between propagation parameters and isotopic ratios. The point is that table 1.5 tells us that unstable nuclei are a unique tool to have clues about our local environment, more than a probe for galactic halo. In [36] this idea has been developed introducing a cylindrical hole centered at the sun position. Inside this hole the density is lower than in the galactic disk leading to a lowering of the spallation source term, fragmentation and energy losses. The effect of this local bubble surrounding the sun is a reduction of the unstable secondaries because they are not produced in the gas depleted region. Accordingly the influence on the halo height is a overestimation since this forces the nuclei to decay before reaching us. This explain why the fitting on the isotopic ratios predicts a large value of the halo height and shed light on the misleading nature of the connection between halo and unstable nuclei. A proper analysis can be focused, for instance, on the estimate of the hole dimensions by exploiting the unstable nuclei. This

approach can be applied to realistic modelling of the local bubble as found in [76; 108].

The grid scan of the present work do not include a local bubble but it is interesting to realize how the propagation parameters are changed by a fitting on the isotopic ratios that leaves fixed the halo height at 4 Kpc. The best fits for this last case are found in table 4.19.

Model-Number	D_0 (cm^2/s)	δ_1	δ_2	γ_1	γ_2	dV_C/dz $(Km\,s^{-1}$ $Kpc^{-1})$	$V_A(km/s)$	$\tilde{\chi}^2$
$DC-6024$	2.7×10^{28}	0	0.48	2.42	2.22	5	0	33.98
$DR-2344$	6.7×10^{28}	0.37	0.37	2.53	2.53	0	22	9.05

Table 4.19: Best DC and DR models reproducing the isotopic ratio data.

Concerning the DC model we do not have a clear trend but this reflects the high disagreement with data. The DR model, that is more effective in reproducing secondary over primary ratio even in the unstable case, clearly confirms the above comments about the lowering effects of a local bubble. In fact the diffusion parameters reach their maximum value and reacceleration is strongly damped by lowering the Alfvén velocity. In conclusion there is a tendency to reduce the isotopic ratio as expected by the presence of a local low density zone around the solar system.

Conclusions

In this work we explored the possibility of a statistical approach to the GALPROP model. The idea has been to include all the knowledge about cosmic ray physics in order to fix the free parameters in the GALPROP model. Among the data that we considered we remember the B/C and SubFe/Fe secondary over primary ratios, protons, helium and isotopic ratios ($^{10}Be/^{9}Be$, $^{26}Al/^{27}Al$, $^{36}Cl/Cl$, $^{54}Mn/Mn$) taken from a plenty of satellite and balloon borne experiments for a total of 313 points. Since we chosen to analyze a grid in the parameter space, the analysis has been very time consuming, so that in order to reduce the required time (that strongly depend on the number of parameters), we applied a two step method where on a first stage the relevant propagation parameter are tuned to reproduce the B/C and SubFe/Fe secondary over primary ratios, protons, helium and the halo height has been left fixed to the value of 4 kpc. On a second stage we considered the best fits obtained from the first step to gain information about the halo height from isotopic ratios. The main result is that we obtained the best fits based on almost all the public data on cosmic ray fluxes taking into account all the known physics about cosmic ray. Among the universe of choices presented by the GALPROP model we focused on two particular models, namely diffusion+reacceleration (DR model) and diffusion+convection (DC model), since these are the minimum combinations which can reproduce the key observations. It turns out that the DR model is not able to produce a primary flux that leads to a satisfactory agreement with observations that furnish very precise data. The reason may be due to the parameter space that we considered but it is more likely that it is intrinsic in the GALPROP model as suggested by observing that the authors of the model usually introduce a break in the injection spectrum to fit observations. This conclusion is supported by the fact that after introducing this breaking in the DC model a more accurate prediction of the primary flux is achieved. The isotopic ratio

data strongly suggests that the halo height may be greater than previous predictions but, despite the usual approach found in the literature, it has to be underlined that for the available data on isotopic ratios, the distance covered is not enough to give information about the halo height (if not indirectly). A more proper approach can use unstable nuclei to shed light on local propagation environment, suggesting the existence of a gas-depleted region around the sun (local bubble). We showed that the overestimation of the halo size can be interpreted as a clue of the local bubble presence. All our best fits show a somewhat large value of the $\tilde{\chi}^2$. Among the reasons, a key role is played by a possible incompatibility of the various set of data that sometimes becomes manifest (as for the isotopic ratios). The advent of Pamela mission will offer a solution to this problem providing a never reached precision in the determination of cosmic ray fluxes over a very large range of kinetic energy.

Particular attention has been focused on the guidelines for future developments. To this end we derived the interval spanned by each parameter when we consider all the model whose $\tilde{\chi}^2$ do not exceed a fixed value. From one side such intervals showed that our grid do not leave space to local minimum (at least for our step-size) other than the one that gives us our best fits. From another side we deduced the right direction to enlarge the considered parameter space. In conclusion this work has demonstrated that, despite the usual approach to the GALPROP model that is far from being systematic, a statistical analysis can be performed exploiting the GALPROP code. A further improvement of the parameter grid scan by mean of our statistical approach will prepare the way to find the best model and parameter values exploiting the upcoming data from PAMELA.

Appendix A

Debye Lenght

If we consider a neutral plasma (i.e. null total charge), then the energy from coulombic interaction is generated by the anisotropy in the charge distribution so that we have a correlation between energy and positions of the charged particles. Following the Boltzmann law, the distribution density of the type a particles, reads

$$n_a \;=\; n_{0a} e^{-\frac{z_a e\phi}{T}} \;, \tag{A.1}$$

where n_{0a} is the mean distribution density. We assume that the plasma has small deviations from the perfect gas behaviour which is equivalent to say that the kinetic contribution to the energy, which is proportional to the temperature T, is still much larger than the contribution due to electric interaction. This condition can be written as

$$T >> e z_a \phi \;, \tag{A.2}$$

allowing the expansion of (A.1)

$$n_a \;\simeq\; n_{0a} - \frac{z_a e\phi}{T} \;. \tag{A.3}$$

The field ϕ is linked to the charge distribution through the Poisson equation

$$\Delta\phi \;=\; -4\pi e \sum_a z_a n_a \;. \tag{A.4}$$

Substituting the expansion (A.3) into the Poisson equation we are left with

$$\Delta\phi - \lambda^{-2}\phi \;=\; 0 \tag{A.5}$$

where we introduced the Debye length

$$\lambda \;=\; (\frac{4\pi e^2}{T}\sum_a n_{0a} z_a^2)^{\;-2} \;. \tag{A.6}$$

The equation (A.5) can be easily solved by imposing that the field ϕ vanish at infinity and it reduces to the coulombic field $\phi \;=\; \frac{ez_b}{r}$ of a particle of charge ez_b in the neighbour of $r \;=\; 0$. The solution turns out to be

$$\phi \;=\; ez_b \frac{e^{-\frac{r}{\lambda}}}{r} \;, \tag{A.7}$$

from which it is clear that the field intensity rapidly decrease if r exceeds the Debye length. In this sense λ characterizes the extension of the ionized cloud.

Appendix B

Leaky Box Model

An extremely simplified version of the diffusion model is the so called "leaky-box" model. It can be understood as a limit of a diffusion model providing that there is a strong reflection at the galaxy boundary and little leakage. The first property forces the particles to traverse the galactic plane many times before escaping to intergalactic medium. The second one allow us to consider spatially averaged quantities all over the galaxy thus leading to a density of cosmic rays that is constant. Physically, it can be justified by saying that the diffusion take place rapidly so that, concerning the diffusion term, we can perform the replacement

$$\nabla \cdot (D_i \nabla N_i) \rightarrow -\frac{N_i}{\tau_{esc}}\,, \tag{B.1}$$

where τ_{esc} characterizes the escaping time of cosmic rays from the galaxy. After this substitution we have to think to the motion of particles inside the propagation region as a free motion, taking a distance from a true diffusion model. After the above considerations we are left with the following propagation equation

$$\frac{\partial N_i}{\partial t} = \bar{q}_i - \frac{N_i}{\tau_{esc}} - \frac{\partial}{\partial \epsilon_k}(\bar{b}_i N_i) - (\bar{n} v \sigma_i + \frac{1}{\tau_i}) N_i + \sum_{j<i} (\bar{n} v \sigma_{ij} + \frac{1}{\tau_{ij}}) N_j\,, \tag{B.2}$$

which can be solved straightforwardly, having only the time as differential variable. We can even think that an equilibrium situation has been reached so that the cosmic rays density evolution is stationary in order to have $\partial N_i/\partial t = 0$ leading a further simplification of the propagation equation

$$\bar{q}_i - \frac{N_i}{\tau_{esc}} - \frac{\partial}{\partial \epsilon_k}(\bar{b}_i N_i) - (\bar{n} v \sigma_i + \frac{1}{\tau_i}) N_i + \sum_{j<i} (\bar{n} v \sigma_{ij} + \frac{1}{\tau_{ij}}) N_j = 0\,, \tag{B.3}$$

Introducing the path length function $G(x)$ as in paragraph (2.1) and disregarding ionization, we get

$$\begin{gathered} \frac{\partial G}{\partial x} + \frac{G}{\tau_{esc}} = \chi\delta(x) \\ \Downarrow \\ G(x) = \chi e^{-x/\tau_{esc}}\,, \end{gathered} \tag{B.4}$$

that clarifies the meaning of τ_{esc} governing the exponential decay of cosmic rays density with the increasing of the length of the distance of traversed medium. In fact we can easily find the average amount of matter traversed by a particle of velocity v

$$\lambda_{esc} \equiv < x >= \frac{\int dx\, x\, G(x)}{\int dx G(x)} = \bar{n} v \tau_{esc}\,, \tag{B.5}$$

which leads to the conclusion that the leaky box model is actually characterized only by the parameter λ_{esc} as a consequence that all the nuclei have the same propagation history. Finally, following the steps of the analysis made in paragraph (2.1), we can use the function $F_i(t, \mathbf{r})$ to get a very simple equation for the densities N_i which is

$$N_i \left(\frac{1}{\tau_{esc}} + \bar{n} v\, \sigma_i \right) = \bar{q}_i \tag{B.6}$$

$$\Downarrow$$

$$N_i = \frac{\bar{q}_i}{\bar{n} v} \frac{\lambda_{esc}}{1 + \sigma_i \lambda_{esc}} = \frac{\bar{q}_i\, \tau_{esc}}{1 + \sigma_i \lambda_{esc}}\,. \tag{B.7}$$

Concerning the secondary nuclei, we can directly exploit (B.3) with $q_i = 0$, neglecting ionization losses, to get the equation

$$\lambda_{esc} = \left[\left(\sum_{j<i} (\sigma_{ij} + \frac{1}{\bar{n} v \tau_{ij}}) \right) \frac{N_j}{N_i} - (\sigma_i + \frac{1}{\bar{n} v \tau_i}) \right]^{-1}\,. \tag{B.8}$$

The general strategy to embed a set of cosmic ray data coming from an experiment into a leaky box model, is to consider the secondary to primary ratios, that determine the factor N_j/N_i in (B.8) and consequently λ_{esc} (nuclear cross sections and decay time are assumed to be known a priori). Once that λ_{esc} is known, the primary spectrum can be used to determine the source $\bar{q}_i$ as in (B.6).

Bibliography

[1] Prishchep V.L. & Ptuskin V.S., *AP&SS* **32** 265 (1975).

[2] Jones F.C. et al., *ApJ* **547** 264 (2001).

[3] Jones F.C., *Phys. Rev.* **2** 2787 (1970).

[4] Chandrasekhar S., *Rev. Mod. Phys.* **15** 1 (1943).

[5] Gaisser, T. K., "Kashiwa 2006, Energy budget in the high energy universe", 45-55, astro-ph/0609534.

[6] Fermi, E., Phys. Rev. **75** 1169 (1949).

[7] Engelmann, J.J. et al, *A&A* **148**, 12, (1985).

[8] Blandford, R. D. and Ostriker, J. P., *ApJ* **237** 793 (1980).

[9] Bell, A.R., MNRAS **182** 147 (1978).

[10] Blandford, R.D. and Ostriker, J.P., *ApJ* **221** L29 (1978).

[11] Mannheim, K., & Schlickeiser, R., *A&A* **286** 983 (1994).

[12] Dermer, C. D., *ApJ*, 295, 28, (1985).

[13] Ginzburg, V. L., Theoretical Physics and Astrophysics (Oxford: Pergamon Press, 1979).

[14] Dermer, C. D., & Liang, E. P., *ApJ* **339** 512 (1989).

[15] Moskalenko, I. V., & Jourdain, E., *A&A* **325** 401 (1997).

[16] von Stickforth J., Z. Physik, **164** 1 (1961).

[17] Haug E., Z. Naturforsch., 30a, 1546, (1975).

[18] Koch, H. W., & Motz, J. W., Rev. Mod. Phys., **31** 920 (1959).

[19] Jones F. C., *Phys. Rev.* 137 B1306 (1965).

[20] Bradt H.L. and Peters B., *Phys. Rev.* **77** 54 (1950).

[67] Letaw J. R., Silberberg R. & Tsao C. H., *APJSS* **51** 271 (1983).

[22] Sihver L. et al., *Phys. Rev. C* **47** 1225 (1993).

[23] Wellish H.P. & Axen D.,*Phys. Rev. C* **54** 1329 (1996).

[24] Silberberg R., Tsao C. H. & Barghouty A.F., *ApJ* **501** 911 (1998).

[25] Silberberg R. & Tsao C. H., *APJSS* **25** 315 (1973).

[26] Webber W.R., Kish J.C. & schrier D.A., *Phys. Rev. C* **41** 566 (1990).

[27] Reimer O. et al., *ApJ* **496** 490 (1998).

[28] Audi G. et al., *Nucl. Phys. A* **624** 1 (1997).

[29] Donato F. et al., *Nucl. Phys. A* **381** 539 (2002).

[30] Hagen F. A., Fisher A.J., Ormes J. F., *Astrophys. J.* **212** 262 (1977).

[31] Webber W. R., Lezniak J. A., Kish J. C., Simpson G. A., *Astrophysical Letters* **18** 125 (1977).

[32] Garcia-Munoz M., Mason G. M. & Simpson J.A., *ApJ* **217** 859 (1977).

[33] Freier P. S., Young J.S, Waddington C.J., *ApJ* **240** L53 (1980).

[34] Wiedenbeck M.E., *ICRC 19* **2** 84 (1985).

[35] Leske, R. A., *ApJ* **405** 567 (1993).

[36] Donato F., Maurin D., Taillet R., *A&A* **381** 539(2002); Donato F., Maurin D. and Taillet R., *Proc. 28th Int. Cosmic-Ray Conf.* (Tsukuba) 2003, 1953-1956.

[37] Goldman D.T., *American Institute of Physics Handbook, third edition*, (§**8**) (1982).

[38] Soutoul A. et al., *A&A* **336** L61 (1998).

[39] Maurin D., Donato F., Taillet R., & Salati P., *ApJ* **555** 585 (2001).

[40] Webber, W.R. et al., *ApJ* **390**, 96, (1992).

[41] Berezinskii V.S., Bulanov S.V., Dogiel V.A., Ginzburg V.L. & Ptuskin V.S., *Astrophysics of Cosmic Rays* (Amsterdam: North Holland) 1990.

[42] Akhiezer, I.A. et al., "Plasma Electrodynamics", (Pergamon Press, Oxford, 1975).

[43] Kennel, C.F. and Engelmann, F., Phys. Fluids **9** 2377 (1966).

[44] Gleeson, L. J. and Axford, W. I., *ApJ* **154** 1011 (1968).

[45] Lukasiak, A. et al. *ApJ* **423**, 426, (1994).

[46] Phyllipps, S., et al., *A&A* **103**, 405, (1981).

[47] Stanek,K.Z. and Garnavich, P.M., *ApJ* **503**, L131, (1998).

[48] Alves, D.R., *ApJ* **539**, 732, (2000).

[49] Strong A. W. and Mattox J. R., *A & A* **308** L21 (1996).

[50] Case G. & Bhattacharya D., *A& A* **120 C** 437 (1996).

[51] Meyer J.-P., Drury L. O'C. & Ellison D. C., *ApJ* **487** 182 (1997).

[52] Gordon, M. A. & Burton, W. B., *ApJ* **208** 346 (1976).

[53] Cox P., Krügel E. & Mezger P. G. , *A& A* **155** 380 (1986).

[54] Bronfman, L., et al., *ApJ* **324** 248 (1988).

[55] Strong, A. W. and Moskalenko, I. V., *ApJ* **509** 212 (1998).

[56] Reynolds R. J., *ApJ* **339** L29 (1989).

[57] Cordes J. M. et al., Nature **354** 121 (1991).

[58] Grevesse N., Noels A. & Sauval A. J., in *ASP Conf. Series* **99** 117 (1996).

[59] Hernandez F. P., & Christensen-Dalsgaard J., *MNRAS* **269** 475 (1994).

[60] Ohno H. & Shibata S., *MNRAS* **262** 953 (1993).

[61] Rand R. J. & Lyne A. G., *MNRAS* **268** 497 (1994).

[62] Heiles C., *ApJ* **462** 316 (1996).

[63] Mathewson D.S. & Ford V.L., *MNRAS* **74** 139 (1970).

[64] Ptuskin V. S., Völk H. J., Zirakashvili V. N. & Breitschwerdt, D., *A& A* **321** 434 (1997).

[65] Ptuskin V. S., Völk H. J., Zirakashvili V. N., & Breitschwerdt D., *A& A* **321** 434 (1997).

[66] Lionetto A.M. et al., *JCAP* **0509** 010 (2005).

[67] Letaw J. R., Silberberg R. & Tsao, C. H., *ApJ* **414** 601 (1993).

[68] Seo E. S. & Ptuskin V. S. *ApJ* **431** 705 (1994).

[69] Heinbach U. & Simon M., *ApJ* **441** 209 (1995).

[70] Simon M. & Heinbach U., *ApJ* **456** 519 (1996).

[71] Ellison D.C., Slane P. & Gaensler B.M., *ApJ* **563** 191 (2001).

[72] Moskalenko, I. V., and Strong, A. W., *ApJ* **493** 694 (1998).

[73] Strong A. W. and Moskalenko I. V., *Adv. Space Res.* **27** 4 717 (2001).

[74] Moskalenko I. V., Mashnik S.G. & Strong A. W., Proc. 27th Int. Cosmic Ray Conf. 1836 (2001).

[75] Webber W. R. and Soutoul A., *ApJ* **506** 335 (1998).

[76] Ptuskin V. S. and Soutoul A., *A&A* **337** 859 (1998).

[77] Davis et al., AIP proceeding **528** 421.

[78] Caldwell, J. H. and Meyer P. 1977 *Proc. 15th Int. Cosmic-Ray Conf.* (Plovdiv) **1** 243.

[79] Chapell, J. H. and Webber, W. R., Proc. 17th Int. Cosmic Ray Conf. (Paris), 2, 59 (1981).

[80] DuVernois, M. A. et al., *A&A* **316**, 555, 1996.

[81] DuVernois, M. A. et al., *ApJ* **481**, 241, 1997.

[82] Dwyer, R. et al. *ApJ* **224** 691, 1978.

[83] Garcia-Munoz, M. et al., *ApJs* **64** 269, 1987.

[84] Engelmann, J. J. et al. *A&A* **233** 96, 1990.

[85] Juliusson E. et al., *ApJ* **191** 331, 1974.

[86] Lezniak, J. A. and Webber, W. R., *ApJ* **223** 676, 1978.

[87] Maehl, R. C. et al., *Ap& SS* **47** 163, 1977.

[88] Orth, C. D. et al., *ApJ* **226** 1147, 1978.

[89] Simon, M., et al. *ApJ* **239** 712, 1980.

[90] Webber, W. R. et al. *ApJ* **457** 435, 1996.

[91] Hareyama, M. et al. 1999 *26th ICRC* (Salt Lake City) **3** 105-108, OG.1.1.28.

[92] Simpson, J. A. et al. *ApJ* **497** L85, 1998.

[93] Connell, J.J. et al. *ApJ* **509** L97, 1998.

[94] Yanasak N.E. et al., *Proc. Symp. ACE 2000* **528**.

[95] Lukasiak, A. et al. *ApJ* **423** 426, (1994).

[96] Wang, J. Z. et al. *ApJ* **564** 244, (2002).

[97] Sanuki, T. et al. *ApJ* **545** 1135 (2000).

[98] Mitchell, J. W. et al. *Nucl. Phys.*B (Proc. Suppl.) **134** 31, 2004.

[99] Boezio, M. et al. *ApJ* **561** 787, 2001.

[100] Boezio, M. et al. *ApJ* **583** 504, 2003.

[101] Maurin D., Taillet R. & Donato F., *A&A* **394** 1039 (2002).

[102] Maurin D., Cassé M. & Vangioni-Flam E., *Astropart.Phys* **18** 471 (2003).

[103] Castellina A. & Donato F., *Astrop. Phys.* **27** 155 (2007).

[104] Moskalenko I. V. et al., Proc. 28th Int. Cosmic Ray Conf. (Tsukuba) 1921 (2003).

[105] Moskalenko, I. V., Strong, A. W., Ormes J.F. & Potgieter M.S., *ApJ* **565** 280 (2002).

[106] Moskalenko I. V. & Mashnik S.G., *Proc. 28th Int. Cosmic Ray Conf.* (Tsukuba) 1917 (2003).

[107] Moskalenko I. V., Strong A. W., Mashnik S.G. and Jones F.C., *26th ICRC* (Tsukuba 2003) 1917.

[108] Ptuskin V. S. and Soutoul A., *A&A* **237** 445 (1990).

Acknowledgments

I would like to acknowledge Professor Piergiorgio Picozza that gave me the opportunity to develop this line of reaserch. I also would like to thanks Fiorenza Donato for fruitful discussion and priceless suggestions. A special thanks goes to Professor Riccardo D'Auria who gave me the chance to conclude this thesis.